AN EVALUATION OF THE RELATIONSHIP BETWEEN SMALL CETACEAN TAG DESIGN AND ATTACHMENT DURATIONS: A BIOENGINEERING APPROACH

Morris Bradley Hanson

A dissertation submitted in partial fulfillment of the requirements for the degree of

Doctor of Philosophy

University of Washington

2001

Program Authorized to Offer Degree: Aquatic and Fishery Sciences

University of Washington
Graduate School

This is to certify that I have examined this copy of a doctoral dissertation by

Morris Bradley Hanson

and have found that it is complete and satisfactory in all respects,
and that any and all revisions required by the final
examining committee have been made.

Chair of Supervisory Committee:

Ray W. Hilborn

Reading Committee:

Robert E. Breidenthal

Robert L. ~~DeLong~~

Ray W. Hilborn

Karyn S. Kunzelman

Glenn R. VanBlaricom

Date: 16 May 2001

In presenting this dissertation in partial fulfillment of the requirements of the Doctoral degree at the University of Washington, I agree that the Library shall make its copies freely available for inspection. I further agree that extensive copying of the dissertation is allowable only for scholarly purposes, consistent with "fair use" as prescribed in the U.S. Copyright Law. Requests for copying or reproduction of this dissertation may be referred to Bell and Howell Information and Learning, 300 North Zeeb Road, Ann Arbor, MI 48106-1346, or to the author.

Signature Morris Bradley Hanson

Date 16 May 2001

University of Washington

Abstract

AN EVALUATION OF THE RELATIONSHIP BETWEEN SMALL CETACEAN TAG DESIGN AND ATTACHMENT DURATIONS:
A BIOENGINEERING APPROACH

Morris Bradley Hanson

Chair of the Supervisory Committee:

Professor Ray Hilborn
School of Aquatic and Fishery Sciences

An unresolved problem with radio-tagging small cetaceans is premature tag loss associated with dorsal fin tissue degeneration and attachment pin out-migration. Pressure necrosis at the pin/tissue interface has been suspected of causing this tissue degeneration. However, it is unknown if the stresses that the tags generate are sufficient to cause tissue breakdown, or if it is associated with dynamic loads that disrupt the tissue healing process. The objective of this dissertation was to determine if a relationship exists between these load-related tissue degradation factors and the duration of small cetacean tag attachments. The specific approach included estimating the loads that previously deployed tag configurations generated using a model porpoise mounted in a wind tunnel. Based on these results and the incorporation of basic hydrodynamic/engineering principles, the load of a new, lower drag, tag design was quantified. The major structural components of the harbor porpoise dorsal fin (epidermis/dermal papillae, ligamentous sheath, and central core) were determined using histological techniques. This aspect was

complimented by quantifying the material properties of these component tissues using standard mechanical testing. The data from these efforts were incorporated into a finite element analysis (FEA) to quantify the stress levels of each tag design. The final aspect of this study was to deploy the redesigned tag on small cetaceans with a dedicated resighting effort to assess its attachment performance. This paired side-mount tag appeared to provide a longer duration of attachment compared to the other two designs, exceeding a year, with some tags causing no apparent tissue damage. The FEA showed that paired side-mount also consistently developed only low to moderate stresses compared to the front-mount, which generally had the highest stresses and shortest attachment durations. The single side-mount tag had stresses and attachment durations which were intermediate of the other tag designs. Several limitations to the FEA preclude determination if any of the tags generate stresses sufficient to cause tissue degeneration. Future improvements in attachment performance will likely result from investigations which use the general approach outlined in this study.

TABLE OF CONTENTS

Page

List of Figures ii

List of Tables iv

Chapter 1: Introduction 1

Chapter 2: Drag measurements of small cetacean telemetry tags from wind tunnel testing 13

Chapter 3: Considerations in the redesign of a telemetry tag system for small cetaceans 40

Chapter 4: An analysis of the structure of the harbor porpoise dorsal fin in relation to telemetry tag attachments 64

Chapter 5: Material properties of the tissue layers of the harbor porpoise dorsal fin: implications for tagging 82

Chapter 6: Factors influencing tag attachment duration for small cetaceans: a finite element analysis of telemetry tags on a harbor porpoise dorsal fin 106

Chapter 7: Attachment performance of a redesigned small cetacean telemetry tag system 145

Chapter 8: Conclusions and recommendations 170

List of References 179

Appendix A: Estimates of free-ranging harbor porpoise velocities 193

Appendix B: Mallory's aniline blue collagen stain 199

Appendix C: Verhoeff elastic stain 200

Appendix D: Collagen percent area analysis protocol 203

Appendix E: Determination of engineering constants 205

LIST OF FIGURES

Figure Number Page

2.1a-c. Previously deployed telemetry tag designs tested on a harbor porpoise model in a wind tunnel.....16, 17, 18

2.2. Mean drag coefficients versus mean Reynolds number for a harbor porpoise model and three previously deployed telemetry tag designs 25

2.3. Mean drag forces (N) plotted against simulated velocity for a model harbor porpoise and three previously deployed telemetry tag designs 27

2.4. Mean proportional drag increase plotted against simulated velocity for three previously deployed telemetry tag designs.....28

2.5. Mean proportional drag increase contributed by the components of three previously deployed telemetry tag designs.....31

3.1a-c. Streamlined telemetry tag designs tested on a harbor porpoise model in a wind tunnel.....47, 49

3.2. Mean drag coefficients versus mean Reynolds number for a harbor porpoise model and three streamlined telemetry tags.....53

3.3. Mean drag forces (N) plotted against simulated velocity for a model harbor porpoise and three streamlined telemetry tag designs 55

3.4. Mean proportional drag increase plotted against simulated velocity for three streamlined telemetry tag designs.....56

4.1. Major tissue types and features of the harbor porpoise dorsal fin 69

4.2a-c. Photomicrographs of a harbor porpoise dorsal fin 70-72

4.3. Photomicrograph of the fiber orientation of the ligamentous sheath and subpapillary layer 74

5.1. Generalized plot of a stress/strain relationship for a viscoelastic biological tissue 85

5.2.a,b. Tissue sectioning pattern for harbor porpoise dorsal fins 88

5.3a-d. Stress/strain characteristics of the three primary harbor porpoise dorsal fin tissue layers. 93, 94

6.1a-c. Finite element model geometry of a harbor porpoise dorsal fin with three different telemetry tags 114, 115

6.2.a,b. Estimated maximum principal compressional stress levels for static load cases associated with typical swimming 122,123

6.3a-c. Compressional stress contours in the epidermal/dermal papillae tissue layer of a harbor porpoise dorsal fin finite element model 125,126

6.4. Estimated maximum principal compressional stress levels for impact loads at the air/water interface 127

6.5. Change in estimated maximum principal compressional stress levels from acceleration to deceleration 128

6.6. Change in estimated maximum principal compressional stress levels between 0° and -10° 130

7.1a-c. Tag position on Dall's porpoise 99-02 at time of capture and approximately one year after attachment 157

A.1. Frequency distribution of velocity readings obtained from a time–depth recorder during 37.7 hours of a deployment on a free-ranging harbor porpoise 195

A.2. Depth and velocity readings from a time-depth recorder plotted against time from 1600-1700 on 17 June 1998 during a 38.7 hour deployment on a free-ranging harbor porpoise 196

LIST OF TABLES

Table Number Page

2.1. Drag coefficients (C_D) for a harbor porpoise model and three previously deployed tag designs from wind tunnel testing.....24

2.2. Loads (N) for a harbor porpoise model and three previously deployed tag designs (less model load) from wind tunnel testing 26

2.3. Loads (N) from a harbor porpoise model and three previously deployed tag designs (less model load) from wind tunnel testing at 0°, -5°, and -10° yaw 29

3.1. Clax mockup tag designs tested on a full scale model of a harbor porpoise in a wind tunnel 44

3.2. Drag coefficients for a harbor porpoise model and three streamlined tag designs as tested in a wind tunnel.....52

3.3. Loads (N) for a harbor porpoise model and three streamlined tag designs (less model load) as tested in a wind tunnel 54

3.4. Loads (N) from a harbor porpoise model and three streamlined tag designs (less model load) as tested in a wind tunnel at 0°, -5°, and -10° yaw 58

4.1. Number of harbor porpoise dorsal fins used by analysis type.....65

4.2. Thickness of harbor porpoise dorsal fin tissue layers.....73

4.3. Percent collagen fiber composition of harbor porpoise dorsal fin 75

5.1. Sample dimensions of harbor porpoise dorsal fin tissue specimens subjected to uniaxial testing 89

5.2. Significant terms or interactions from a generalized linear model to the coefficients obtained from a spline fit to the stress/strain relationships for the central core and ligamentous sheath 96

5.3. Mean coefficients from a spline fit of the central core and ligamentous sheath by orientation and crosshead speed 98

6.1. Material properties of components of the dorsal fin/telemetry tag finite element models 117

6.2. Load cases (N) used in the finite element models 119

6.2. Estimated maximum principal compressional stress levels for static load cases associated with typical swimming 121

6.4. Estimated maximum principal compressional stress levels for an impact load at the air/water interface.....127

6.5. Change in estimated maximum principal compressional stress levels from acceleration to deceleration 128

6.6. Change in estimated maximum principal compressional stress levels between 0° and -10° yaw 129

7.1. Summary of tag designs and attachment systems deployed on porpoises and dolphins 153

ACKNOWLEDGMENTS

General

I would like to extend my appreciation to my supervisory committee. I am particularly grateful to the chairman, Dr. Ray Hilborn, for agreeing to take on a student outside his area of expertise and for his interest, encouragement, and the good company of he and his family in the field. This project would not have been possible without the support of my supervisor, Dr. Robert DeLong, for providing the opportunity to pursue this problem and related projects without restraint, in lieu of other program responsibilities. Dr. Robert Breidenthal provided guidance on hydrodynamics and wind tunnel testing. Dr. Karyn Kunzelman provided guidance on the bioengineering aspects of the project and her mitral valve research served as a framework for the bioengineering aspects of this project. Dr. Glenn VanBlaricom's interest and encouragement were greatly appreciated. I would probably never undertaken this particular project had it not been for committee member Dr. Albert Erickson, who provided numerous opportunities, encouragement, and guidance over the past 25 years. By giving an unknown undergraduate student an opportunity to work on a killer whale radio-tagging project in 1976 he set my career in this field in motion and sparked my longstanding interest in the problem addressed in this dissertation. Dr. David Manuwal's participation as the Graduate School Representative was greatly appreciated.

Colleagues Robin Baird, Jeff Foster, and William Walker deserve special mention for their continued interest and assistance through this all, and in particular, for their humor and support during some very challenging field conditions.

I am grateful to NMML colleagues Jeff Laake and Jim Thomasen for their genuine interest and encouragement. The considerable literature that had to be acquired for this project would not have been possible without the cheerful and persistent efforts of NMML librarian, Sonja Kromann. Funding for tuition support was made available by the Egtvedt Foundation and through the NMFS Advanced Studies Program. Project funding was provided by the NMFS Recover Protected Species Program and the Wendy P. McCaw Foundation.

Chapter 2

Steve Osmek provided a tremendous amount of effort in conjunction with the design of Tag 1, and directed the capture and tag deployment on a harbor porpoise off the Washington coast in 1995. Robin Baird designed and built the TDR/tag system used to collect the velocity data from free-ranging porpoises. Todd Burroughs produced excellent porpoise models for wind tunnel use. Brad and Jeff Pratt skillfully modified the models to mount on the wind tunnel drag balance. Andy Read, Andrew Westgate, and Jonas Teilmann willingly provided their tags for testing. Dr. Bob Breidenthal and student test engineers Brad Pratt, Seung Chung, Esther Carlson, and

Matt Craw of the University of Washington's Department of Aeronautics and Astronautics, provided considerable assistance and advice with the wind tunnel testing. Testing and data analysis would not have been possible without the enthusiastic cooperation of Brian Geppert and the staff of the University of Washington Aeronautical Laboratory's Kirsten Wind Tunnel. Jeff Laake provided statistical assistance. Frank Fish provided helpful discussions. Roberta Scholz skillfully translated Bannasch 1996. Robin Baird provided many useful comments.

Chapter 3

Todd Burroughs produced excellent porpoise models for the wind tunnel. Brad and Jeff Pratt skillfully modified the models to mount on the wind tunnel drag balance. Dr. Bob Breidenthal and student test engineers Brad Pratt, Seung Chung, Esther Carlson, and Matt Craw of the University of Washington's Department of Aeronautics and Astronautics, provided considerable assistance and advice with the wind tunnel testing. Testing would not have been possible without the enthusiastic cooperation of Brian Geppert and the staff of the University of Washington Aeronautical Laboratory's Kirsten Wind Tunnel. Lloyd Murrey and Dave Molegro of Moeller Design were of considerable assistance in urethane fairing production. Roberta Scholz skillfully translated Bannasch 1996.

Chapter 4

Bill Walker was integral in the development of this fin structure evaluation, providing assistance with interpretation and acting as a sounding board for the significance of the observations. Terry Spraker did some of the initial histological specimen preparation. Frank Morado provided staff support for development of the histologic techniques. Lisa Appesland spent a considerable amount of time refining the staining process for the histological analysis to yield slides suitable for assessment from these specimens. Jeff Laake graciously upgraded the statistical analyses. Wendy Carlson of the AFSC graphics unit skillfully produced several of the figures. This study would have been severely limited without the foresight of Tamara Guenther and Robin Baird of the Marine Mammal Research Group, Victoria, B.C. to retain the large number of specimen fins as part of their stranding response program.

Chapter 5

I am indebted to Dr. Sue Herring for making her uniaxial tester available, to Betty Sindelar and Tracy Popowics for teaching me how to use it, and to Chris Marshall for assistance with scheduling its use.

I am extremely grateful to Jeff Laake for his development of the Laake Analysis of the Modulus of Elasticity (LAME) spline power curve fitting routine and

his additional assistance with appropriate statistical analyses. Wendy Carlson of the AFSC graphics unit skillfully produced several of the figures.

This study would have been severely limited without the foresight of the Tamara Guenther and Robin Baird of the Marine Mammal Research Group, Victoria, B.C. to retain the large number of specimen fins as part of their stranding response program

Chapter 6

The finite element analysis would not have been possible without the hard work and skill of Joy Xu. Her familiarity with the software used in this analysis and her code-writing ability allowed me to successfully complete these analyses.

Chapter 7

Lloyd Murrey and Dave Molegro of Moeller Design were of considerable assistance in urethane fairing production. The capture and tagging portion of this project would not have been possible without the skilled efforts and moral support of Artur Andriolo, Robin Baird, Jeff Foster, Nolan Harvey, William Walker, Stephen Claussen, Jen Schorr, and Greg Schorr in tagging Dall's porpoises. Robin Baird, Stephen Claussen, Jeff Foster, Kirt Hughes, Chris Malcolm, Karen McCrea, Greg Schorr, Jen Schorr, and Pam Willis assisted with tracking these porpoises. Scott Hill, Doug Schlieger, Paul Wade, and William Walker assisted in capture of the harbor porpoises and Robin Baird and Sacha Hooker with tracking the harbor porpoise.

Capture and tagging of harbor porpoises was conducted under NMFS MMPA permit 967 and capture and tagging of Dall's porpoises was conducted under MMPA permit 782-1349.

I am deeply indebted to the staff of the Friday Harbor Laboratory, University of Washington. Dr. Dennis Willows generously made moorage available. Particular thanks go to staff members Joyce Smith and Sharon Beach for their ever-pleasant assistance with accommodations. David Duggins and Megan Dethier, and Jim and Mary Guard graciously allowed access to their San Juan Island properties for monitoring VHF transmitter signals.

Larry Hansen provided the initial opportunity to deploy tags on bottlenose dolphins. Aleta Hohn diligently kept track the tagged dolphins, deployed additional tags and provided additional information. Sue Barco, Keith Rittmaster, and Kristen Mazzerella graciously provided their unpublished resight information.

Wendy Carlson of the AFSC graphics unit skillfully produced the figure. Roberta Scholz skillfully translated Bannasch 1996.

CHAPTER 1

INTRODUCTION

Determining the movements of individual small cetaceans over periods of months or years can provide potentially critical information for the proper management of these species. These data are particularly valuable for investigations of population stock structure and habitat use. Because seasonal movements are important in determining population subunit interchange, and habitat use may vary seasonally, seasonal knowledge of movements over periods of months is necessary. Additionally, information on local movements and distribution relative to potential sources of anthropogenic disturbance or mortality can be gained. However, because these species live in an aquatic environment and range widely, they are difficult to visually monitor. Thus, the attachment of radio-telemetry devices to their dorsal fins has become an attractive method for researchers attempting to collect movement data.

In most studies which attempted to obtain long-term movement data, the tags were surgically attached to the dorsal fin because this procedure was generally thought to have less impact on the skin and behavior of animals than if attached using a body harness (Leatherwood and Evans 1979). Researchers have attached a variety of telemetry devices to the fins of numerous species of small cetaceans over the past 30 years (Norris et al. 1974, Leatherwood and Evans 1979, Dietz 1986, Scott et al. 1990, Reeves 1998). These tags have typically included a single transmitter (usually satellite-linked or VHF), and a saddle, to which the transmitter is attached. The saddle also

serves as a support plate for the one or more plastic or metal bolts or pins (threaded at both ends), which were made from a biocompatible material. The tagging process includes surgically punching or drilling holes (of about the same diameter as the pins) through the fin tissue. The tag is then positioned on the fin and the bolts or pins are inserted through the tissue, and then secured with nuts that are usually made of a corrodible material. This design theoretically allows the tag to be shed after the batteries have been exhausted.

The underlying problem with these tags is that, until recently (Westgate and Read 1998, Martin and da Silva 1998, Larsen et al. in prep.), movement data for small cetaceans using telemetry-tags has typically been collected for only relatively short time periods because signals were received from the tags for only a few weeks (Scott et al. 1990). However, despite longer durations of contact, some of these studies also experienced a substantial amount of unexplained variability in attachment durations (boto, *Inia geofrennsis*, 0-290 days, n=10, Martin and da Silva 1998, harbor porpoise, *Phocoena phocoena*, 33-212 days, n=9, Westgate and Read 1998). Much of this variability has remained unexplained because most tagging studies did not (or could not) undertake systematic follow-up monitoring to determine causes of signal loss. This was generally because the primary focus of these studies have been to obtain movement data. Consequently, most were not designed to collect resight data and in many cases the existence of these species in the aquatic environment, their wide-ranging nature, and the lack of ready access due to remote or pelagic distribution, has further limited the ability of researchers to closely monitor the animals to observe problems. The limited

resight data that have been gathered have been extremely valuable in assessing the general problems associated with these shorter than expected deployments.

Although signal loss has been documented or suspected due to animals moving out of VHF monitoring range (Read and Gaskin 1985, Erickson 1978), the two sources of failure that are of primary concern and that have been documented or suspected were related to the: 1) transmitter (Irvine et al. 1982, Tanaka et al. 1987); or 2) attachment (Irvine et al. 1979, Read and Westgate 1997)). However, conspicuously lacking in published reports is any detailed, comprehensive assessment of the sources of these failures. Many studies did not conclude or speculate on the factors associated with these failures. Those that did sometimes described these in only general terms, thus not conveying a clear understanding of the underlying factor (s) related to the observed problems, or did not provide supporting rationale for their comments. Most of these comments appear to be related to the attachments. Reports from some of the earliest tagging studies noted that "water drag, tissue rejection and attempts by the dolphin to shed tags may have contributed to tag loss and fin damage" (Irvine et al. 1982). In a review of tagging techniques a decade ago Scott et al. (1990) reiterated the importance of the findings in previous studies of tissue responses to small, dermal implants (Geraci and Smith 1990). They highlighted the need for "a composite material that encourages growth in the implanted portion of the tag to immobilize the tag and prevent rejection, an epidermal seal to prevent wicking of pathogens, and an elasticity of the implanted portion which matches that of the tissue but is strong enough to resist mechanical stress." More recently, a more comprehensive list of factors based on three major

concerns (attachment methods, tag reliability, and potential effects on the animals), were developed by Brill and Friedl (1993). They went on to identify the factors associated with these problems and suggest some areas of research. As for attachment methods they noted that pressure necrosis, tag migration, and enlargement of holes with large or heavy transmitters were the important factors. Suggested research requirements included: material testing (mount, biocompatible pins, and antifouling treatments, etc.), flow dynamics testing (water flow around tag and tag mounts, migration of pins), redesign of dorsal fin mount (reflecting concerns about the role of fin vascularization for reproduction, (see Rommel et al. 1992, 1993)), and research into pin attachment and size, and placement of the mount on the dorsal fin. For tag reliability, they suggested the use of both satellite and VHF transmitters to allow for resightings of coastal animals. In order to test the effects on the animals flow tank testing was suggested in order to develop an optimal design for the tag and its attachment. It was considered essential to test the tags on active animals. This could be done with captive animals, but ultimately should be undertaken on free-ranging animals, preferably in populations that already have baseline data and where individuals can be readily observed. In addition, Brill and Friedl (1993) also noted the need for tests on the physiological and energetic effects of tags, inclusion of behavioral/social considerations, evaluation of tissue damage and other health issues (biocompatible materials research), and a failure analysis on existing tags. Most recently, it was only noted that size reduction in tags would solve retention problems (Stone et al. 1998). These varied and lengthy lists of factors demonstrate both the complexity of the tag attachment problem and the lack of a

comprehensive understanding of the factors associated with the observed problems. This is further demonstrated by the lack of any stated rationale for tag/attachment designs and the continuing occurrence of failures. Taken together, this indicates researchers have been unable to anticipate the full spectrum of conditions to which tags are subjected. An underlying association of all failure modes is that they appear to be a result of inadequate engineering. Consequently, it is in an enginerring context that these problems need to be considered.

The factors associated with transmitter or attachment failures are likely numerous, with potentially complex interactions. Specific aspects of transmitter failure have or could include several components: i.e. batteries; signal sending unit; antenna; or saltwater switch (if equipped). Placing transmitter electronics in the ocean exposes them to an extremely hostile environment, compromising their function because saltwater is very corrosive (requiring enclosure in waterproof housings or materials). In addition, the cold temperatures in many regions reduce battery performance. The dive depths marine mammals reach (e.g., Hooker and Baird 1999) can subject transmitters to extremely high pressures, possibly causing structural failure, which can allow saltwater intrusion. Fouling by marine organisms may reduce or inactivate the transmitters' sending capabilities. In addition, the transmitter may be exposed to excessive mechanical forces by the animal itself (e.g., rubbing) or by conspecifics (e.g., biting or rubbing) resulting in damage to the transmitter (Irvine et al. 1982) or its components such as antennas (Irvine et al. 1982, Tanaka et al. 1987). Providing robust packaging (i.e., pressure cylinders or solid epoxy castings) has substantially reduced many of these

problems, however, damage, corrosion, and marine fouling remain as continuing challenges to successful transmitter design. In addition, the sophistication of these transmitters varies substantially such that problems associated with the inherent complexity of the electronics can result in unforeseen malfunctions.

Factors affecting the attachment system range from fouling by marine organisms (Irvine et al. 1982, Tanaka et al. 1987) to the drag forces created by the tag while the animal swims, surfaces, etc., or contact forces applied while an animal rubs or interacts with other animals (Irvine et al. 1982). The contact forces are exerted in varying magnitudes and may cause the physical loss of the tag resulting from two potential sources of material failure; that of the attachment system components or the dorsal fin tissue. Attachment system failures have been noted from a failure of the tag's attachment to the saddle, the saddle itself, or attachment pins (Irvine et al. 1982, Read and Westgate 1997, Mate et al. 1995). Attachment system components include the devices, which secure the transmitter to the saddle (e.g., hose clamps, plastic tie-wraps, adhesives), the saddle (typically some type of thermoplastic or polycarbonate), the surgical pins (usually plastic or metal) and the fastening nuts (e.g., zinc, magnesium, stainless steel, steel, nylon). Failures have been documented for the first three components (transmitter attachment to saddle; Read and Westgate 1997, B. Mate pers. comm., the entire saddle; Irvine et al. 1982, Read and Westgate 1997, pins; Read and Westgate 1997). In order for these failures to occur, the forces applied must have exceeded the structural properties of these materials. Based on the relatively short durations of some of the attachments it is likely that some of these failures occurred

suddenly, due to extreme loads. Others potentially occurred over time, as a result of fatigue of the materials. Researchers that used more or larger diameter pins, rather than modify the saddle, did so in an apparent effort to provide a more secure attachment. Attachments have used from one to six pins, and diameters have varied from 3.1 mm to 7.9 mm, with 6.4 mm being most commonly used. However, no data are currently available on the loads and associated vectors that could induce the failure of these tag attachment materials, nor has a quantitative comparison been conducted of the strength of the attachment materials.

The other type of failure leading to tag loss is that of dorsal fin tissue degradation. It may occur from two sources, depending on the forces involved. Large forces exerted on the tissue may cause the pins to tear out. Alternatively, under lighter loads, tissue degradation can develop at the pin sites, resulting in their out-migration. The frequency of tag loss due to the tag rapidly tearing out of the fin tissue is unknown, but maybe rare as there are no reports in the literature. Tissue degeneration and subsequent pin out-migration has been more commonly observed and although this can occur over a period of days (Irvine et al. 1982), it more typically takes months (Irvine et al. 1982, Hanson unpubl. data, Martin and da Silva 1998, Orr et al. 1998). In order to evaluate the factors influencing tissue degradation, it is also necessary to redefine the problem in terms of what the tag attachments actually are, i.e., percutaneous devices experiencing dynamic loads in an aquatic environment. For percutaneous devices, tissue degeneration might be expected to occur at these sites resulting from: 1) a foreign body response due to the interaction of the pinning material and adjacent tissue (von

Recum and Park 1981, Geraci and Smith 1990); 2) an infection due to bacterial invasion of the wound (von Recum and Park 1981, Geraci and Smith 1990); 3) pressure necrosis, due to chronic stress concentrations which occlude blood flow (Mak et. al 1994); or 4) mechanical stresses disrupting the healing process (von Recum and Park 1981, Geraci and Smith 1990).

Tissue response to the pinning materials in small cetaceans has been examined in implant studies conducted on captive animals (Geraci and Smith 1990). Because most of the test materials were readily rejected it was suggested that the constant exposure of open wounds to the infectious organisms in the aquatic environment allowed infections to develop (Geraci and Smith 1990). Although stainless steel was the most readily rejected material in this implant study, this same material yielded one of the longest attachment durations recorded for cetaceans when it was used for the attachment pins on a killer whale (*Orcinus orca*) tag (4.5+ months, Erickson 1978). In addition, infections have typically not been observed at pin out-migration sites (Irvine et al. 1982, Tanaka et al. 1987, Martin and da Silva 1998, Orr et al. 1998). The lack of infections may be associated with the saline content of seawater or robust immune systems of the animal. These results suggest that a tissue's response to loading stress (caused by the additional drag of the tag or other loads) may be of greater influence on tag retention than a foreign body response or infection process.

The dorsal fin potentially serves several important functions that may be impacted by tags. Although its vascularization likely serves an important thermoregulatory function for the reproductive organs of respective sexes (Rommel et

al. 1992, 1993), its most obvious function is to act as a stabilizer to resist yawing and rolling (Fish and Rohr 1999). The dorsal fin is essentially a small hydrofoil that produces a force perpendicular to the axis of motion (sometimes referred to as “lift” - Webb 1975), and likely improves turning efficiency in small cetaceans. As a result, it must be of sturdy construction to be resistant to applied loads during an animal’s maneuvers. Because it contains no skeletal elements, it derives its structural integrity from its dense fibrous connective tissue (Fraser 1952, Felts 1966, Elsner et al. 1974), consisting primarily of collagen fibers (Felts 1966). However, dorsal fins are more elastic than the pins and tag saddles that are typically attached to them. This mismatch in their material properties may result in stress concentrations in the tissue surrounding the attachment site when the tag is under load. The stress distribution within the fin will be a function of the load being applied, the structural composition of the tissue, and the attachment scheme’s configuration (i.e., the position of the tag on the fin and the number, diameter, and location of pins). At least part of this load will be dependent on the velocity of the animal, but little information is available on the velocities these animals typically maintain in a free-ranging condition. If the stress levels in the dorsal fin tissue were sufficient to occlude blood flow and were sustained over a period of hours, pressure necrosis and tissue degradation would be expected to ensue. Although observations of tissue degradation have been attributed to pressure necrosis (Brill and Friedl 1993, Mate et al. 1995), it is unknown if the pressure that any previously deployed tags cause is sufficient to occlude blood flow. This type of tissue breakdown is likely a function of the load per unit area (i.e., stress) such that minimizing pressure

necrosis should be achievable by reducing the load per unit area; i.e. increasing the unit area of the load bearing surface or reducing the total load. This could be achieved by increasing the number of pins or their diameters, whereas reducing total load can only be accomplished by reducing tag drag. This appeared to be the intent in one study that used five pins (Mate et al. 1995). The other potential source of pressure related tissue degradation is due to the disruption of the healing process because of the tag's movement (Geraci and Smith 1990). The underlying mechanism will be dynamic loads that are associated with several fundamental aspects of these animal's behaviors. These aspects include the frequency and magnitude of the changes of an animal's velocity and direction while swimming under water, the impact loads of the tag entering water after an animal surfaces to breathe, as well as the animal's interactive contact with conspecifics or rubbing on substrate. Tag movement is likely to be related to the tag's stability on the fin, associated with the position and number of pins and the tolerances of the pins with the holes in the saddle and the fin. The use of several pins by some researchers may have been an attempt to better stabilize the tag.

Although tissue necrosis has been recognized as a problem for a long time (Irvine et al. 1979), little has been done to address this problem. The lack of a quantified approach to this problem is likely due to the fact that measuring the pressure created by the tag requires estimating loads, a task not easily accomplished due to the complexity of the forces involved and the difficultly associated with their measurement. The logistics of direct measurements of the load at the pin/tissue interface in vivo are impractical. Even estimating the drag generated by a tag is difficult because it requires

testing with models in wind or water tunnels, or on captive animals where deceleration can be accurately measured while gliding. In a few tagging studies hydrodynamic drag was suggested to be of importance (Martin et al. 1971, Evans 1974, Würsig 1982, Norris et al. 1985, Scott et al. 1990, Mate et al. 1995, Davis et al. 1996), but only two have actually quantified the drag of tag designs that deployed (Tanaka et al. 1987, Stewart et al. 1995). Although minimizing drag can be accomplished by streamlining the tag design, it may not be possible to match the efficiency of a small cetacean's body, which exceeds those of most man-made shapes (Nachtigall 1981). Consequently, telemetry tags, in the shape of their typical square and cylindrical components, might be expected to add a substantial amount of drag to these animals, which also may create significant loads on their dorsal fin tissues. Tags that are streamlined should generate less drag, and therefore, less pressure for similar attachments.

The objective of this dissertation was to determine if the forces generated by telemetry tags are sufficient to cause pressure necrosis or other load-related tissue degradation and if these factors correspond with observed tag attachment duration. The general approach was to conduct a finite element analysis, using computer-based mechanical models of the tags mounted on a fin, to visualize and quantify the stress distribution generated by these tag designs, for comparison to their attachment performance. This approach required the determination of load cases generated by the tags, the geometry of the fin tissue layers, and their material properties. In addition, a more streamlined design would need to be developed and its attachment performance assessed. The specific approach was to first estimate the loads generated by the three

most commonly used tag configurations using a model porpoise mounted in a wind tunnel at typical swim velocities. Based on the results of these investigations and the incorporation of basic hydrodynamic/engineering principles, transmitter constraints, and field assessment needs, a new tag design was developed and evaluated in the wind tunnel. This redesigned tag was then deployed on small cetaceans and its attachment performance was assessed with a dedicated resighting effort.

In order to better understand the structural integrity of the dorsal fins, a detailed examination of the structural components of the harbor porpoise dorsal fin was undertaken using histological techniques. This effort was complimented by quantifying the material properties of the component tissues (identified from the histological analysis) using standard mechanical testing.

CHAPTER 2

DRAG MEASUREMENTS OF SMALL CETACEAN TELEMETRY TAGS FROM WIND TUNNEL TESTING

Introduction

Small cetaceans are known to have very hydrodynamically efficient body forms (Hertel 1963, Lang and Pryor 1966, Bannasch 1996, Fish and Rohr 1999). Hydrodynamic efficiency is necessary to minimize the energetic costs associated with movement at relatively high speeds through a dense medium. The body design of small cetaceans creates less drag than most man-made shapes (Nachtigall 1981). Consequently, even well designed telemetry tags might be expected to add a substantial amount of drag to these animals while swimming underwater. The additional drag the tag creates is a load. This force is a function of the animal's velocity, and because these devices have typically been attached with pins through the animal's dorsal fin (Evans 1974, Leatherwood and Evans 1979, Scott et al. 1990), the load is transferred through the pins to the adjacent tissue. Pin out-migration and premature tag loss due to tissue degradation at the pin/tissue interface has been observed (Irvine et al 1982, Tanaka et al. 1987, Orr et al. 1998). While it has been suggested that the observed tissue degeneration was a function of pressure necrosis (Brill and Friedl 1993, Mate et al. 1995), it is unknown if the loads these tags generate are sufficient to cause this type of necrosis. Because the amount of drag a tag (or any object) creates is a function of its shape (Vogel 1994) and the animal's velocity, the

rate of pin out-migration (and thus attachment duration) might be related to the amount of drag a tag adds. Consequently, quantifying the additional drag of previously deployed tags may help explain the differences that have been observed in attachment durations, as inferred from signal durations. Some researchers have noted hydrodynamics as a factor to consider in a tag's design (Martin et al. 1971, Evans 1974, Würsig 1982, Norris et al. 1985, Scott et al. 1990, Mate et al. 1995, Davis et al. 1996). Although in one case it was stated that their tag was hydrodynamically shaped (Davis et al. 1996), there were no test data to support this claim. The drag of only two previously deployed tags have ever been quantified, one test having been conducted in a water tunnel and the second through glide tests on live animals (Tanaka et al. 1987, Stewart et al. 1995).

Wind tunnels are routinely used to assess the drag characteristics of a variety of objects (Rae and Pope 1984) and can provide qualitative (flow visualization) or quantitative (drag loads) information. Determination of the additional burdens of telemetry packages which have been previously deployed on flying birds and penguins have been made using this technique (Obrecht et al. 1988, Culik et al. 1994). In this study, the drag coefficients, loads, and proportional increase in drag were determined for three tag designs that had been previously deployed on wild harbor porpoises (*Phocoena phocoena*), from measurements on a model porpoise in a wind tunnel.

Methods

Drag forces generated by the tag designs were measured by attaching them to a full-scale fiberglass model of a harbor porpoise mounted in a wind tunnel. The porpoise model was constructed from a mold that was taken off an adult male porpoise. This animal had been killed incidental to commercial fishing operations and was subsequently frozen in the glide position by hanging it by its tail. This model was configured to mount on the drag balance strut of the University of Washington Aeronautical Laboratory's Kirsten wind tunnel, a subsonic, closed-circuit, double-return tunnel (test section dimensions - 2.4 m high, 3.6 m wide, 3.0 m long).

Three different tags designs, all of which had been previously deployed on harbor porpoises, were tested. Tag 1 is referred to as a dual-side mount because it consisted of two transmitters, each attached with two hose clamps to a thermoplastic saddle, lined with 3.2 mm neoprene foam, which wrapped around each side of the dorsal fin (Figure 2.1a). On the left side was a cylindrical split-board configuration of a Telonics ST-10 satellite Platform Terminal Transmitter (PTT - 2.54 cm diameter, 11.7 cm long), with a 19.0 cm long rigid stainless steel wire antenna (1.2 mm diameter) exiting the tag at 45° from the back of the transmitter. On the right side was an ATS model 201 VHF transmitter with 2 AA batteries (1.9 cm diameter, 14.6 cm long) arranged in line. This transmitter had a 0.16 cm diameter, 34 cm long, rigid

Figure 2.1.a. Tag 1 - dual side mount telemetry tag. Telonics split board ST-10, left side, ATS Model 201, right side.

stainless steel wire antenna, also exiting from the posterior end of the transmitter at 45°. The pack was attached with three 4.8 mm diameter Delrin pins. This design was deployed on one animal off the Washington coast in 1995 and signals were received for 20 days from both transmitters (Osmek et al. in prep.). Tag 2 is described as a front-mount (Figure 2.1b), which consisted of the cylindrical ST-10 (except with a 2.1mm diameter flexible braided wire antenna). In the first two deployments the transmitter was secured with plastic tie wraps (subsequent versions used three hose clamps) to a thermoplastic saddle that fit around the leading edge of the dorsal fin with a open cell foam liner. It was attached with three 7.8 mm high-density polyethylene or Delrin pins. It was deployed on five animals in the Bay of Fundy in 1994 and 1995

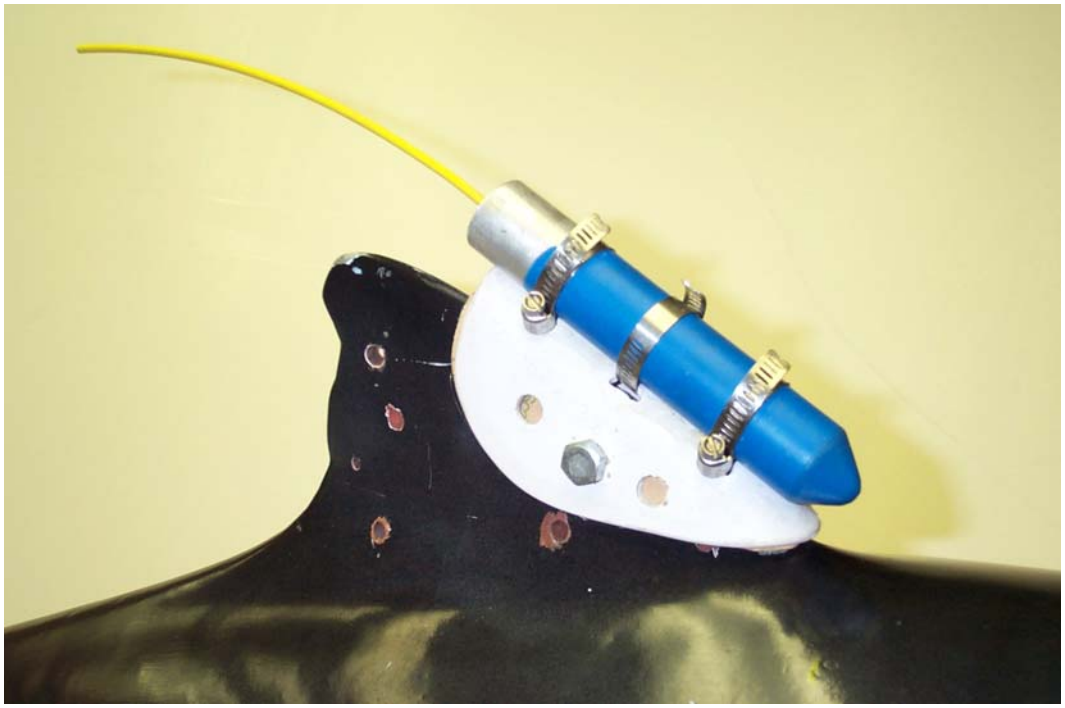

Figure 2.1.b. Tag 2 – front mount telemetry tag. Telonics split board ST-10.

with signals received for 2-21 days (Westgate and Read 1998). The tag used in these tests was a mock-up of the original tag but lacked an antenna, which was determined to add negligible drag from preliminary tests using the actual tag. Tag 3 is described as a single side-mount (Figure 2.1c) and is a rectangular configuration of the ST10 (2.1 cm high, 9.1cm long, 4.8 cm wide). The Lexan transmitter housing was epoxied to a 2 mm thick flat plastic saddle, lined with open cell foam, which was fit on the right side of the dorsal fin and fastened with three 6.3 mm Delrin pins. The same size flexible antenna used on Tag 2 was mounted vertically near the front of the transmitter. This design was deployed on 9 animals in the Bay of Fundy in 1995 and 1997 and yielded signals for 33 to 212 days (Westgate and Read 1998).

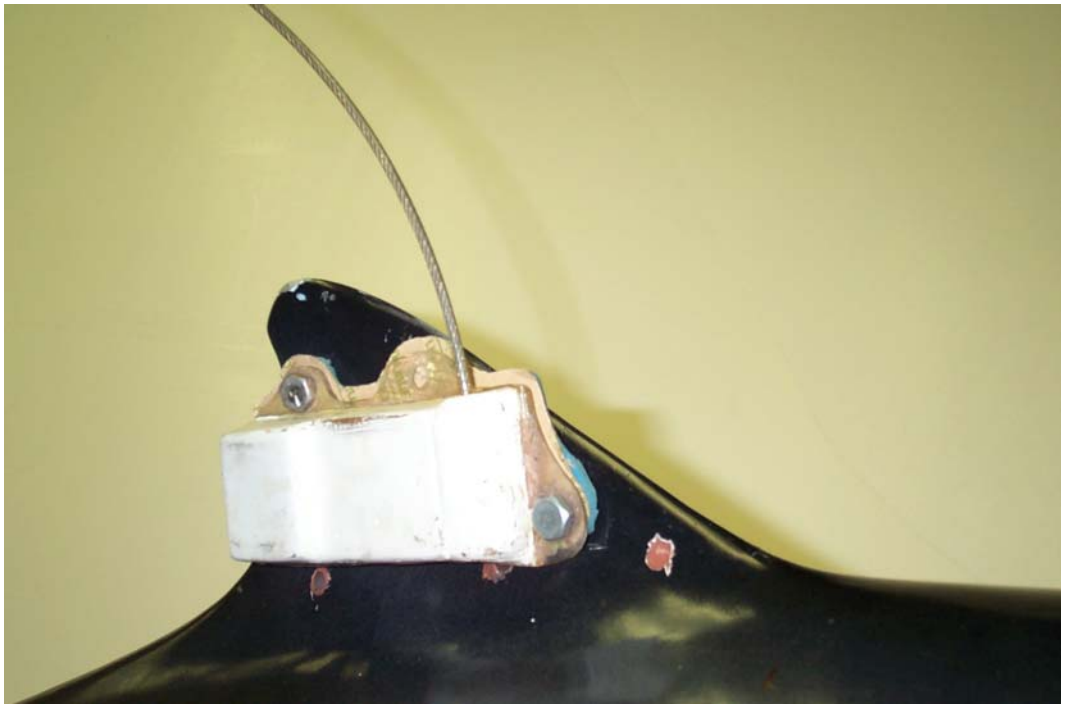

Figure 2.1.c. Tag 3 – side mount telemetry tag. Telonics ST-10.

Because loads are velocity dependent, testing was conducted over a range of typical swim speeds of free-ranging porpoises. This velocity range was estimated for a free-ranging porpoise from data collected by a suction-cup attached time-depth recorder (TDR/VHF radio tag, Hanson and Baird 1998) equipped with a velocity turbine (Mk6, Wildlife Computers, Redmond,WA) during a 38.7 hr deployment on a female harbor porpoise in Presidents Channel and the southern Strait of Georgia, Washington State (Appendix A). Median velocity was 1.25m/s, with 90% of the speeds being between 0.4 and 2.3 m/s. The maximum velocity was 6.5 m/s.

In order to determine the forces on the swimming porpoise from the wind tunnel tests, it is important to match a dimensionless parameter, the Reynolds number,

according to the differences in viscosity between air and water. This can be accounted for using the principle of dynamic similarity (Hansen 1987). The Reynolds's number (Re) is defined as:

$$\mathrm{Re} = \frac{VL}{\nu} \tag{1}$$

where V is velocity, L is model length, and ν is kinematic viscosity. Consequently, it follows that:

$$\mathrm{Re} = \frac{V_{saltwater} L}{\nu_{saltwater}} = \frac{V_{air} L}{\nu_{air}} \tag{2}$$

such that:

$$V_{air} = \frac{V_{saltwater} \nu_{air}}{\nu_{saltwater}} \tag{3}$$

where $V_{saltwater}$ varied as porpoise swim speed, ν_{air} depended on the air temperature and pressure in the tunnel, and $\nu_{saltwater}$ was 1.260×10^{-6} m^2/s based on an average water temperature of 12.7^{o} C obtained from the TDR deployment.

At the same Reynolds number, the two flows are similar, so that all forces are proportional to the dynamic pressure:

$$q = \frac{\rho V^2}{2} \tag{4}$$

where ρ is the density of the fluid in question.

The dimensionless drag coefficient, C_D, was calculated for the model as:

$$C_{Dm} = \frac{D_m}{qA_m} \tag{5}$$

where D_m is the time-averaged drag force on the model in Newtons at a specific q, and A_m is the cross-sectional frontal reference area of the model. Tag C_{Dt} was calculated as:

$$C_{Dt} = \frac{C_{Dm+t} - C_{Dm}}{A_t / A_m} \tag{6}$$

where C_{Dm+t} was the drag coefficient of the model and the tag, and A_t is the cross-sectional frontal reference area of the tags (Hoerner 1965). Cross-sectional frontal areas were determined using the area morphometry function of Optimas 6.51 running on a PC with frontal, digital photographs. All C_D values were corrected for the drag

tare effect of the model support strut by subtracting the strut-only drag measurements taken at the same dynamic pressure.

The testing protocol included a baseline test of the model without tags at the beginning of the testing session and a subsequent test, either in the middle or near the end of the testing session. The model was initially tested without tags at dynamic pressures of 480, 960, 1200, 1900, 2400 and 2900 Pa, pitch was varied from -10.0^o to +10.0^o in 2° increments, and yaw was varied from 0° to +10.0^o in 2° increments. Drag values were typically lowest at 6° pitch and 0° yaw. Subsequent testing typically used dynamic pressures of 95, 190, 240, 290, 380, 480, 1200, and 1900 Pa. Although porpoises swim slower than the equivalent dynamic pressure of 95 Pa (~1.0m/s), this was the minimum q that the tunnel could be accurately maintained. Pitch angles used for most tests were either +4.0^o to +8.0^o with 0.5^o steps, or +5.0^o to +7.0^o with 1.0^o steps. All comparisons in the data analyses were made at 6° pitch. Various yaw settings were used, including –10°, -8 ^{o}, -5 ^{o}, -2 ^{o}, 0 ^{o}, 2 ^{o}, 5 ^{o}, 8 ^{o}, 10 ^{o}. Analyses of the effect of yawing on tag load were conducted for Tags 2 and 3 and limited to yaw angles of -5 ^{o}, and –10 ^{o} because conventional airfoils typically stall at about a 15° angle of attack (Fish and Rohr 1999).

Impact loads at the air/water interface that occur at the beginning of a dive were estimated as:

$$D_{tI} = C_{DtI} q A_t \qquad (8)$$

where the $C_D \cong 2$ for a blunt-faced tag. Porpoises typically submerge at about 1.1 m/s (Appendix A), which is approximately equivalent to a q of 95 Pa.

Tag loads were estimated by subtracting the average load of the model with the tag from all tests for a given q and yaw, from the average load of the model without the tag from all the tests. The proportional increase in drag was calculated by:

$$P = \frac{D_{m+t} - D_m}{D_m} \qquad (9)$$

where D_{m+t} is the average load of the model with the tag.

In order to evaluate the relative drag contribution of each of the tag's components (saddle, transmitter, antenna), test runs were made with the saddle and transmitter with antenna, the saddle and transmitter without antenna, and the saddle only. All tests were conducted at 1900 Pa with pitch angles of -10.0^o to +10.0^o and 0° yaw. All analyses were conducted at 6° pitch.

Results

The model without tags had average C_D values that decreased with increasing Re, ranging from 0.076 to 0.053 at Re of 0.91×10^6 to 5.03×10^6 (Table 2.1, Figure 2.2). A similar trend was observed for the average C_D of all the tags, but these values were much higher than the porpoise model. Over all dynamic pressures, Tag 2 had the lowest C_D of the three tags.

The average load that the model generated with or without tags generally increased with swim velocity, with the exception of the interval between 1.5 and 1.9 m/s (Table 2.2, Figure 2.3). All three tags added more drag to the model, generating loads that ranged between 0.16 N and 5.36 N over all dynamic pressures. The average proportional increase of these tags showed that they all added a substantial amount of drag to the model, ranging from 0.17 to 0.68 across all tags and simulated velocities (Figure 2.4). However, there was a particularly rapid increase in the proportion of drag added between about 1.5m/s and 2.4 m/s. Tag 1 added substantially more drag to the model than Tags 2 and 3 at all but the lowest velocities. Tags 2 and 3 both generated similar proportional increases from 1.1 to 1.9 m/s, but Tag 2 added slightly more drag at velocities above 1.9 m/s. Tag 1 was estimated to generate the largest impact load at 0.60N compared to 0.43 N for Tag 2 and 0.32 N for Tag 3.

During the tests when the model was yawed to -5° and -10°, the loads of Tags 2 and 3 showed no consistent pattern of change with increasing angle of attack (Table 2.3). The drag loads of Tag 2 declined at all three dynamic pressures from 0° to -5°

Table 2.1. Drag coefficients (C_D) for a harbor porpoise model and three previously deployed tag designs from wind tunnel testing. All values were taken at 0° yaw.

Dynamic pressure, q (Pa)		95	190	240	290	380	480	1200	1900
Simulated swim velocity (m/s)		1.1	1.5	1.7	1.9	2.2	2.4	3.8	4.8
Configuration (frontal area)									
Porpoise model (710 cm^2)	Mean	0.08	0.07	0.04	0.04	0.03	0.05	0.06	0.06
	SE	0.001	0.002	0.002	0.002	0.002	0.02	0.001	0.001
	n	9	5	6	5	5	7	6	15
Tag 1 (30.8 cm^2)	Mean	0.97	0.88	0.94	0.86	0.87	0.91	0.90	0.89
	SE	0.06	0.07	0.07	0.07	0.07	0.07	0.07	0.04
	n	4	3	3	3	3	3	3	7
Tag 2* (21.6 cm^2)	Mean	0.81	0.69	0.69	0.63	0.66	0.72	0.72	0.69
	SE	0.07	0.09	0.09	0.09	0.09	0.09	0.09	0.06
	n	4	3	3	3	3	3	3	6
Tag 3 (17.5 cm^2)	Mean	0.96	0.81	1.04	0.79	0.87	0.87	0.74	0.69
	SE	0.09	0.09	0.10	0.12	0.09	0.09	0.09	0.07
	n	6	5	5	3	5	5	5	9

* without antenna

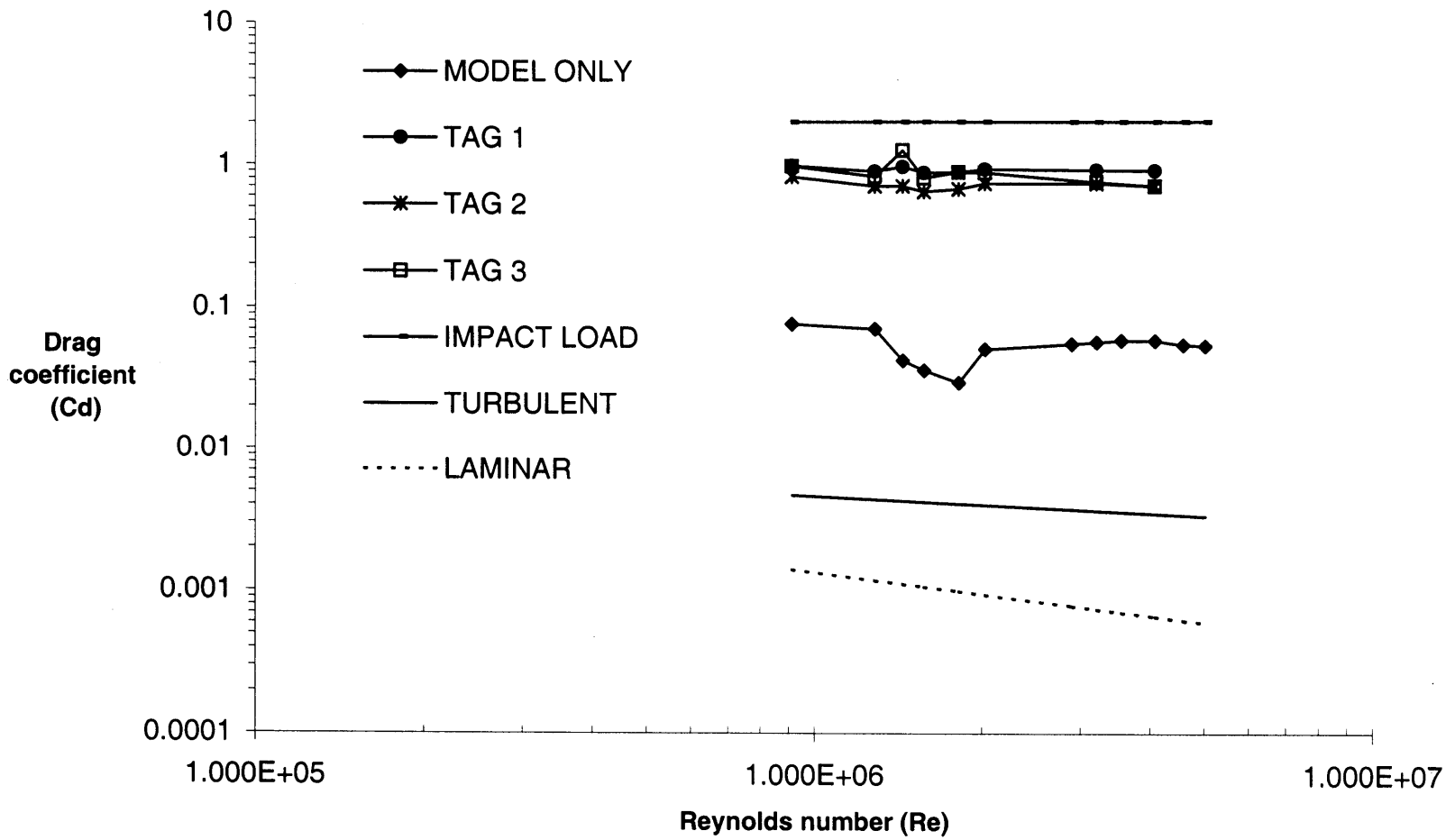

Figure 2.2. Mean drag coefficients versus mean Reynolds number for a harbor porpoise model and three previously deployed telemetry tag designs in a wind tunnel. Turbulent flow line is the drag coefficient for a flat plate with a turbulent boundary layer ($C_D(\text{turbulent})=0.072Re^{-0.2}$). Laminar flow line is for a flat plate with a laminar boundary layer ($C_D(\text{laminar})=1.33Re^{-0.5}$). Drag coefficients are based on frontal area for the porpoise model and the plan form area for the flat plates.

Table 2.2. Loads (N) for a harbor porpoise model and three previously deployed tag designs (less model load) from wind tunnel testing. All values are at 0° yaw.

	Dynamic pressure, q (Pa)	95	190	240	290	380	480	1200	1900
	Simulated swim velocity (m/s)	1.1	1.5	1.7	1.9	2.2	2.4	3.8	4.8
Configuration									
Model	Mean	0.91	1.67	1.63	1.51	1.82	2.22	5.09	7.82
	SE	0.08	0.11	0.10	0.11	0.11	0.09	0.10	0.06
	n	9	5	6	5	5	7	6	15
Tag 1	Mean	0.30	0.56	0.71	0.85	1.11	1.40	3.44	5.36
	SE	0.10	0.12	0.12	0.12	0.12	0.12	0.12	0.07
	n	4	3	3	3	3	3	3	7
Tag 2*	Mean	0.18	0.33	0.37	0.47	0.61	0.79	1.93	2.90
	SE	0.06	0.07	0.07	0.07	0.07	0.07	0.07	0.05
	n	4	3	3	3	3	3	3	6
Tag 3	Mean	0.16	0.27	0.36	0.48	0.55	0.70	1.52	2.30
	SE	0.04	0.05	0.05	0.06	0.05	0.05	0.05	0.04
	n	6	5	5	3	5	5	5	9

* without antenna

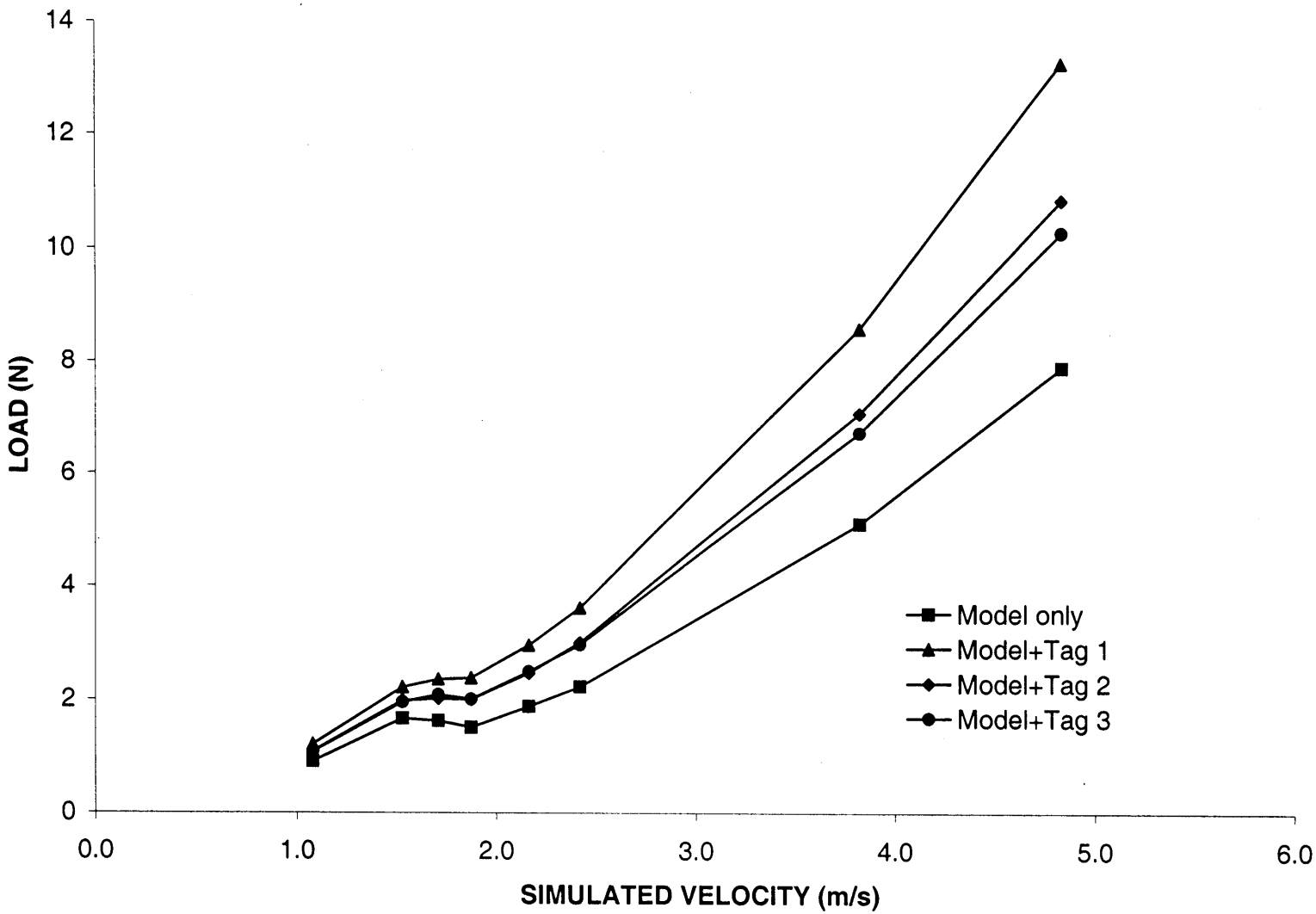

Figure 2.3. Mean drag forces (N) plotted against simulated velocity for a model harbor porpoise and three previously deployed telemetry tag designs.

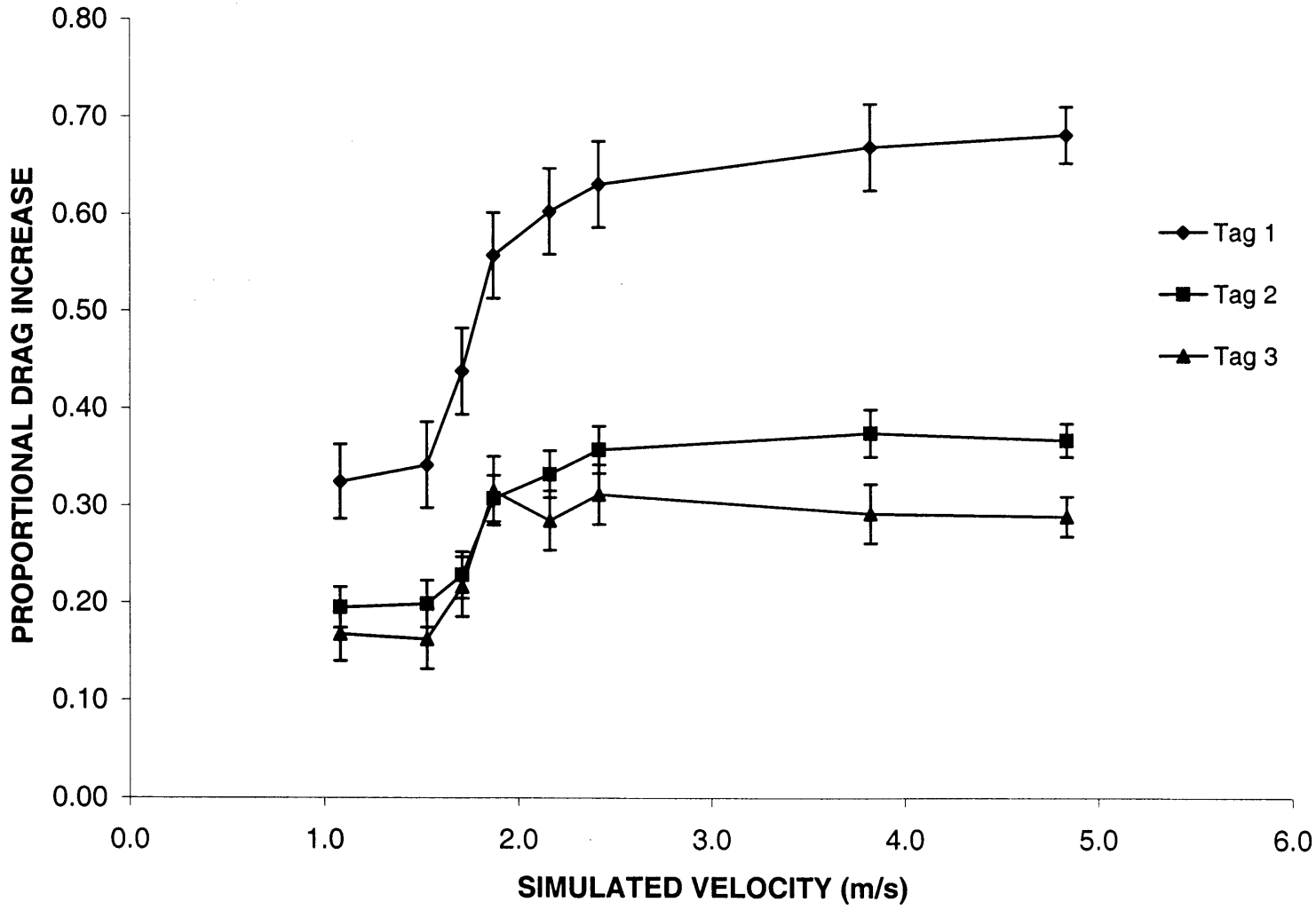

Figure 2.4. Mean proportional drag increase plotted against simulated velocity for three previously deployed telemetry tag designs. Vertical bars are the CI.

Table 2.3. Loads (N) from a harbor porpoise model and three previously deployed tag designs (less model load) from wind tunnel testing at 0°, -5°, and –10° yaw.

	Dynamic Pressure	95	380	1900
	Simulated swim velocity (m/s)	1.1	2.2	4.8
Configuration	Yaw angle			
Model only	0°	0.91	1.88	7.87
	-5°	1.09	2.46	11.1
	–10°	1.58	4.75	20.6
Tag 2	0°	0.17	0.61	2.95
	-5°	0.15	0.56	2.79
	–10°	0.18	0.64	3.48
Tag 3	0°	0.15	0.55	2.26
	-5°	0.14	0.53	2.42
	–10°	0.12	0.43	2.62

and then increased from -5° to -10°. For Tag 3, loads declined with increasing angle of attack with the exception of the increase observed at 1900 Pa and -10°. The relative contribution of tag components to the total drag varied substantially between all three tags (Figure 2.5). Whereas the transmitters of Tag 1 contributed the greatest drag of the three components, the saddles represented the largest amount of drag for Tags 2 and 3.

Discussion

Although interest in quantifying small cetacean drag characteristics began in the early 1960s, there has been limited use of rigid body models to develop these estimates. This may have been because hydromechanical model estimates for the power output of actively swimming animals were several times higher than rigid models (due to tail oscillation), suggesting rigid models underestimate total drag (Fish and Rohr 1999). However, recent work from robotic swimming fish suggests that the drag this model created may actually be less than when it was passively dragged (Anderson and Kerrebrock 1997). In addition, it has also been recently noted that many marine mammals, including small cetaceans, spend sizable proportions of dives gliding, likely to conserve energy (Williams et al. 2000). Consequently, the drag estimates derived from rigid body models may be representative of a substantial proportion of a porpoise's overall drag budget.

The C_D values for the model in this study followed the same general trend of decline with increasing Re that has been observed in several other studies (Purves et

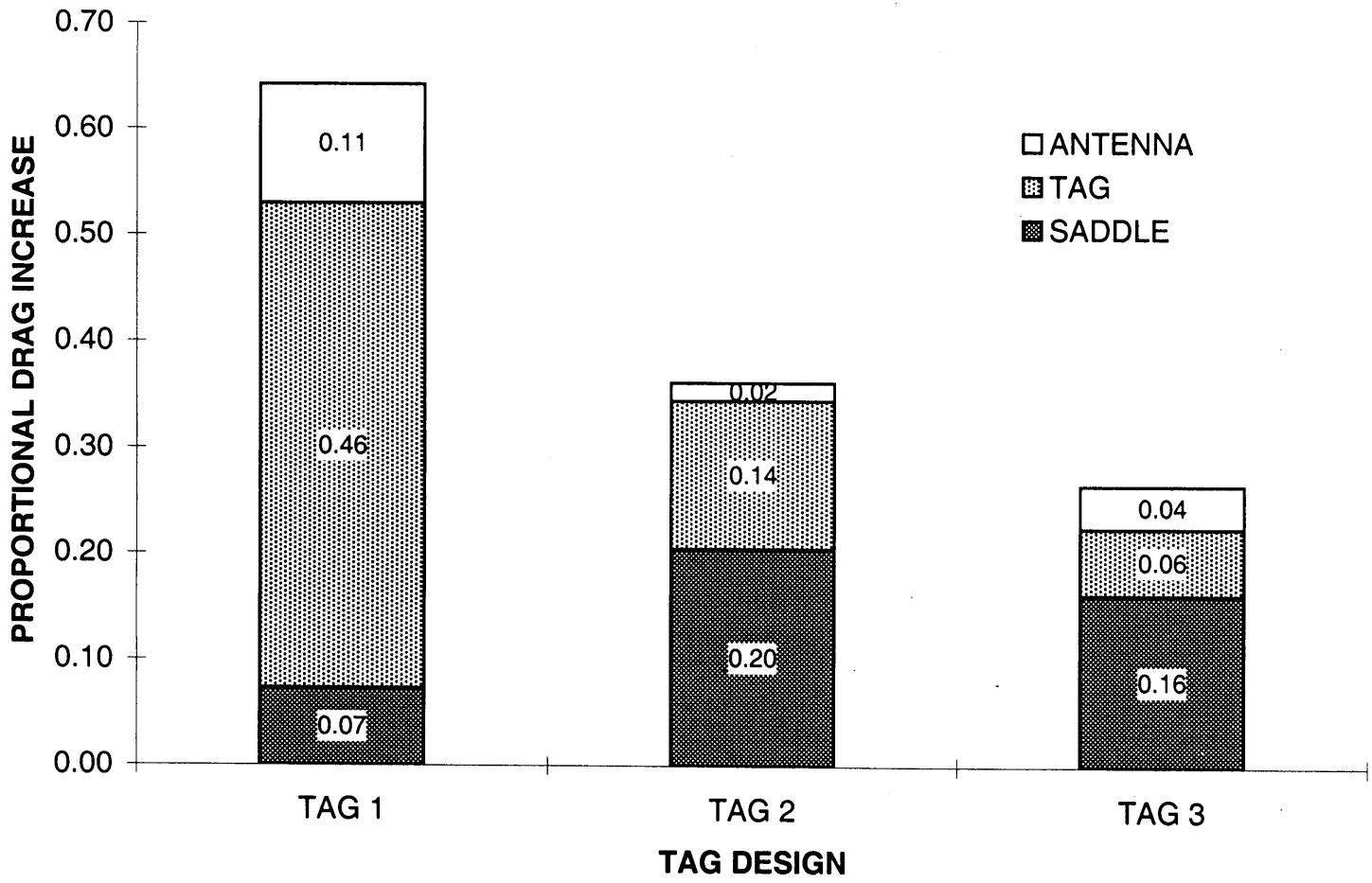

Figure 2.5. Mean proportional drag increase contributed by the components of three previously deployed telemetry tag designs. Tests were conducted at a dynamic pressure of 1900 Pa (n=2).

al. 1975, Bannasch 1996, Fish and Rohr 1999). However, the C_D values in this study were generally higher compared to previous studies that measured the drag of rigid models of small cetaceans (see Purves et al. 1975, Bannasch 1996) as well as for other towed bodies or gliding animals (see Fish and Rohr 1999). Although Purves et al. (1975) and Bannasch (1996) used water tunnels, the differences noted were likely related to differences in model size and configuration. In particular, the study by Bannasch (1996) used a smaller harbor porpoise model (1.23m) that also lacked flippers and flukes. It was noted by Yasui (1980) that the flippers and flukes of a harbor porpoise contribute 18.0% and 13.4%, respectively, to its drag. When the observed values in this study were adjusted by these percentages, they were still slightly higher at the lowest Re but in about the same range as Bannasch (1996) at higher Re. These differences may be due to the angles of attack for the flippers or the surface condition of the model in this study. Flow visualization might provide some insight as to the source of this additional drag.

An interesting phenomenon was the consistent decrease in C_D values observed at mid-range Re. Although testing of other small cetacean rigid models has been limited, a similar pattern appears to be present in some other tests (see Figure 17, Fish and Rohr 1999). It is possible that this temporary decrease in drag is associated with the boundary layer transition to turbulence (Streeter et al. 1998), or changes in the reattachment point of the separated regions. However, whereas the C_D values from other studies fall in the Re region where the flow transitions between laminar and turbulent (see Figure 17, Fish and Rohr 1999), the values obtained in this study are

above this transition region (Figure 2.2). Consequently, the source of the mid-range Re drag decrease in this study remains unclear. Although this model has provided a reasonable approximation of drag, an alternative approach to validating these wind tunnel results would be to conduct deceleration glide studies on live porpoises (see Williams 1987) with these tag designs temporarily attached.

The C_D values obtained for the tags in this study confirm that none are particularly hydrodynamically efficient compared to the body of the porpoise. Tags 1 and 3 had values that were similar to generally round or square objects previously tested in a wind tunnel (Hoerner 1965). Even Tag 2, the design of which had a rounded shape and attempted to minimize frontal area with its alignment on the leading edge of the fin, generated a substantial amount of drag. It seems likely that drag generated by telemetry tags could be reduced through the application of basic principles associated with the shape of attached secondary bodies (see Hoerner 1965).

The observed pattern of the model and all three tags contributing more drag with increasing velocity (Figure 2.3) was similar to the results of a study of tags on a penguin model in a wind tunnel (Bannasch et al. 1994). However, based on proportional increase, Tag 3's drag only increased initially with a slight decreasing trend observed from mid- to high velocities. This pattern is similar to that of a tag prototype tested on a harbor porpoise model in a water tunnel (Bannasch 1996). While the trends observed in this study are likely valid, the accuracy of the drag estimates obtained at lower q settings may be limited because the resolution of the drag balance used in this study was only approximately 0.05 N. Given that the added

drag at 95 Pa for Tag 2 or 3 is approximately 0.15 N, the resolution limitations of the drag balance may contribute up to 30% of the observed variation in drag at this dynamic pressure. At 1900 Pa, this factor only accounts for 3% of the potential variability. A similar situation was encountered during testing of transmitters on birds in a wind tunnel (Obrecht et al. 1988). Testing of these tags on a model of the dorsal fin only in a smaller wind tunnel with a more sensitive drag balance would be the most viable approach in enumerating drag differences at typical swim speeds.

This study was the first to attempt to measure the drag of tags on a yawed model in order to estimate loads incurred while turning. Although insights into the results are limited by small sample size, it is also likely that a lack of consistent trends was due to the porpoise body dominating the flow patterns. The cross-sectional frontal areas of the tags represented only about 2-4% of the frontal area of the model. Although these angles of attack may not be unrealistic for a fin, they may be for the body of the porpoise, resulting in an unsteady flow regime. Consequently, anything less than the model positioned to minimize drag could overwhelm the contribution of tags. Flow visualization would likely prove useful in providing some insight into the complexities of these results. As previously noted, the best approach may be to test the tags on a model of only the dorsal fin at various angles of attack using a higher resolution drag balance in a smaller wind tunnel. This approach would also help evaluate the impact of these tags on lift generation. The dorsal fin, with its position posterior and dorsal to the animal's center of gravity, acts as a stabilizer that resists yawing and rolling moments and prevents side slip during maneuvers (Fish and Rohr

1999). Given the large area and prominent profile of most tags, lift production might be expected to be severely impacted by telemetry tags.

The relatively low drag observed for Tag 3 and its longer signal durations (33 to 212 day for Tag 3 versus approximately 21 days for Tags 1 and 2; Westgate and Read 1998, Osmek et al. in prep.) suggest that lower drag might be related to longer tag attachment durations. However, it is important to note that considerable variability existed in the signal durations from Tag 3, and Tags 2 and 3 appeared to have very similar drag values at simulated velocities close to typical porpoise swimming speeds. Consequently, it is possible other types of failures, other than tissue attachment failure may have been occurring with these tags. Although it has not possible to determine the source of attachment component failures (see Read and Westgate 1997, Irvine et al. 1982), it is unlikely that the loads generated during typical swimming behavior would been sufficient to cause these failures (see Chapter 6).

It is possible that drag differences may have existed but were not detected due to limitations associated with the underlying assumptions, or that other load-related factors may be affecting tag attachment duration. Although the range of velocities examined in this study covered a wide range of the expected swim speeds, the load regime that a tag likely creates on free-ranging animals is potentially greater. Load increases quadratically with velocity, and velocities as high as 6.5 m/s have been recorded for a free-ranging harbor porpoise (Appendix A). Additionally, the estimated velocities used in this study may have been underestimated by up to 15% due to the to potential impairment of water flow into the TDR turbine (Appendix A). The drag the

tag creates as measured at 0° yaw in this study is only a one-dimensional model for the load that the tissue experiences. This load may increase significantly due to another type of inertial force, wave drag, when the porpoises are near the surface, due to the effect of gravity on the wakes generated at the water-air interface (Hertel 1963, Hoerner 1965).

Other load-related factors that might affect attachment duration may be associated with changes in the loads. Consequently, the loads the tags generate on the fin likely also have a dynamic component in addition to the static analysis conducted in this study. While swimming, these animals frequently accelerate and decelerate (Appendix A), as well as turn. In addition, depending on a tag's position on the fin, a tag will also likely generate rotational acceleration associated with its moment relative to the center of lift of the fin during swimming and turning. Even low-level dynamic loads can result in fatigue, and ultimately failure (Sandor 1972) of the tag attachment components. Alternatively, dynamic loads could result in disruption of the tissue healing process (von Recum and Park 1981).

There may also be high loads that occur over a short period of time from several different sources. The impact load that is generated when the tag reenters the water after the porpoise surfaces to breathe is one of these loads. These load estimates were based on an approximation for C_{DtI} of 2. While this value has not been measured, it is likely to be in approximately the correct range for blunt objects because when a tag with flat front enters the water, which splashes the water perpendicularly, all the incident momentum (density times velocity squared) is lost, yielding a value of

2 for the C_D (equations 4 and 5). This value seems reasonable given that impact loads are expected to be substantially greater than those generated during submerged swimming, which for these tests ranged from 0.81N to 0.97N. High impact loads are also possible due to rubbing or biting interactions with conspecifics. Further, if an animal rubs the tag on the bottom substrate, extremely high impact loads may be generated. In both cases, the frequency of such occurrences is difficult to determine, but damage to tags and tissue appear to have been observed from these types of activities (Irvine et al. 1982, Chapter 7). Consequently, all the potential loads that may be applied to the tags need to be identified, and development of tags should try to minimize the effect of all these forces. In addition, a finite element analysis would be useful in analyzing how the loads these different tags generate are actually distributed in the fin in order to minimize them (Chapter 6).

The tag component tests provided insights as to which components to focus on in redesigning tags in order to reduce drag. Of particular note was that the saddles of Tags 2 and 3 were the predominant drag component for these tags. Tag 2's saddle had the highest drag value, which was not unexpected given that it likely had more cross-sectional frontal area than the saddles of the other two designs. However, the large contribution by Tag 3's saddle was surprising given that it likely had lowest cross-sectional frontal area. It is possible that the relatively large contribution to drag is due to the abrupt edge just posterior to the leading edge of the fin, which is unique to this tag’s saddle. This also suggests that more attention should be paid to the design of the junction between the tag and the fin. Although antenna design likely deserves

some attention, the high values associated with Tag 1 were due to the presence of two antennas. However, even when divided in half, this value (7%) is still greater than those for the antennas on Tags 2 and 3 and is probably a result of Tag 1's VHF transmitter, which had a much longer antenna than the satellite transmitter. The extremely low amount of drag from the antenna of Tag 2 is most likely because it was oriented almost parallel to flow. Although additional testing with higher resolution equipment will be necessary to better quantify the loads of these small scale features, future design work can likely reduce tag drag by paying closer attention to saddle and antenna configurations.

Consideration should also be given to how much of a burden the additional drag created by these tags represents to an animal the size of a harbor porpoise, and what effects this might have on the tagged animal. Although swimming motion may increase total drag such that the tag's relative contribution is possibly lessened, this study has demonstrated their potential to add a substantial amount of drag to these animals. This effect may have been manifested as relatively obvious changes in behavior, such as the unusual surfacing observed in bottlenose dolphins (Irvine et al. 1982), or the longer foraging trips in penguins and seals (Croll et al. 1991, Walker and Boveng 1995), or more subtle changes such as slower swim speeds in penguins (Bannasch et al. 1994). Quantifying the drag for a swimming porpoise is not possible because the same body parts produce thrust and drag, which cannot be separated (Vogel 1994). However, it may be possible to determine the energetic burden these tags impose, which may ultimately be the most important measure to the animal.

While no empirical data are currently available for the energetic costs associated with carrying these or other tags by harbor porpoises, greater energy output has been documented in tagged penguins (Bannasch et al. 1994). In that study, a tag that added 15-25% more drag at typical swim speeds on a wingless wind tunnel model was determined to increase the mean energy expenditure by 5.6% for a live bird. The extent to which harbor porpoises can "afford" to carry tags is unknown but it has been noted that energy reserves may be marginal, particularly for reproductive age females (Yasui 1980). The only reliable approach is to quantify additional energetic demands by direct metabolic evaluation on this species. Such a study would be an important addition in assessing the impact of these or other tag designs.

CHAPTER 3

CONSIDERATIONS IN THE REDESIGN OF A TELEMETRY TAG SYSTEM FOR SMALL CETACEANS

Introduction

Numerous efforts to attach telemetry devices to the dorsal fins of small cetaceans have been undertaken over the past 30 years (Norris et al. 1974, Leatherwood and Evans 1979, Dietz 1986, Scott et al. 1990, Reeves 1998). Until recently, duration of transmitter signal contact with tagged small cetaceans was typically for only a few days or weeks (Scott et al.1990). More recently, several studies have had longer durations of contact using tags attached to the side of the dorsal fin (Read and Westgate 1997, Martin and da Silva 1998, Larsen et al, in prep.). Despite increased durations of contact, in some cases the tags have failed to attain their expected service-life. Some of these failures have been due to dorsal fin tissue breakdown at the attachment pin/tissue interface, leading to pin migration and premature tag loss (Irvine et al. 1982, Tanaka et al. 1987). It has been suggested that the tissue breakdown is due to pressure necrosis (Brill and Freidl 1993, Mate et al. 1995). This pressure is a result of the drag the tag generates on the fin tissue as the animal swims.

Several researchers have suggested the potential importance of hydrodynamics in marine mammal tag designs (Martin et al. 1971, Evans 1974, Würsig 1982, Scott et al. 1990, Mate et al. 1995), and while one study suggested that the tag used was

streamlined (Davis et al. 1996), only three studies have ever attempted to assess the hydrodynamic characteristics of deployed tags (Tanaka et al. 1987 and Stewart et al 1995, Chapter 2). However, only one study quantified the drag of a tag design prior to deployment (Bannasch 1996). The amount of drag any object (including a telemetry tag) creates will be a function of its shape and the animal's velocity (Vogel 1994). The shapes of telemetry tags are constrained to a certain extent by the available components and the need to attach the tag to the fin, in order to transmit radio signals in air. Typical tag component (battery and transmitter) shapes are cylinders and brick-like. These shapes are known to generate a relatively large amount of drag (Hoerner 1965, Chapter 2), while streamlined shapes could generate much less drag (Hoerner 1965). If pressure is a factor in tissue breakdown, and drag (i.e., static load) could be reduced, it might be possible to increase tag attachment durations.

It is also possible that other factors may affect tissue degradation. Small cetaceans often change speed (Appendix A) and direction, causing dynamic loads. Dynamic loads have the potential to continually disrupt the interfacial tissue bonds that develop adjacent to the pins as part of the wound response, which can also lead to tissue necrosis (von Recum 1984). Like static loads, if dynamic loads (i.e., changes in momentum), are a factor, and can be reduced, duration of tag attachment may be increased.

In addition to these normal (parallel to direction of forward motion) static and dynamic loads, there are rotational force components (moments) for each of these forces that exert a load as a function of the distance from the center of each axis of

rotation. Consequently, the load a tag generates will also be a function of its position on the fin.

In most of the previous tagging studies little, if any, rationale was presented for the tag/attachment design or its potential to adversely affect dorsal fin tissue. As the preceding review demonstrates, tag/attachment design is essentially an engineering problem. Consequently, it is in that context that this issue will be investigated in this study.

The purpose of this study was to develop a telemetry tag system that would minimize the effect of static and dynamic loads. The focus of the present analyses is to evaluate the potential for drag reduction (static loads) using wind tunnel testing. Other aspects that were not evaluated here were considered indirectly through modeling (Chapter 6), or field deployments (Chapter 7).

Methods

General design concept

A prerequisite of this tag design was the incorporation of two transmitters, which would not only provide redundancy in the event that one failed, but would also potentially allow for an assessment of the failure mode of the other transmitter because it could possibly be relocated and observed. By using a single attachment system for both transmitters, transmitter failure (single signal loss) could likely be differentiated from attachment failure (loss of both signals within a short time of each other).

Mockup design and testing

Eight mockup tag designs were developed in clax (a mixture of clay and wax) based on incorporation of the most commonly used tag electronic components available in 1997 and basic fluid-dynamic design principles that would reduce pressure and interference drag (Hoerner 1965). The components included combinations of VHF and satellite transmitters (Telonics ST-10) with either 2/3 A or AA batteries (Table 3.1). The designs were positioned on the leading edge, side, or trailing edge of the dorsal fin with the objective of staying above the optimal 10:1 fineness ratio (length to height) for a secondary attached body (Hoerner 1965). Where possible, every attempt was made to lengthen and flatten the forebody to avoid flow separation. One model incorporated a blunt trailing edge and the rest were tapered, the latter feature was also to reduce the potential for flow separation. The widths of the tapered trailing edges were designed to be approximately one third the maximum width, even if the afterbody extended beyond the trailing edge for the dorsal fin, to reduce drag (Hoerner 1965). Interference drag also occurs at the junction of two adjoining bodies but this can be reduced if the junction angle is decreased from 90°, the effect of which can also be enhanced in combination with afterbody fairings (Hoerner 1965).

The load generated by each of these prototypes was measured by attaching each design to a full scale, fiberglass model of an adult male harbor porpoise mounted in a wind tunnel. The porpoise model was constructed from a mold of an adult male that

Table 3.1. Clax mockup tag designs tested on a full scale model of a harbor porpoise in a wind tunnel.

Mockup #	Number of transmitters/type	Location of transmitters	Location/orientation of batteries	Saddle configuration	Proportional increase in drag
1A	1 VHF/ 2/3A battery	trailing edge	trailing edge/vertical	posterior wraparound /blunt trailing edge	0.05
1B	1 VHF 2/3A battery	trailing edge	trailing edge/vertical	posterior wraparound/tapered trailing edge	0.01
2	1 VHF AA battery	trailing edge	trailing edge/vertical	posterior wraparound/tapered trailing edge	0.04
3A	1 PTT*	side	trailing edge/vertical	posterior wraparound/tapered trailing edge	0.03
3B	1 PTT*, 1VHF 2/3 A	leading edge, side	leading edge/vertical, trailing edge/vertical	anterior/posterior wraparound/tapered trailing edge	0.04
4	1VHF, 2/3A battery	leading edge	leading edge/vertical	leading edge/vertical	0.03
5	1 PTT*	leading edge	leading edge/vertical	leading edge/vertical	0.17
6	1 PTT*, 1 VHF AA battery	side, side	side/vertical, side/horizontal	posterior wraparound/tapered trailing edge	0.05

*flat board ST10, rectangular

had been killed incidental to commercial fishing operations and subsequently frozen in the glide position by hanging it by its tail. This model had been configured to mount on the drag balance strut of the University of Washington Aeronautical Laboratory's Kirsten Wind Tunnel, a subsonic, closed circuit, double return tunnel with a 2.4 m high, 3.6 m wide and 3.0 m long test section.

The test protocol in this study was similar to the one used in Chapter 2. It included a baseline test of the model without tags at the beginning of the testing session and a subsequent test of the untagged model later, either in the middle or near the end of the testing session. All tests of mockups were conducted at a dynamic pressure (q) of 1900 Pa for comparison to the previous tests of actual tags (see Chapter 2). Pitch was varied from -10.0^{o} to +10.0^{o} in 2° increments. Drag values were typically lowest at 6° pitch and 0° yaw, thus yaw was maintained at 0° for all further tests. All comparative analyses of the data were made at 6° pitch and 0° degrees yaw. Estimates of proportional drag increases were determined using the same methodology as outlined in Chapter 2.

Production tag design and testing

The configuration of the final design was a tag mounted on the sides of fin. The decision for this placement was based on the results of the mockup tests, which indicated that unless the front transmitter width could be constrained to the fin width, a front/aft mount would generate substantial drag. In addition, the generally longer

duration of radio-signal contact in studies using single side-mount tags suggested that this position would be more advantageous (Read and Westgate 1997, Martin and daSilva 1998). Based on the prerequisite design concept of incorporating a second transmitter, its placement would likely be optimal on the other side of the fin because the moments associated with each tag would cancel out (assuming the designs were symmetrical). This design, termed the paired side-mount, was initially developed to incorporate two transmitters for deployment on Dall's porpoises (Tag 4, Figure 3.1a). The overall configuration that would accommodate the battery and transmitter was based on mockup #6 and reproduced in low sulfur clay on a fiberglass replica of a Dall's porpoise dorsal fin. The locations of the three-pin attachment system (based on the pattern used on tags deployed by Read and Westgate 1997) were integrated into this clay prototype with two anterior pins located approximately 2.5 cm posterior to the leading edge of the dorsal fin, approximately 4.1 cm apart. A pair of posterior pin locations was located in line, approximately 15.9 cm and 16.5 cm from the leading edge, in order to account for the average inter-arterial distance. The spacing of the two holes would provide alternate penetration sites to avoid primary vascular trunks (see Chapter 4), which play an important thermoregulatory role for the reproductive organs (Rommel et al. 1992, 1993). The relative positions of these three pins were designed to act similar to a truss system and limit the tag's movement in all three principal axes. The 0.64 cm diameter pin holes were incorporated into the mold to provide a close tolerance fit between the saddle and the pin in order to minimize the effects of momentum associated with dynamic loads. The pin shaft depth of each of the pin sites

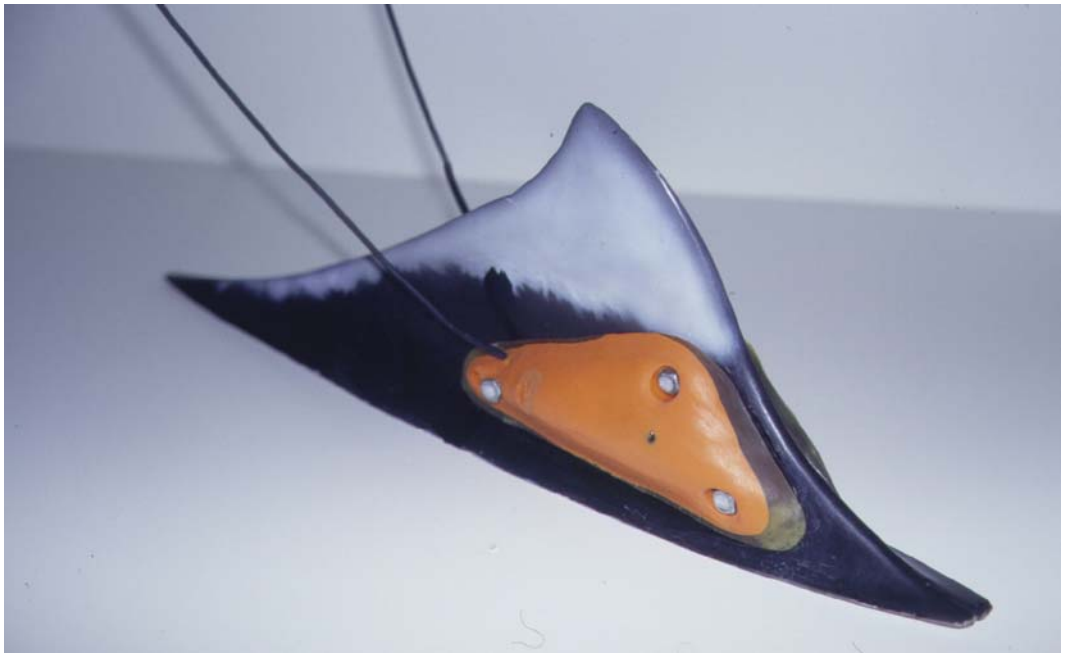

Figure 3.1a. Tag 4 - Paired side mount telemetry tag. ATS model 201, left, ATS model 201, right.

was approximately 0.95 cm. Each site incorporated a recess for the pin/nut, which was 1.27 cm in diameter and varied in depth from 0.32 cm to 0.64 cm. The recess was designed to keep debris from accumulating on these assemblies. In addition, recessed nuts were likely to generate less drag compared to protruding nuts (Hoerner 1965). In order to minimize nut size, the pins were threaded for 6mm nuts. The tag was 16.5 cm in length and 1.9 cm in height yielding a fineness ratio of approximately 11.5. The trailing edge of the fairing was approximately 2.5 cm wide, corresponding to 0.3 of the tag's maximum width. A silicone mold was made of the clay mockup and the surrounding dorsal fin. An ATS model 201 transmitter powered by a size 1035 battery (which initially incorporated a saltwater switch - the saltwater switch was eliminated

from the design in subsequent tags due to malfunction during field deployments) was used with a 34.3 cm long, rigid stainless wire antenna exiting the dorsal posterior part of the tag fairing at approximately 45 degrees. Tag 4's transmitters were potted in the silicone mold with 65 A scale durometer urethane with 0.64 cm diameter stainless steel washers imbedded in the urethane at each pin location to provide reinforcement. A urethane of this durometer was used because its material properties were more similar to those of dorsal fin tissue (Chapter 5) than the plastics typically used, thus potentially allowing the saddle to buffer transmission of dynamic loads to the tissue.

Two additional paired side mount tag designs (Tag 8 and Tag 16), were designed to allow incorporation of a satellite transmitter (Telonics ST-10) on the left side and a VHF transmitter powered by two AA cells on the right side (Figure 3.1b, c). Tag 8 was a standard flat board configuration of the ST-10 powered by two 2/3 A cells. Tag 16 consisted of a ST-10 that was custom packaged with two A cells by SirTrack, Ltd, NZ. The overall dimensions of these tags were: Tag 8; left, 18.8 cm x 7.5 x 2.0 cm, and right, 17 cm x 7.5cm x 2.0 cm, and Tag 16; left, 16.8 cm x 7.2 x 2.0 cm, and right, 17 cm x 7.5cm x 2.0 cm. The tag bodies had fineness ratios ranging from 8.4 to 9.4, however, the afterbodies were two-thirds of the maximum width in order to incorporate the batteries. A fourth pin site with two holes was incorporated into the bottom edge of the tag fairing.

All three of the production tag designs were also tested in the Kirsten wind tunnel under the same general protocol as the mockups except that dynamic pressures of 95, 190, 240, 290, 380, 480, 1200, and 1900 Pa were used. Although porpoises

Figure 3.1b. Tag 8 – Paired side mount telemetry tag. Telonics ST-10 left, ATS model 201 right.

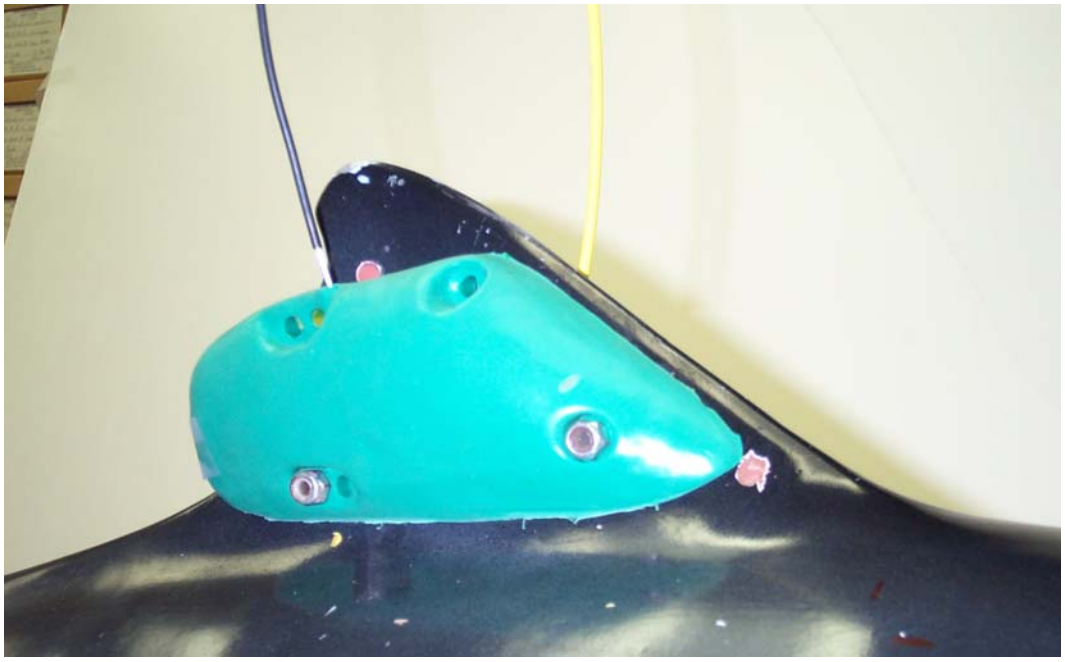

Figure 3.1c. Tag 16 – Paired side mount telemetry tag. Custom packaged Telonics ST-10 left, ATS model 201 right.

swim slower than the equivalent dynamic pressure of 95 Pa (~1.0m/s), this was the minimum dynamic pressure that the tunnel could be accurately maintained. Pitch angles used for most tests were either +4.0^o to +8.0^o with 0.5^o steps, or +5.0^o to +7.0^o with 1.0^o steps. All comparisons in the data analyses were made at 6° pitch because this level consistently yielded the lowest drag during baseline runs. Various yaw settings were used, including –10°, -8 ^{o}, -5 ^{o}, -2 ^{o}, 0 ^{o}, 2 ^{o}, 5 ^{o}, 8 ^{o}, 10 ^{o}. Analyses of the effect of yawing on tag load were conducted for all tags and limited to yaw angles of -5 ^{o}, and –10 ^{o} because conventional airfoils typically stall at about a 15° angle of attack (Fish and Rohr 1999). Determination of drag coefficients (C_D), tag loads, and proportional drag increases used the same methodologies outlined in Chapter 2.

Impact loads at the air/water interface that occur at the beginning of a dive were estimated as:

$$D_{tI} = C_{DI} q A_t \qquad (1)$$

where, $C_{DI} \cong 1$ for a streamlined tag of frontal area A_t as it impacts the water, and q is the dynamic pressure at the time of impact. Porpoises typically submerge at about 1.1 m/s (Appendix A), which is approximately equivalent to a q of 95 Pa. In order to evaluate the relative drag contribution of antennas on Tag 4, test runs were made with and without antennas. All tests were conducted at 1900 Pa with pitch angles between

-10.0^o to +10.0^o and all comparisons were made at 6° pitch and 0° yaw. Determination of drag coefficients, loads, and proportional increases in drag, followed the same approaches outlined in Chapter 2.

Results

The proportional increase in drag loads created by the mockup designs was generally very low, with seven of the eight designs only adding between approximately 1% and 5% more drag to the porpoise model (Table 3.1). The exception was mockup #5, a front mount, which added about 17% more drag to the model.

For the three production tags, the C_D generally decreased with increasing Re (Table 3.2, Figure 3.2). In a comparison of tags, Tag 4 and Tag 16 had similar C_D values while Tag 8 was slightly greater. All tags added more drag to the model with increasing velocity, particularly between 1.1 and 1.5 m/s (Table 3.3, Figure 3.3). Tag 4 generated the smallest increases, ranging from 0.13N to 1.90N and Tag 8 the greatest (range, 0.18N to 2.86N). However, the average proportional increase of these tags over the model showed that they all added substantially more drag starting at about 1.5m/s before leveling off at 2.4 m/s (Figure 3.4). The same pattern of differences between tags observed for absolute loads were reflected in a comparison of their proportional increases, but they added relatively similar amounts of drag to the model.

During the tests when the model was yawed at – 5° and –10 ^{o}, the drag loads

Table 3.2. Drag coefficients for a harbor porpoise model and three streamlined tag designs as tested in a wind tunnel. All tests were conducted at 0° yaw.

Dynamic pressure, q (Pa)		95	190	240	290	380	480	1200	1900
Simulated swim velocity (m/s)		1.1	1.5	1.7	1.9	2.2	2.4	3.8	4.8
Configuration (frontal area)									
Porpoise model (710 cm^2)	Mean	0.08	0.07	0.04	0.04	0.03	0.05	0.06	0.06
	SE	0.001	0.002	0.002	0.002	0.002	0.02	0.001	0.001
	n	9	5	6	5	5	7	6	15
Tag 4 (25.9 cm^2)	Mean	0.50	0.47	0.41	0.39	0.46	0.44	0.39	0.37
	SE	0.06	0.06	0.07	0.07	0.06	0.06	0.06	0.06
	n	5	5	4	5	5	5	5	5
Tag 8 (37.4cm^2)	Mean	0.60	0.63	0.53	0.77	0.51	0.50	0.46	0.46
	SE	0.13	0.13	0.16	0.16	0.13	0.13	0.13	0.13
	n	3	2	2	2	2	3	3	3
Tag 16 (37.0cm^2)	n=1	0.49	0.48	0.24	0.38	0.40	0.39	0.37	0.37

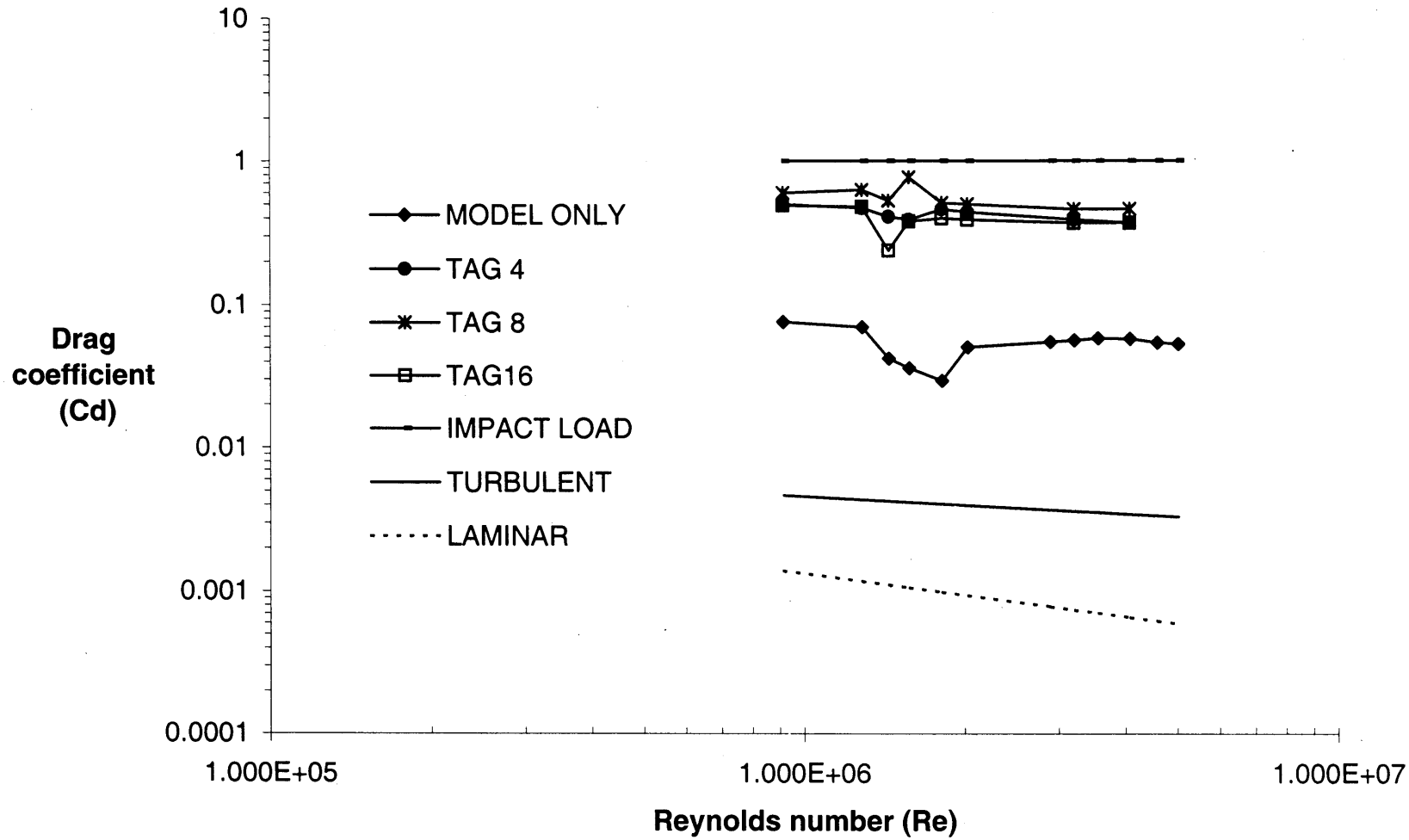

Figure 3.2. Mean drag coefficients versus mean Reynolds number for a harbor porpoise model and three streamlined telemetry tag designs in a wind tunnel. Turbulent flow line is the drag coefficient for a flat plate with a turbulent boundary layer ($C_D(\text{turbulent})=0.072Re^{-0.2}$). Laminar flow line is for a flat plate with a laminar boundary layer ($C_D(\text{laminar})=1.33Re^{-0.5}$). Drag coefficients are based on frontal area for the porpoise model and plan form area for the flat plates.

Table 3.3. Loads (N) for a harbor porpoise model and three streamlined tag designs (less model load) as tested in a wind tunnel. All tests were conducted at 0° yaw.

	Dynamic pressure, q (Pa)	95	190	240	290	380	480	1200	1900
	Simulated swim velocity (m/s)	1.1	1.5	1.7	1.9	2.2	2.4	3.8	4.8
Configuration									
Model	Mean	0.91	1.67	1.63	1.51	1.82	2.22	5.09	7.82
	SE	0.08	0.11	0.10	0.11	0.11	0.09	0.10	0.06
	n	9	5	6	5	5	7	6	15
Tag 4	Mean	0.13	0.24	0.30	0.38	0.47	0.56	1.26	1.90
	SE	0.06	0.06	0.07	0.07	0.06	0.06	0.06	0.06
	n	5	5	4	5	5	5	5	5
Tag 8	Mean	0.18	0.37	0.39	0.63	0.61	0.76	1.84	2.86
	SE	0.08	0.08	0.10	0.10	0.10	0.08	0.08	0.08
	n	3	3	2	3	3	3	3	3
Tag 16	n=1	0.16	0.29	0.41	0.46	0.56	0.67	1.54	2.26

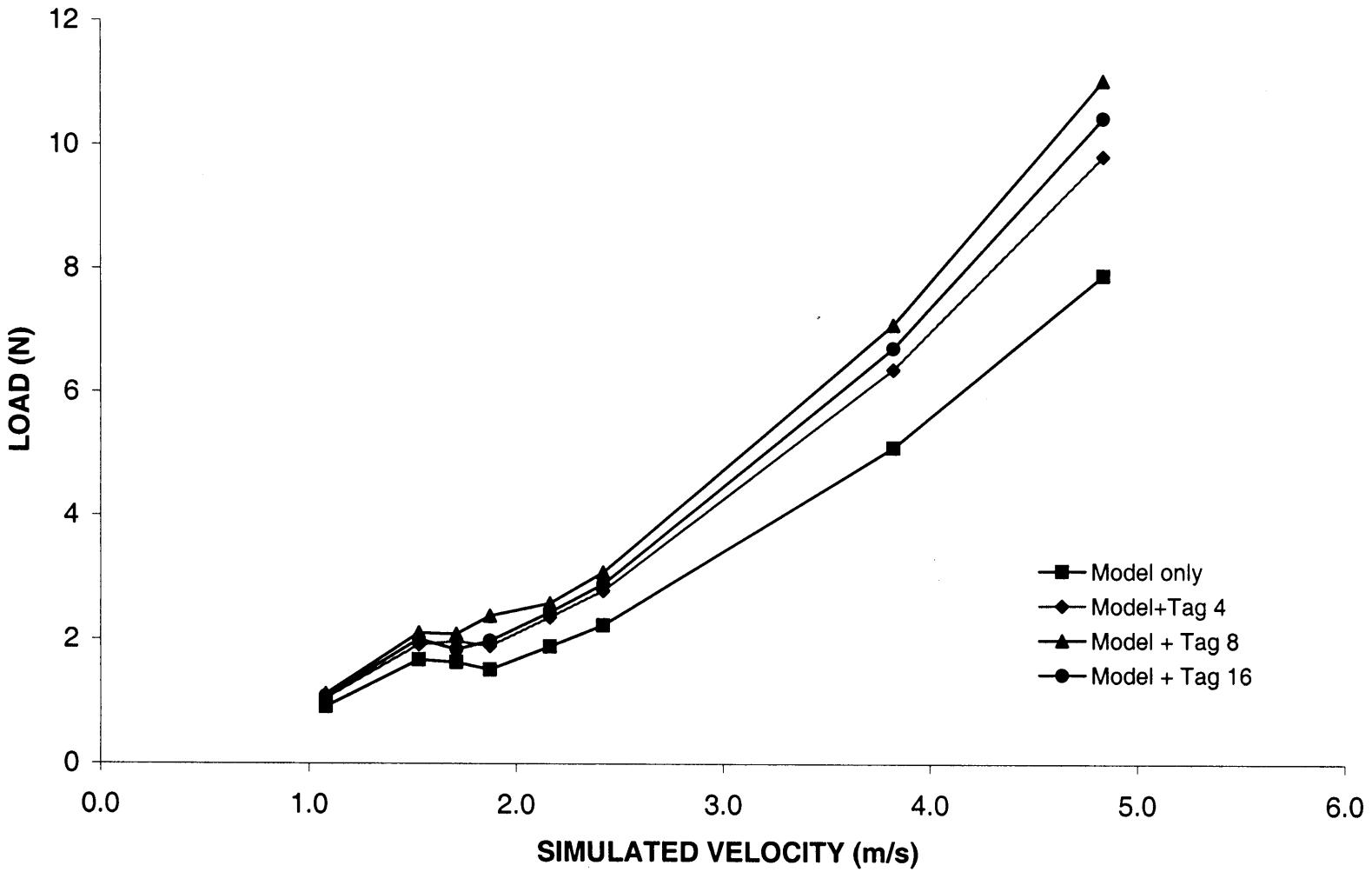

Figure 3.3. Mean drag forces (N) plotted against simulated velocity for a model harbor porpoise and three streamlined telemetry tag designs.

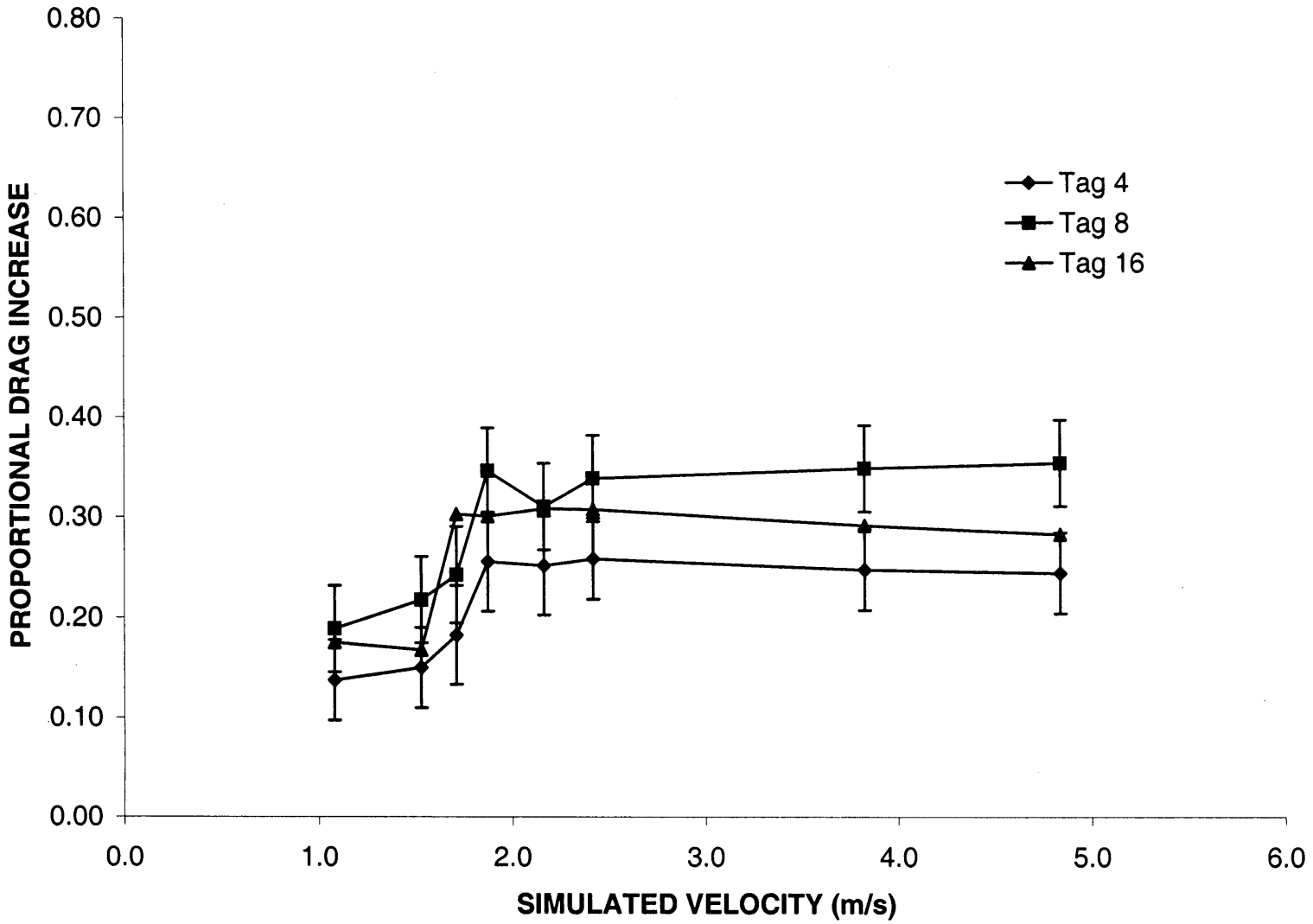

Figure 3.4. Mean proportional drag increase for three streamlined telemetry tag designs plotted against simulated velocity. Vertical bars are the CI.

that for these designs produced variable results (Table 3.4). Although Tags 4 and 16 tended to increase drag at all dynamic pressures, the reverse pattern was present for Tag 8.

For impact loads, Tag 4 was estimated to have the lowest at 0.26N, while Tag 8 and Tag 16 were higher at 0.31N, and 0.34N, respectively. Tag 4 was the only one of the three designs tested without antennas (n=2). With an average proportional increase of only 0.16 at 1900 Pa, the lack of antennas reduced the tag's drag by a third.

Discussion

This study demonstrated that by incorporating some basic fluid-dynamic principles into the designs of telemetry tags for small cetaceans, the drag tags generate could be substantially reduced. Tag 4 had less drag than both the front mount (Tag 2, Chapter 2) and single side mount (Tag 3, Chapter 2), while Tag 8 was similar to Tag 2, and Tag 16 was similar to Tag 3. Despite the presence of two transmitters for both Tag 4 and 16, theses tags generated about the same drag as Tag 3 with its rectangular shaped single transmitter. Consequently, it is expected that a single side of Tag 4 or 16 would produce about half the drag of Tag 3. This difference is of note because single sides of Tag 4 and 16 have volumes similar to Tag 3.

The drag performance of this paired design compares favorably with a similar optimized design (see Bannasch 1996). The tag designs in both studies are somewhat similar (a pair of elongated, half-body teardrop) except that the tags in that study are

Table 3.4. Loads (N) from a harbor porpoise model and three streamlined tag designs (less model load) as tested in a wind tunnel at 0°, -5°, and –10° yaw.

	Dynamic pressure, q (Pa)	95	380	1900
	Simulated swim velocity (m/s)	1.1	2.2	4.8
Configuration	Yaw angle			
Model only	0°	0.91	1.82	7.82
	-5°	1.09	2.46	11.1
	–10°	1.58	4.75	20.6
Tag 4	0°	0.13	0.47	1.90
	-5°	0.17	0.62	2.14
	–10°	0.15	0.51	2.13
Tag 8	0°	0.18	0.61	2.86
	-5°	0.20	0.53	2.14
	–10°	0.17	0.46	2.31
Tag 16	0°	0.16	0.56	2.26
	-5°	0.17	0.57	2.63
	–10°	0.18	0.70	3.42

larger and extend anterior and posterior of the harbor porpoise dorsal fin in order to contain transmitter components. Interestingly, the tag in that study added proportionally more drag at lower velocities, 31% at 1.0 m/s, before decreasing to 17-18% at velocities of 1.5 m/s and greater. This pattern is the opposite of the sharp increase observed at 1.9 m/s in this study. Reasons for the differences between studies in the patterns of drag increase between the two tag designs are unclear. However, a direct comparison is confounded because the porpoise model used by Bannasch (1996) lacked pectoral fins and flukes and was smaller (1.23m) than the model in the present study. It was noted by Yasui (1980) that the flippers and flukes of a harbor porpoise contribute 18.0% and 13.4%, respectively, to its drag. Consequently, the Bannasch (1996) tag may actually contribute proportionally less to a larger, “complete” animal. However, it is important to note that this tag lacked any antennas, likely reducing drag substantially. In addition, because the tag in that study extended well beyond front and back of the fin, it is likely that it would create a substantial bending moment during turns.

Although the reliability of the mockup test results are limited due to the small number of trials, the limited dynamic pressures used, and the small loads obtained relative to drag balance resolution (Chapter 2), these results suggest that additional reductions in tag drag are still possible. The primary differences between the mockups and production tags were the lack of pin hole recesses, and a lack of antennas. Based on the test of Tag 4, with and without antennas, it is apparent that over a third of the drag on this more streamlined design is contributed by the antennas, compared to

about 7% for previously tested tags (Chapter 2). While antennas are typically of small diameter, their cylindrical shapes exhibit poor hydrodynamic performance (Hoerner 1965, Vogel 1994). Therefore, modifying the antenna to a more streamlined shape should be investigated, with special attention to ensuring that signal transmission quality is not degraded.

The other primary approach to drag reduction that is likely to be productive is reducing tag size. Although satellite transmitter components will not currently fit the fairing of Tag 4, they may in the future as miniaturization of these parts occurs. The potential for long-term attachments of small tags on dolphins and porpoises is evident from documentation of several, documented long attachment durations of disk and roto tags (see Scott et al. 1990). The success of these tag designs likely lies in their optimized fineness ratio. It was appropriately noted at the time the roto tag technique was described that these small tags have little “hydrodynamically induced strain” (Norris and Pryor 1970). The challenge of tag size reduction lies in the miniaturization of transmitter components, more efficient power use (reliable saltwater switches and duty cycles), and more efficient packaging of the components and attachment system. Although it has been suggested that tag size reduction will be important to advancing this technique (Stone et al. 1998), improving tag attachment longevities will also require a thorough evaluation the factors influencing the problem. By defining the problem in terms of what the tags actually are (percutaneous devices experiencing dynamic loads in an aquatic environment), the issue becomes more tractable. For percutaneous devices, tissue degeneration can be expected to occur at

these sites from: 1) a foreign body response due to the interaction of the pinning material and adjacent tissue (von Recum and Park 1981, Geraci and Smith 1990); 2) an infection due to bacterial invasion of the wound (von Recum and Park 1981, Geraci and Smith 1990); 3) pressure necrosis, due to chronic stress concentrations which occlude blood flow (Mak et. al 1994); or 4) mechanical stresses disrupting the healing process (von Recum and Park 1981, Geraci and Smith 1990).

Biocompatibilty of the pinning materials with marine mammal skin has been examined in implant studies conducted on captive animals (Geraci and Smith 1990). The observation that none of the test materials were readily accepted may stem from the constant exposure of the open wounds to the non-sterile aquatic environment, allowing an infection to develop (Geraci and Smith 1990). Although stainless steel was the most readily rejected material in this implant study, it yielded one of the longest attachment durations recorded for cetaceans when used for pins with a killer whale tag (4.5 months, Erickson 1978). In addition, infections associated with pin out-migrations have typically not been observed (Irvine et al. 1982, Martin and da Silva 1998). These results suggest that tissue structure response to loading stress may be of greater influence on tag retention than pin biocompatibility or infection. However, the extent to which reducing these loads, by minimizing tag drag, might increase attachment duration remains unclear. While pressure necrosis has been suggested as the source of tag loss in some previous studies (Brill and Friedl 1993, Mate et al. 1995) it is unknown if the pressure that these, or any other recently deployed tags cause, were sufficient to occlude blood flow. The stress distribution within the fin due

to the drag caused by the tag will be a function of the structural composition of the tissue and the attachment scheme's load distribution in the tissue, which is dependent on the position of the tag on the fin and the number, diameter, and location of pins. Because the dorsal fin tissue is not as strong as the pins and tag saddles typically used in attachments, stress concentrations in the tissue are likely to form due to a mismatch in material properties. The flexibility of the urethane fairing used in the present study may be beneficial in reducing stress concentrations.

An additional level of complexity results from frequent changes in velocity and direction while swimming, and from surfacing to breathe. As a result, the loads and associated vectors will be dynamic, possibly disrupting the healing process in the dorsal fin tissue (von Recum and Park 1981). The loads developed by tags in this study between different yaw angles and estimated for impact at the water surface would be similar to those associated with dynamic loads. Similar to the yaw results from Chapter 2, there were no consistent patterns associated with increasing angle of attack. The substantial amount of variability observed likely stems from the model body dominating the flow regime (Chapter 2). A more accurate estimate of the drag developed by these tags during turns would likely be obtained from mounting the tags on fin-only models in a smaller tunnel with a more sensitive drag balance. The other dynamic load is that associated with the tag impacting the water surface when the animal submerges after breathing. The estimates of impact loads suggest that Tag 4 generates less drag than any of the previously tested tags, while Tags 8 and 16 are about the same as the single side mount (Chapter 2). However, it is important to note

that while the assumption for the value of the C_{DI} used is likely in the range of valid values, its accuracy is unknown. Impact of the tags at the air/water interface will certainly generate greater loads than those that occur during submerged swimming. Therefore, the estimate of a C_{DI} of 1, which is approximately double the C_D of these tags during submerged swim drag, appears reasonable. However, the complexity of the frontal shapes of the tags that actually impact the water surface may exceed the capability of some of the complex theoretical models (see Gollwitzer and Petereson 1996, Xu et al. 1999). Consequently, accurate impact estimates will likely be most readily obtained through empirical tests.

Drag measurements obtained from a model or an animal in the glide position represent simplified estimates of the loads the tissue likely actually experiences. Consequently, these analyses are likely of only limited application in understanding the stresses generated in the tissues. Modeling the stress distribution in the fin using a finite element analysis (FEA) during the surfacing/diving cycle, which incorporates loads estimates from wind tunnel tests over typical swim velocities determined from time-depth recorder data will be an important step in better understanding the roles of factors suspected to influence tag attachment longevity (Chapter 6). This approach will require determining the structurally important tissue layers in the dorsal fin and quantifying their strength. While FEA studies will be important in evaluating some of the features incorporated in this design, others can only be evaluated in field deployments with a dedicated resighting effort.

CHAPTER 4

AN ANALYSIS OF THE STRUCTURE OF THE HARBOR PORPOISE DORSAL FIN IN RELATION TO TELEMETRY TAG ATTACHMENTS

Introduction

The anatomical structure of the dorsal fin of small cetaceans has only received limited attention and as such, no comprehensive analyses have been conducted. As a result, no common terminology has been used to describe the discrete layers that have been observed. The earliest examination described the basic structural components as the skin, a ligamentous layer, and a central core of fibrous tissue (Fraser 1952). Subsequent studies have only discussed the fin's structural makeup as an aside to consideration of the structure of skin (Sokolov 1982), or in comparison to the flukes (Felts 1966, Green 1972, Simpson and Gardner 1972). While the role of the vascularization in dorsal fins has been noted for thermoregulation of the reproductive organs (Rommel et al. 1992, 1993), it has only been recently described and considered relative to dorsal fin tag attachment (Scott et al. in prep.). Despite using the fin as an attachment site for telemetry tags, none of the tagging studies to date have provided more than cursory consideration of fin composition, potential load bearing qualities, or the potential adverse affect of attachments.

A detailed examination of the harbor porpoise dorsal fin was undertaken in the context of the typical attachment of telemetry devices. Consequently, the focus was primarily on those components in those regions that contribute to the structural

integrity of the fin. In this study, the gross structural features within the fin were identified, described, and measured.

Methods and Materials

Eighteen adult harbor porpoise dorsal fins of similar size (approximately 10 cm high and 23 cm long along the base at the insertion point to the body), collected from both fresh and frozen stranded animals, were examined (Table 4.1). Primary collagen fiber orientation was made from a macroscopic examination of seven of these fins. For one of the fins, which was fresh and still attached to the body, the fiber orientation of the distinct layers was determined by dissecting away each distinct, successive layer and directly measuring the fiber angle with a compass. For the six other fins the angle was measured relative to the base cut during processing for material property testing (see Chapter 5).

Table 4.1. Number of harbor porpoise dorsal fins used by analysis type.

Analysis	Frozen fins	Fresh fins
Collagen fiber angle	6	1
Histological analysis	4	1
Vasculature analysis	6	0

Five of the 18 fins, four frozen, one fresh, which had also been removed at the basal insertion point, were cut into approximately 3 mm thick sections parallel to the base of the fin and fixed in formalin for histological analysis of the tissue layers. Two levels of tissue sections, which corresponded to approximate levels where pins typically attach the tags to the dorsal fin (approximately 2 cm and 6 cm dorsal to the base), were processed. Tissues from these sections were cut into six micron thick slices and stained with Mallory's aniline blue stain to identify collagen (Thompson and Hunt 1966) (Appendix B), and with Verhoeff elastic stain to identify elastin (Carson 1997) (Appendix C). Two slides, which were at least 2.5 cm posterior to the leading edge from the base level, were used to measure tissue layer thickness and percent collagen composition. One slide was processed from the upper level of two of the fins for these analyses. For one of the fins, a slide was made of the leading and trailing edge at the base level for examination of changes in tissue layer thickness. The terminology used in previous studies to describe tissue layers of the dorsal fin has varied. In this study, the epidermis and dermis follow descriptions and terms used by Sokolov (1982). Although the subpapillary layer of the dermis was described by Sokolov (1982) as a general feature of cetacean skin, it has not been previously described in the dorsal fin. The term "ligamentous sheath" was used by Felts (1966) and is suggested to be the best descriptor compared to the other terms used: "ligamentous fibers" (Fraser 1952); "tendon layer" (Sokolov 1982); "radiating fiber" (Purves 1969); and "collagen fiber bundles" (Simpson 1972). The use of "central core" tissue follows Purves (1969). Other terms for this tissue include: "fibrous core"

(Fraser 1952); “core material” (Felts 1966); and “median layer” (Sokolov 1982). The lateral thickness of the epidermis and dermal papillae, subpapillary layer, and ligamentous sheath were measured for each of these tissue layers at the end of each corner of the slide with an ocular micrometer (to the nearest 0.1 mm) under a dissecting microscope (magnification 10x). Tissue thicknesses are summarized as the mean and standard error.

Collagen density was measured for the ligamentous sheath and the central core from cross-sectonal slides by capturing the slide image with a digital microscope camera (Polariod DMC-1) mounted on a microscope (Leica MZ 8), interfaced to a PC, using the percent area determination feature of an imaging software package (Optimus 6.51, see Appendix D). Collagen composition in the ligamentous sheath and central core was compared using a paired t-test (Splus). The variances of the percent collagen values were estimated within and between slides, and between animals, with the VARCOMP function of Splus.

The other six adult harbor porpoise fins were used to determine the spacing of the primary vascular trunks (periarterial venous rete (PAVR), and superficial veins (SV), Pabst et al. 1999). Each fin was cut in a horizontal plane at the approximate level of the anterior ventral tag attachment pin (20 mm above the base of the fin) and the distance from the leading edge of the fin to each PAVR and SV was measured to the nearest 0.5 mm with a ruler. The number of veins per artery for each PAVR was counted from the same slides used for the tissue thickness and percent collagen analyses.

Results

Based on all the examination approaches, the dorsal fin appears to be comprised of two tissue layers with five distinct regions (Figures 4.1, 4.2). The outermost layer is the epidermis, which includes three components (stratum germinativum, stratum spinosum, and stratum corneum). The underlying layer is the dermis, composed of the dermal papillae, the subpapillary layer, the ligamentous sheath, and the central core. The thickness of the epidermis and dermal papillae of the dermis at the base level (2 cm above insertion to body) was slightly thicker than at the upper level (6 cm above insertion to body) (Table 4.2). The dermal papillae were observed to occur in rows that were generally parallel to the body axis near the base level but at the upper level they appeared to be oriented at an angle of about 25° in the posterior-anterior plane relative to the posterior end of the fin. The inside of the dermal papillae are lined with some collagen and elastin fibers, as well as capillary vascularization.

Adjacent to the papillae is a very thin (0.1 mm, at both the base and upper levels) layer of interwoven collagen and elastin fibers. Fibers from this subpapillary layer extend distally to line the papillary walls and proximally between the ligamentous sheath bundles to join with the diffuse collagen bundle plexus of the central core tissue. The collagen and elastin fibers of the subpapillary layer are also oriented parallel to the dermal papillae rows when directly adjacent to that structure,

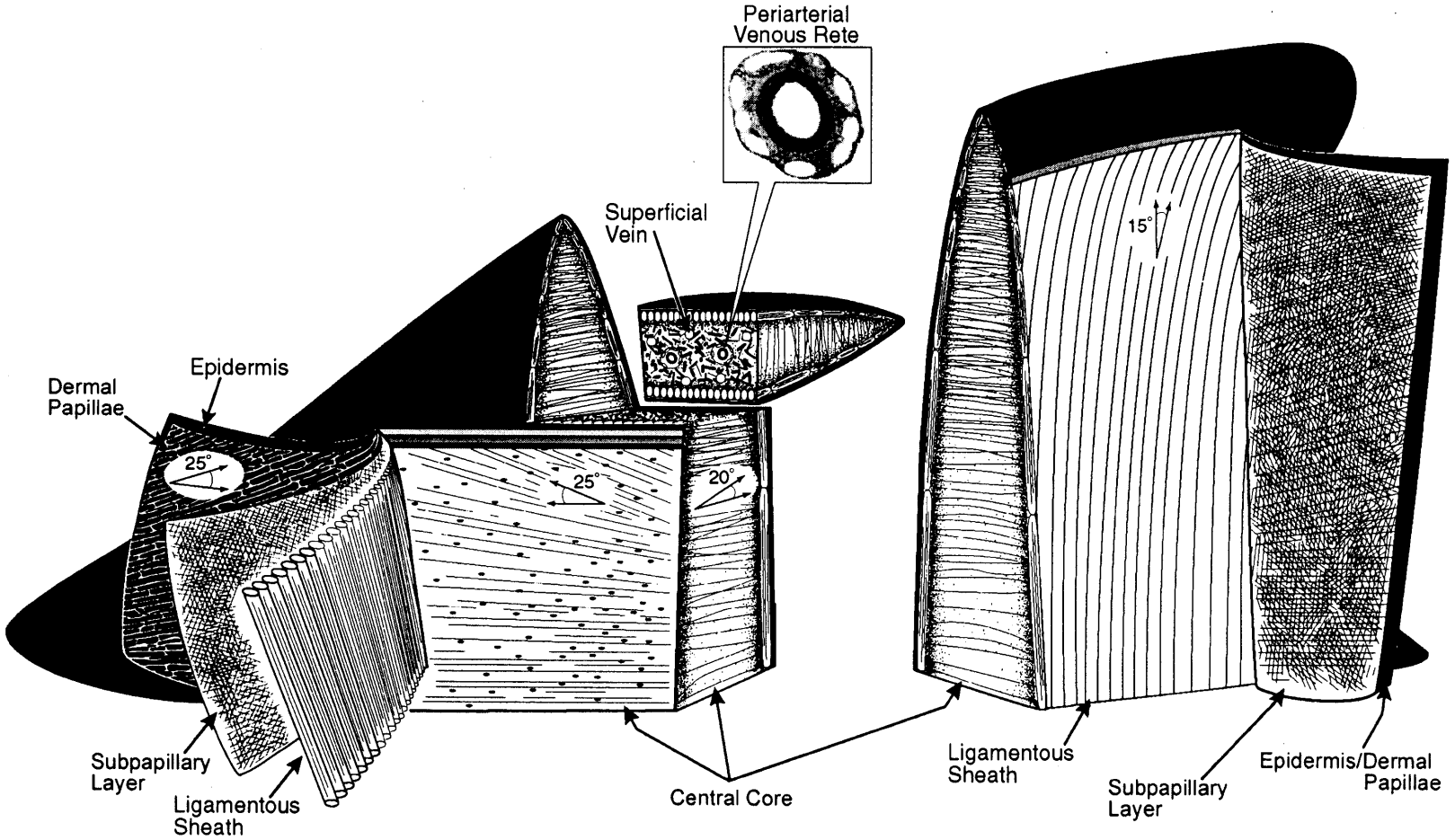

Figure 4.1. Major tissue types and features of the harbor porpoise dorsal fin. The outermost layer is the epidermis and the inner dermal layer consists of (from outside to inside) dermal papillae, subpapillary layer, ligamentous sheath, and central core. Angles indicate typical fiber or feature orientation. The prominent vascularization includes the periarterial venous retes and superficial viens.

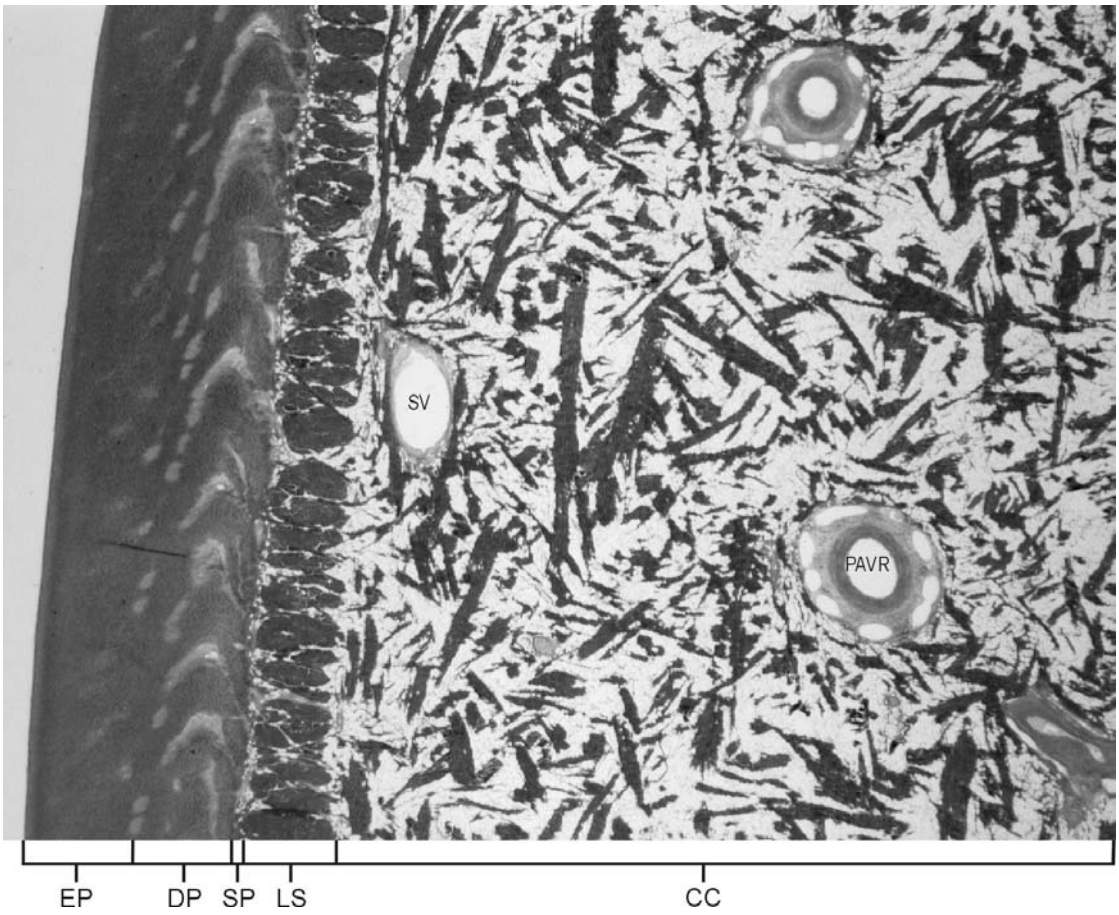

Figure 4.2a. Photomicrograph of a horizontal section from the medial region of a harbor porpoise dorsal fin. Section is approximately 2 cm above its insertion to the body. The distinction between the epidermis (EP) and the dermis is at the dermal papillae (DP). The subpapillary (SP) layer is the very thin region of fine collagen and elastin fibers adjacent to the ligamentous sheath (LS). The central core (CC) is present to the right of the ligamentous sheath. This region also contains a periarterial venous rete (PAVR) and superficial vein (SV). Original magnification 10x.

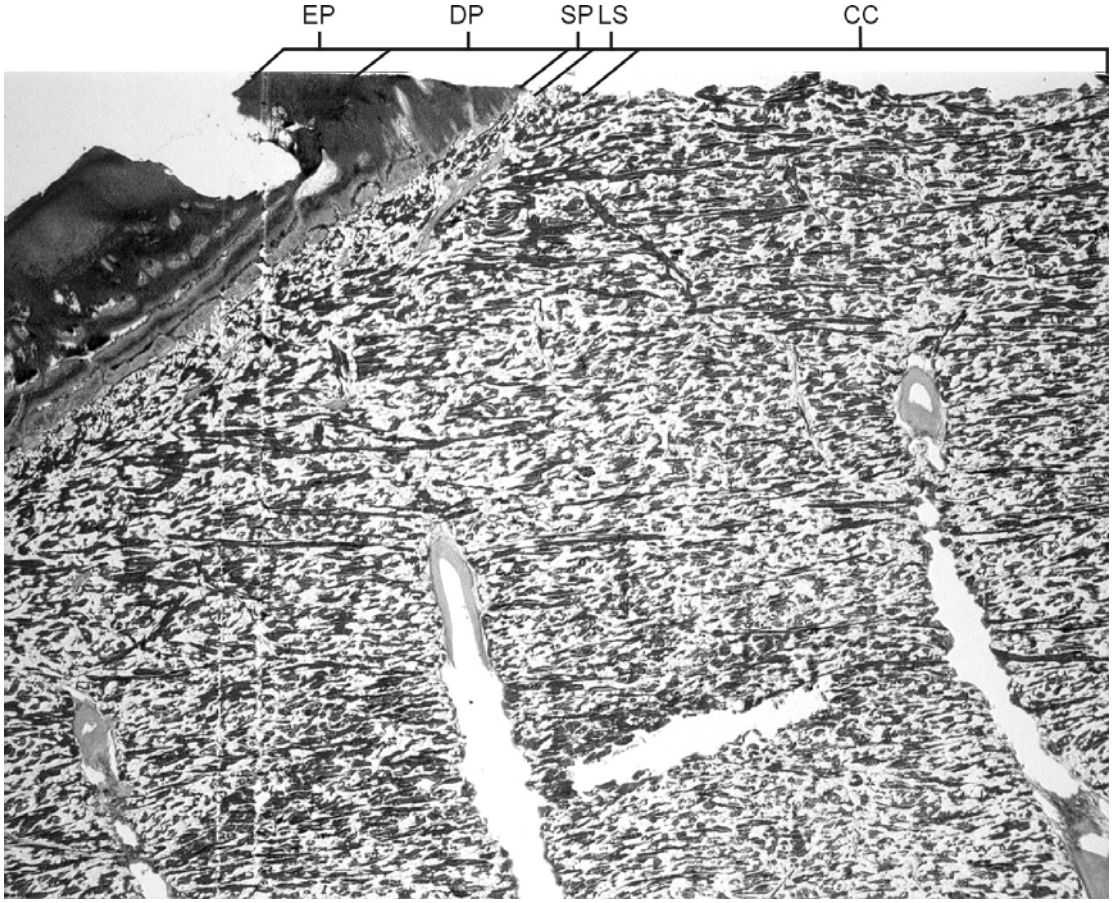

Figure 4.2b. Photomicrograph of a sagittal section of harbor porpoise dorsal fin tissue as viewed from the left side. Region is approximately 2 cm above its insertion to the body, near the leading edge. Tissue features are marked using previously defined symbols. Anterior end of fin on the left. Original magnification 6.3x.

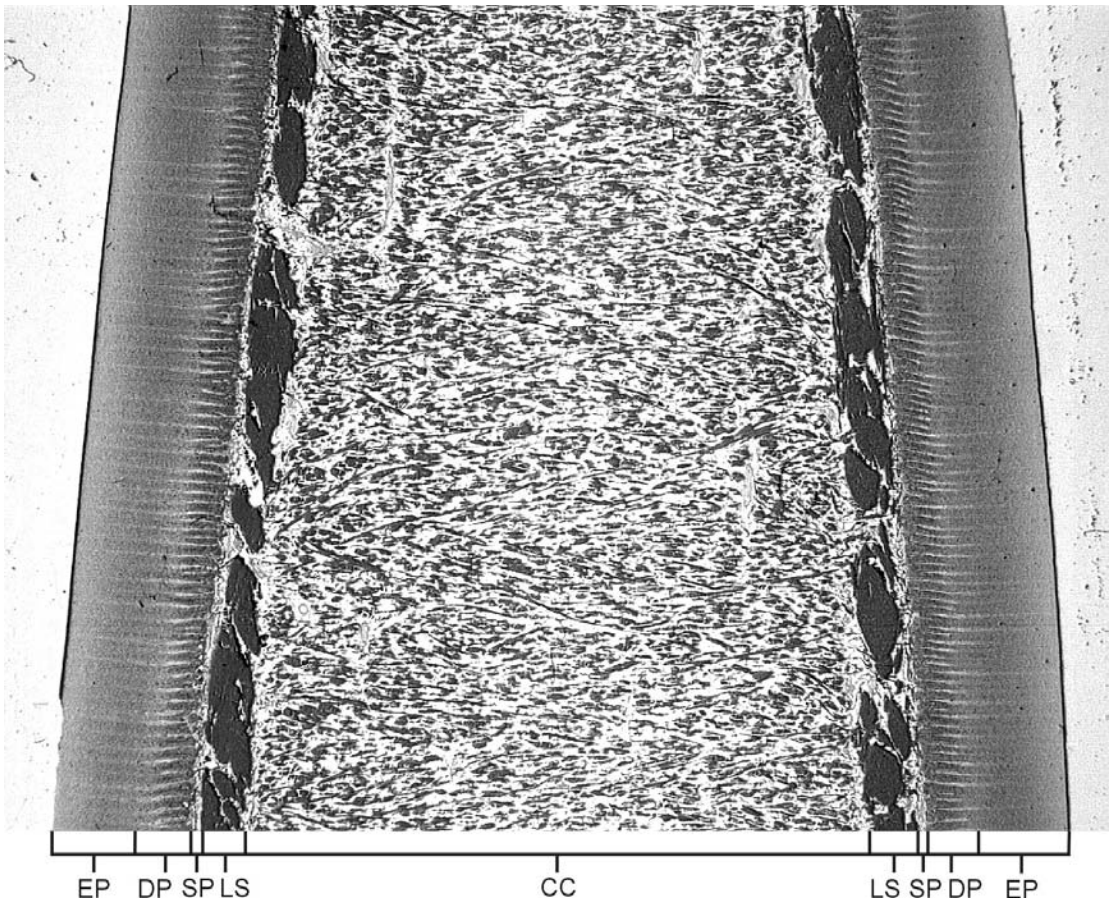

Figure 4.2c. Photomicrograph of a harbor porpoise dorsal fin from a frontal perspective. Region includes area approximately 2 cm above its insertion to the body. Tissue features are marked using previously defined symbols. Note shallow angle ($<20^{o}$) of horizontal fibers. Original magnification 6.3x.

Table 4.2. Thickness of harbor porpoise dorsal fin tissue layers.

Tissue	Lateral thickness (mm)
Epidermis/dermal papillae	
base [a]	3.2 ± 0.2
upper [b]	2.9 ± 0.4
Subpapillary layer	
base [a]	0.1
upper [b]	0.1
Ligamentous sheath	
base [a]	1.1 ± 0.1
upper [b]	0.9 ± 0.2

Values are means± SE. [a] 2 cm above insertion to body [b] 6 cm above insertion to body

but gradually fiber alignment changes to orient parallel to the fibers of the ligamentous sheath bundles (Figure 4.3).

The ligamentous sheath lies beneath the subpapillary layer. It is composed of relatively large diameter, dense, collagen bundles, which are round or oval and form a sheath vertically at the base, sweeping posterior to an angle of approximately 15° relative to vertical, near the tip. This layer is slightly thicker at the base level than it was at the upper level. However, differences in this layer between the base and upper level were apparent from the shape of the bundles and collagen composition. It appeared that the bundles were rounder at the upper level and that the collagen density was higher (Table 4.3). However, in the anterior-posterior plane at the base level, the organization of this layer became less distinct near the anterior and posterior regions. The fiber diameter was 0.5 mm near the leading edge and although the bundle

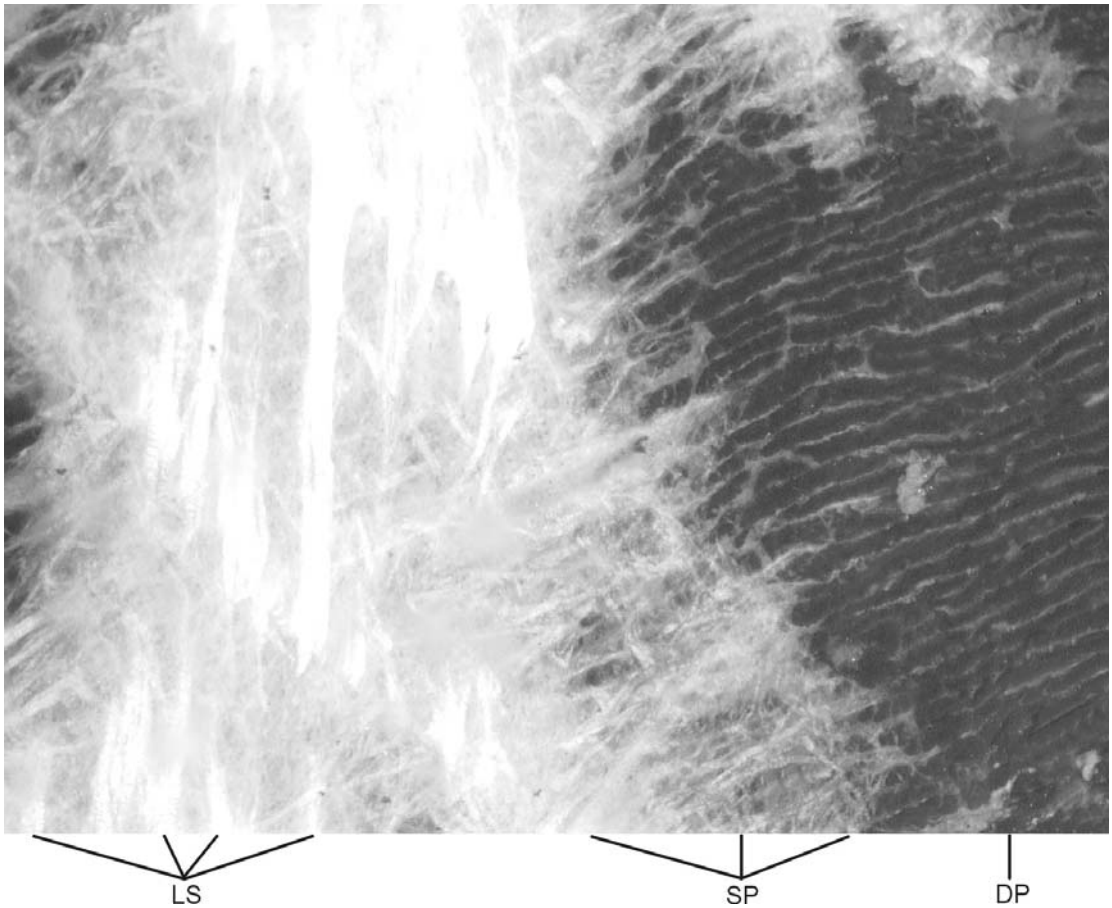

Figure 4.3. Photomicrograph of the fiber orientation of the ligamentous sheath and subpapillary layer. Collagen and elastin fibers line the horizontal rows of dermal pegs visible in the background and the collagen fibers are gradually reoriented to align with those of the vertically arranged ligamentous sheath. Original magnification 20x.

Table 4.3. Percent collagen fiber composition of harbor porpoise dorsal fin tissue layers.

Tissue	Percent collagen	Variance		
		Within slide	Between slide	Between animal
Ligamentous sheath				
base [a]	77.4 ± 3.2	10.2	15.4	41.6
upper [b]	87.4 ± 5.3			
Central core				
base [a]	48.3 ± 4.3*	10.6	24.1	78.2
upper [b]	69.7 ± 8.0			

Values are means± SE. [a] 2 cm above insertion to body [b] 6 cm above insertion to body * P< 0.05 vs. ligamentous sheath, base level.

structure remained distinct near the trailing edge of the fin, the 0.5 mm fiber diameter was similar to the leading edge. Proximal to the ligamentous layer is the central core tissue. It is comprised of an aggregation of collagen fibers, lipid cells, and the major vasculature. Due to the presence of the lipid cells there was a significantly lower percentage of collagen fibers in this layer at this level than for the ligamentous sheath ($t=2.77$, $p=0.002$). Although the cross section in the horizontal plane appears to show little organization in fiber orientation, many of these fibers were oriented at right angles to the ligamentous sheath, in both the sagittal and frontal planes. In general, all these fibers appear to be flattened or oval in cross-section. The anterior/posterior-oriented fibers are more numerous distally. They appear to originate caudally and extend forward parallel to the body axis at the base of the fin, gradually increasing to an angle of approximately 25° degrees near the leading edge in the upper portion of the fin. This fiber orientation appears to run approximately parallel to the alignment of the rows of the dermal pegs. The laterally oriented fibers are generally arranged at

angles less than 20° relative to the base as measured from either side of the base of the fin. At the upper level, the central core had substantially greater collagen density and the lateral fiber orientation predominated the fiber pattern, indicating a much lower fiber angle.

Both major types of blood trunks: the periarterial venous rete (PAVR); and superficial veins (SV), appear to have a substantial amount of collagen reinforcement. The PAVR, with an average of eight veins per artery to provide countercurrent heat exchange, were generally located medially in the central core. The SV, which return peripherally routed blood to the body core, were located near the ligamentous sheath interface. Both types of vascularization were observed to rise vertically and sweep back at angles that parallel the fibers of the ligamentous sheath. Although the first small PAVR occurred at 7.5 mm to 32 mm posterior to the leading edge of the fin, the distances to the arteries with medium to large diameters were 25 mm to 83 mm from the leading edge. The average spacing between PAVR varied substantially between fins ranging from 7.4 mm to 13.1 mm. Similarly, the spacing between SV ranged from 6.7 mm to 10.2 mm for the fins. Considered together, the spacing between both PAVR and SV ranged from 3.5 to 5.4 mm.

Discussion

Structural components

The tissue layers in the dorsal fin are unique compared with typical cetacean skin. Sokolov (1982) describes two primary layers: the epidermis and the dermis (which includes subcutaneous fat). Although the subpapillary layer, ligamentous sheath and central core tissue of the dorsal fin are all components of the dermal layer they are highly modified and should be considered a subgroup of "specialized connective tissue" following the classification terminology of Ross and Reith (1985). The subpapillary layer, which is interwoven with collagen and elastin fibers and lines the walls of the dermal papillae, appears to tie the epidermis to the central core tissue because fibers from this layer also pass between the ligamentous sheath bundles and connect with the central core tissue. The ligamentous sheath layer is unique to the dorsal fin, flukes, and pectoral fins of cetaceans and is not found in other regions of the body. The central core appears to be a modified subcutaneous fat layer in that it is composed of adipose cells surrounded by nearly an equal percentage by collagen fibers. However, in the dorsal fin these collagen fibers are larger in diameter and more densely concentrated than those found in typical adipose tissue.

Functional morphology

In addition to serving as a thermoregulatory device, the dorsal fin also serves as a hydrofoil, which acts as a stabilizer (Fish and Rohr 1999). During turns, it

generates lift, a force perpendicular to the direction of motion (Webb 1975). As a result, the fin needs to be resistant to deformation from loads applied from either side. The loads applied to a fin during turns are likely to be similar to a beam subjected to a bending moment. The arrangement of two ligamentous sheaths of large diameter, dense collagen bundles lateral to the central core would be very resistant to elongation (Wainwright et al. 1982). Consequently, this design is ideal for minimizing deformation from these types of loads. These layers would support the most stress in pure tension of any tissue within the fin when subjected to perpendicular loads associated with turning. In addition, the lateral orientation of the oval shape of the ligamentous sheath bundles would be more resistant to a bending moment than a round shaped bundle (Wainwright et al. 1982). The importance of the ligamentous layers in resisting lateral pressure on the dorsal fin was recognized early on (Fraser 1952), as was a homologous structure in the flukes (Felts 1966, Purves 1969). The fiber matrix of the central core might be expected to provide only limited support to perpendicular loads, but the very low angles of the lateral fibers are likely to constrain deformation (Wainwright et al. 1982). Additionally, the higher proportion of collagen in the upper portion of the fin and the lower lateral fiber angle would be expected to increase resistance to deformation in that region. It had been previously noted that some of the fibers of the central core run at right angles to the ligamentous layer (Fraser 1952). The pattern was also observed in the present study and many of the fibers in the central core were also observed to run at right angles to each other. Arrangements of these elements in this pattern will increase the rigidity of the overall

structure (Wainwright et al. 1982). The presence of numerous, widely distributed, vertically oriented, vascular bundles, which are composed primarily of collagen and elastin, may provide reinforcement to the central core. The Young's moduli for the tissue layers would be expected to reflect the properties of these structural differences. The material property testing confirms this relationship (see Chapter 5).

Potential tag attachment effects

The pins that attach a tag to the dorsal fin are percutaneous devices that perforate all the layers of the dorsal fin, creating a pathological condition in fin tissues. In addition, these pins will likely subject the fin to loads that it did not evolve to support. Both compressive and tensile loads are possible on each tissue layer, depending on the tag/attachment configuration and load vectors. Although the round shape of the pins will minimize stress concentrations (Wainwright et al. 1982), these are expected to develop around perforations (Özkaya and Nordin 1999), particularly because of the likely mismatch in material properties between the soft tissues and the more rigid pins. However, soft tissues do have the advantage of being more resistant to tearing or fracturing than stiffer materials due to their ability to stretch (Vincent 1982) under extreme loads. In addition, the composite structure of the fin will lend itself to stopping the spread of cracks (Alexander 1975, Harris 1980, Wainwright et al. 1982). However, dynamic loads at the pin sites may increase the potential for failures to occur. Consequently, the complexity of predicting the effect of various loads on any specific tissue layer will require a more sophisticated evaluation of these factors.

The most appropriate approach would be the use of a finite element model, which can incorporate several factors simultaneously.

Limitations

Several factors in the methods or analyses of this study may influence the observed results. Although there was a significant difference between the collagen density in the ligamentous sheath and central core, it is important to note that this analysis was based on a relatively small sample. The increasing trend in variances from within slide, between slide, and between animals associated with the percent collagen estimates of both the ligamentous sheath and central core indicates that fewer sampling sites per slide could be used but that more slides per animal, and particularly, more animals should be sampled. Although the observed differences between slides and individuals could be real, it is possible that this variability could have been introduced from factors inherent to the methodology. Although it was attempted to select the same relative height in the fin for the histological slides, the fins were of slightly different sizes and profile shapes. There also may be differences associated with sex or age. Although harbor porpoises are not sexually dimorphic, females are generally slightly larger than males (Read 1999). Differences in dorsal fin morphology between the two sexes may exist but could not discerned. Specimen material came from both stranded and gillnet caught individuals. Specimen condition at the time of collection was variable and some degree of decomposition may have occurred in the stranded specimens. Most specimens were frozen and some had been

stored for up to ten years. All but one specimen used in the histological analysis was frozen and thawed prior to being fixed in formalin. It is evident that the tissues from frozen specimens had a greater tendency for the collagen fibers to tear and stack up, potentially causing the collagen percentage to be underestimated. In addition, stain absorption, which may be a function of tissue condition, could affect color saturation.

This investigation has identified and quantified the dimensions of the primary structural components of the harbor porpoise dorsal fin. Additional gross and histological analyses with larger samples may allow for the identification of more subtle structural features. The tissue layers identified from this analysis will guide further work to determine the material properties of these layers (see Chapter 5). In addition, this study will serve as a basis for the geometry of a finite element model which can be used to quantitatively evaluate the stresses generated by different tag design/attachment schemes (Chapter 6).

CHAPTER 5

MATERIAL PROPERTIES OF THE TISSUE LAYERS OF THE HARBOR PORPOISE DORSAL FIN: IMPLICATIONS FOR TAGGING

Introduction

The dorsal fin of small cetaceans, including harbor porpoises, has typically been the site used to attach telemetry devices for tracking the movements of these animals. However, telemetry devices generate additional forces from static and dynamic loads (Chapter 2, 3), which are transferred to the tissue layers adjacent to the attachment pin sites. Tissue breakdown has been commonly observed at the pin sites and is thought to be, at least in part, related to these additional loads (Irvine et al. 1982, Tanaka et al. 1987, Scott et al. 1990). As part of a comprehensive assessment of the effects of tag generated forces on the dorsal fin, loads generated by the tags were quantified (Chapters 2, 3), fin tissue structure was defined (Chapter 4), and the strength of fin tissues needed to be determined (this chapter). All of these data are required for incorporation into a finite element model (Chapter 6).

The structural response of fin tissues to tag-generated loads will be a function of their mechanical load bearing properties. A material property of a tissue can be defined as its ability to resist deformation from an externally applied force (Nigg et al. 2000). Many biological tissues are considered composite materials because they are comprised of various combinations of collagen, elastin, ground substance (protein-based macromolecules and bound water), and water. The material properties of a

composite will depend on the properties and proportions of their constituents, as well as their arrangement (Harris 1980). The greatest insight to their strength characteristics can be achieved by quantifying the stress/strain relationship of the unique structural components. Based on the composition and arrangement of components, five distinct tissue types were identified in the harbor porpoise dorsal fin; the epidermis, dermal papillae, subpapillary layer, ligamentous sheath, and central core (Chapter 4), and each might be expected to possess different material properties.

The cetacean epidermis is 10 to 20 times thicker than in terrestrial mammals (Sokolov 1982) and is comprised of epithelial cells and melanocytes, which are connected to the dermis by hemidesmosomes on the basement membrane and to each other by desmosomes (Geraci et al. 1986). The outer region of the epidermis is dominated by rows of cells up to 50 layers deep (Geraci et al. 1986), which are gradually flattening and are enroute to being exfoliated.

Because the dorsal fin lacks skeletal support, its structural integrity is derived primarily from fibrous connective tissue (Fraser 1952, Chapter 4). The fibrous connective tissue is located in the subpapillary layer, ligamentous sheath, and central core. The primary structural component of this fibrous connective tissue is collagen (Parry and Craig 1980). The small amount of elastin present is confined to the subpapillary layer (Chapter 4). The ligamentous sheath is comprised of relatively large bundles of individual collagen fibers (Chapter 4). The central core is also primarily comprised of collagen bundles, but of a smaller diameter than those found in the ligamentous sheath, in addition to a substantial number of lipid cells. Collagen

bundles are made up of individual collagen fibers. Individual collagen fibers were observed in the subpapillary layer (Chapter 4). The collagen fibers are in turn composed of bundles of fibrils. These fibrils vary in thickness and a characteristic of their structure is their wavy appearance, commonly called crimp, with a periodicity of 64nm (Wainwright et al. 1982). This crimped structure dictates that when collagen is subjected to a tensile load, the initial elongation that occurs is due to the removal of the crimp, which requires relatively little force. However, once the crimp is removed the stiffness of this material increases significantly. Its overall strength, like that of many biological tissues, is non-linear viscoelastic (Vincent 1982) such that besides being a function of stress and strain, its properties are also time dependent. A stress/strain curve from these types of tissues typically has an initial linear region, a curved region, and second linear region classified as the pre-transition (or “toe”, Vincent 1982), transition, and post-transition (Figure 5.1), respectfully (Duck 1990). Consequently, this type of stress/strain relationship would be expected for the load bearing components of the dorsal fin, particularly if the load was oriented parallel to the fiber arrangement.

The strength of these layers can be measured by subjecting different orientations of each tissue layer present in the dorsal fin to uniaxial tensile testing. Tensile stress (σ) is determined as the load to area ratio:

$$\sigma = F / A_o \qquad (1)$$

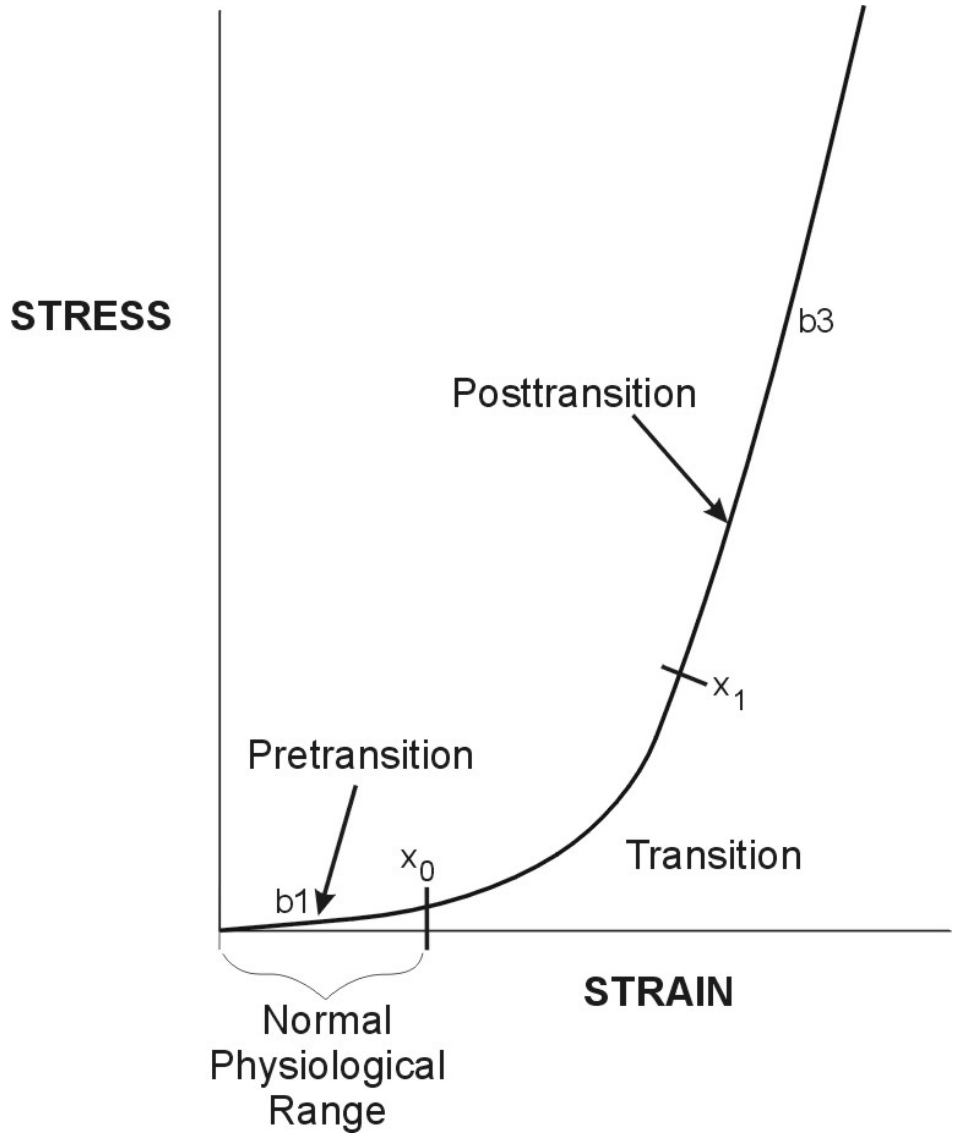

Figure 5.1. Generalized plot of a stress/strain relationship for a viscoelastic biological tissue (modified from Vincent 1982). The slopes of the two linear regions, b_1 and b_3, represent the pre- and post-transition elastic moduli of the tissue and x_0 represents the beginning of the transition region and x_1 the beginning of the post-transition region, as estimated from a spline fitting function.

where F is the applied tensile force and A_o is the original cross-sectional area, normal to the applied force. Strain (ε) is determined as the ratio of specimen elongation to original length:

$$\varepsilon = \delta L / L_o \qquad (2)$$

where δL is the change in length and L_o is the original specimen length. The material stiffness (or strength), E, is Young's modulus of elasticity, the ratio of stress to strain, represented by:

$$E = \sigma / \varepsilon \qquad (3)$$

The pre-transition (E_{pre}) and post-transition (E_{post}) elastic moduli are the local slopes of the linear regions of the stress/strain curves.

The material properties of the tissue components of the harbor porpoise dorsal fin have never been quantified, nor have those of any other small cetacean. Consequently, determination of these material properties was necessary in order to better understand the significance of the observed structural components (Chapter 4), as well as for use as inputs in a finite element model (Chapter 6).

Materials and Methods

Seven dorsal fins from adult harbor porpoises (five frozen, two unfrozen from stranded animals) were removed at the basal insertion to the body. Three fins were sliced dorsal-ventrally (D-V) (parallel to the ligamentous sheath bundles) into approximately 15-30 mm wide sections (Figure 5.2a), and the other four were sliced into similar width sections in an approximately anterior-posterior (A-P) plane (parallel to the fibers of the central core tissue) (Figure 5.2b). For each section, up to two sample strips representing the following three layers were dissected out just prior to testing. The epidermis and dermal papillae were removed as one layer at the interface of the dermal papillae and the subpapillary layer. The ligamentous sheath was then separated from the central core and the central core was then cut into thin strips. Samples that were suitable for testing were cut to length with test group means ranging from 7.6 to 31.5 mm (Table 5.1). In addition, these samples had their ends flared to improve mounting by cutting away approximately 3 mm from each side, yielding hourglass shaped specimens with group means ranging from 9.3-14.3 mm in width. Specimens were placed in a plastic dish and kept moist with 0.9% saline solution.

An MTS uniaxial tester, interfaced with a PC equipped with Testworks 3.0 software, was used in this study. The Sintech 2/S testing system was equipped with a 500N load cell and medium capacity, manual vise-action grips, the bottom being fixed and the upper attached to the load cell. The system was calibrated prior to each day’s

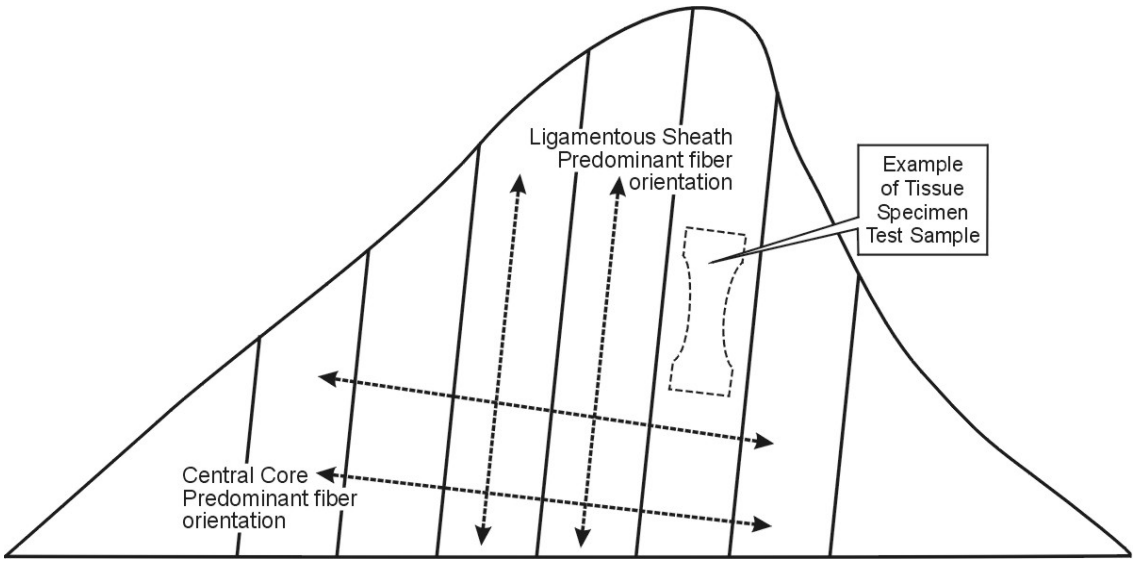

Figure 5.2a. Dorsal-Ventral tissue sectioning pattern for four harbor porpoise dorsal fins. The predominant fiber orientation for the central core and ligamentous sheath tissue layers are illustrated.

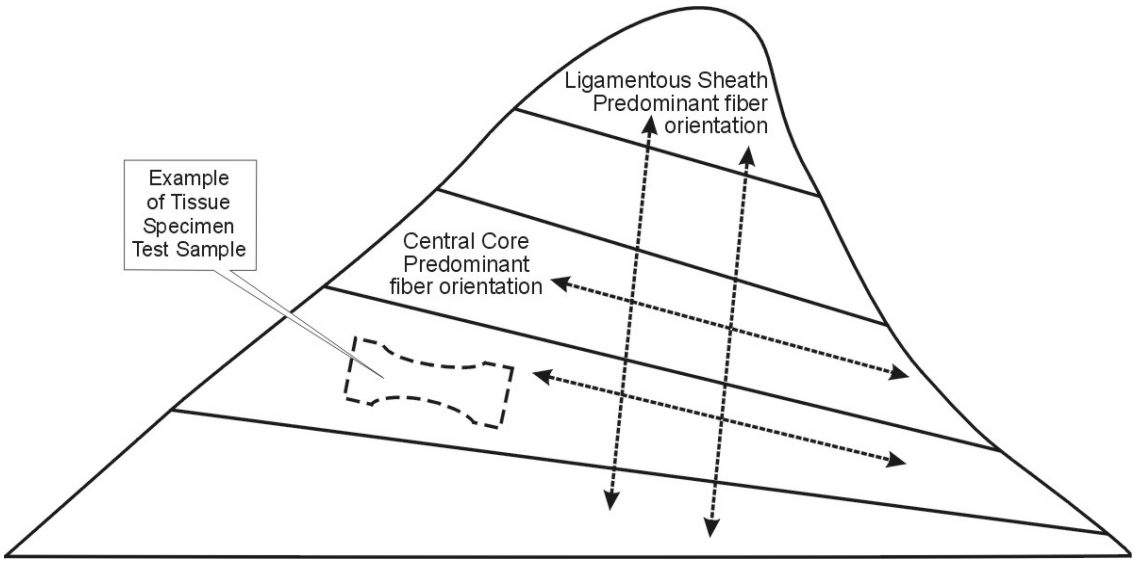

Figure 5.2b. Anterior-Posterior tissue sectioning pattern for three harbor porpoise dorsal fins. The predominant fiber orientation for the central core and ligamentous sheath tissue layers are illustrated.

Table 5.1. Sample dimensions of harbor porpoise dorsal fin tissue specimens subjected to uniaxial testing.

		Anterior-Posterior		Dorsal-Ventral	
		5 mm/sec	5 mm/min	5 mm/sec	5 mm/min
Epidermis/ dermal papillae	(n)	(11)	(4)	(4)	(8)
	Width	9.5 ± 0.5	9.6 ± 0.3	14.3 ± 0.4	9.8 ± 0.4
	Thickness	2.1 ± 0.0	2.3 ± 0.1	2.7 ± 0.2	2.3 ± 0.1
	Length	13.2 ± 1.1	10.9 ± 0.7	10.8 ± 2.2	12.1 ± 0.3
	Cross-sectional area	19.4 ± 0.8	22.1 ± 1.2	38.4 ± 4.0	22.7 ± 1.3
Ligamentous sheath	(n)	(4)	(4)	(6)	(6)
	Width	9.9 ± 0.3	9.3 ± 0.2	10.4 ± 0.4	9.8 ± 0.7
	Thickness	1.5 ± 0.1	1.5 ± 0.0	1.6 ± 0.1	1.5 ± 0.1
	Length	22.1 ± 1.8	31.5 ± 2.2	22.8 ± 1.8	19.4 ± 2.0
	Cross-sectional area	14.8 ± 1.0	14.0 ± 0.2	16.5 ± 1.1	15.2 ± 1.4
Central core	(n)	(5)	(4)	(4)	(6)
	Width	13.1 ± 0.3	10.5 ± 1.3	13.5 ± 0.6	10.4 ± 0.5
	Thickness	3.4 ± 0.1	3.3 ± 0.3	3.1 ± 0.2	3.6 ± 0.3
	Length	7.6 ± 0.5	13.3 ± 2.1	15.5 ± 1.1	9.3 ± 0.4
	Cross-sectional area	44.4 ± 1.9	35.0 ± 6.4	40.7 ± 1.4	38.3 ± 3.5

use and the load cell zeroed before the sample was installed for each test. A 4 cm by 2 cm piece of 240 grit sandpaper was bent in half and placed in each grip. Each specimen was lightly dried with a paper towel before installation between the sandpaper in the upper grip. Its width and thickness were then estimated based on the average of five measurements to the nearest 0.1 mm at five locations using a digital micrometer. After the specimen was lowered manually into the lower grip it was clamped such that buckling was minimized. It was preconditioned by being loaded to approximately 0.5 N and returned to zero five times. With the load gauge indicating no preload, the specimen height was measured. All specimen dimensions were immediately input into the PC and the grips retightened and the test initiated. A crosshead speed setting of 5 mm/sec was used with one set of 34 specimens to approximate the strain rate the tissue is estimated to experience in vivo. Small cetaceans commonly turn at rates of 150 degrees per second (Fish and Rohr 1999). Consequently, the potential load rate for a fin moving from the neutral axis to even a shallow angle of attack of a few degrees would likely occur in a fraction of a second. Although the distance and speed at which a dorsal fin flexes has not been quantified, observations of bowriding species have shown this distance to be small and the movement occurs very quickly. A second set of 32 specimens were tested at 5 mm/min was used to examine rate dependent behavior of the tissues. All tests were run until slippage or failure occurred.

In addition to these tissues, four samples of 50A durometer urethane, which was used for the saddle/fairing for a redesigned tag (Chapter 3), were tested to

slippage at 5mm/min. Specimen sizes averaged 13.5 mm in width, 24.2 mm in length, and 6.3 mm thick.

A spline of the two linear portions (if present) and the power function of the transition portion of the stress/strain curve were fit for each test run, with estimated knot points (Figure 5.1). The parameters were estimated by minimizing the sum of squares using Solver in Excel. It was of the form:

$$y = a_1 + b_1 x_0 \quad \text{when} \quad x \le x_0 \qquad (4)$$

where a_1 is the y intercept, b_1 is the slope of the linear transition region in MPa, x_0 is the knot point at the beginning of the transition region in dimensionless units of strain (i.e., 0.1 strain =10% elongation), and

$$y = a_1 + b_1 x_0 + b_2 (x - x_0)^p \quad \text{when} \quad x_0 \le x \le x_1 \qquad (5)$$

where b_2 and the exponent p are the curve modifier and power function for the transition region, respectively, and x_1 is the knot point of the beginning of the post-transition region in dimensionless strain, and

$$y = a_1 + b_1 x_0 + b_2 (x - x_0)^p + b_3 (x - x_1) \ \text{ when } \ x > x_1 \qquad (6)$$

where b_3 is the slope of the post-transition region in MPa. The post-transition region was truncated at the point the Testworks software had defined as the end of the linear region, based on the program's least squares fit.

A quasi-likelihood generalized linear model (GLM) with a log-link and variance proportional to the mean squared was used to determine if differences in speed and orientation existed for x_0, x_1, and E_{pre}, and E_{post} for each tissue (Splus-GLM, Venables and Ripley 1994). A post-hoc Tukey test was used to evaluate differences between the means of the coefficients (Zar 1996) where overall significant differences from the GLM were found.

Results

The three primary structural tissue layers of the harbor porpoise dorsal fin displayed a variety of stress/strain relationships, with marked differences between tissues, orientations and crosshead speeds.

Epidermis/dermal papillae

The stress/strain behavior of the epidermis/dermal papillae was substantially different from the central core and ligamentous sheath (Figure 5.3). This tissue lacked a distinct pre-transition phase for either orientation or speed, such that the slope was nearly linear through about 0.1 strain (10% elongation) before decreasing slightly over

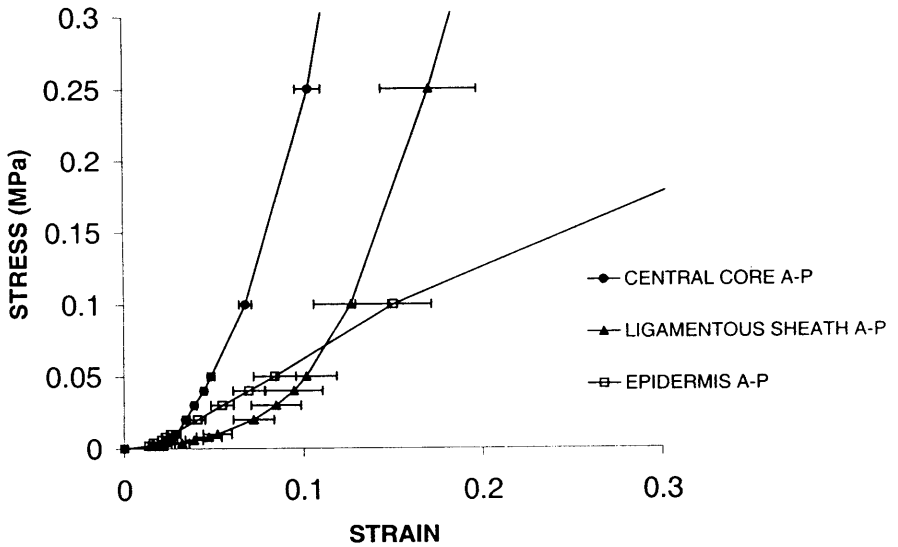

Figure 5.3a. Stress/strain characteristics of the three primary harbor porpoise dorsal fin tissue layers. Anterior-Posterior section orientation at a 5 mm/sec deformation rate. Mean ± SE.

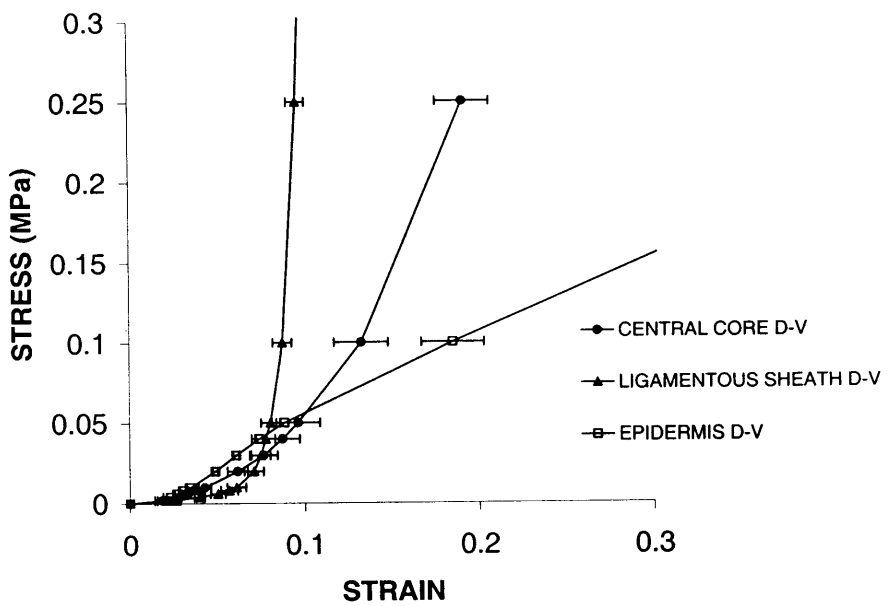

Figure 5.3b. Stress/strain characteristics of the three primary harbor porpoise dorsal fin tissue layers. Dorsal-Ventral section orientation at a 5 mm/sec deformation rate. Mean ± SE.

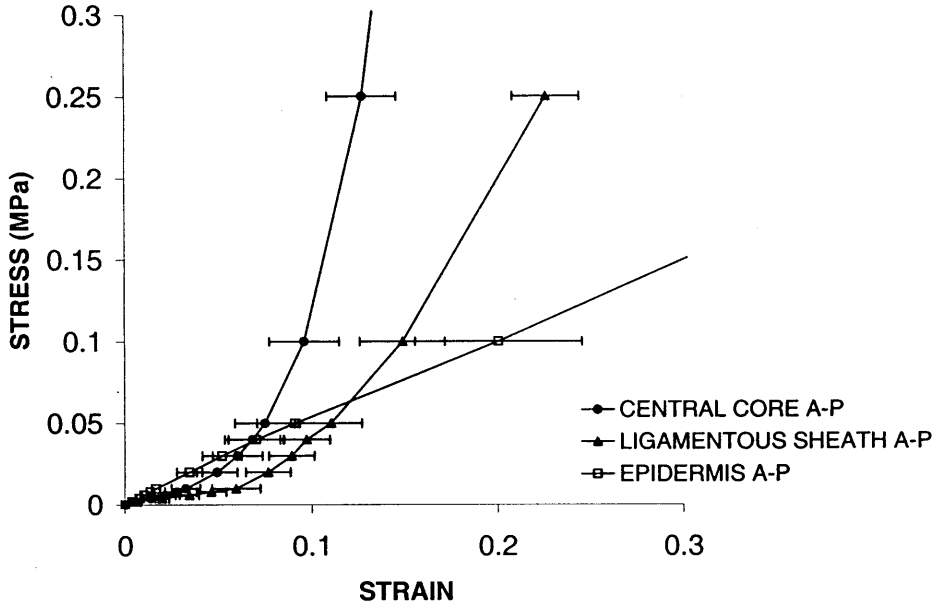

Figure 5.3c. Stress/strain characteristics of the three primary harbor porpoise dorsal fin tissue layers. Anterior-Posterior section orientation at a 5 mm/min deformation rate. Mean ± SE.

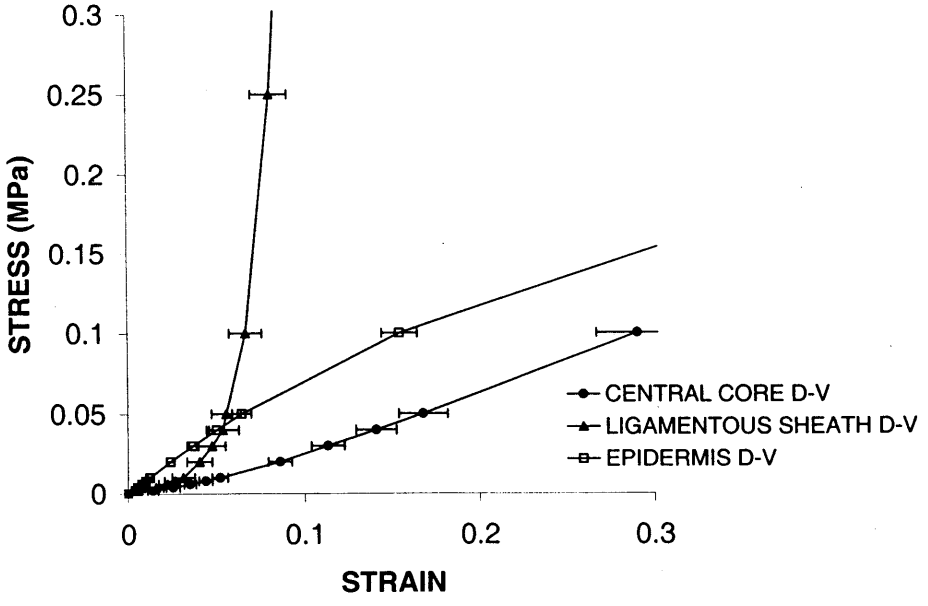

Figure 5.3d. Stress/strain characteristics of the three primary harbor porpoise dorsal fin tissue layers. Dorsal-Ventral section orientation at a 5 mm/min deformation rate. Mean ± SE.

the rest of the elongation. Consequently, the values for all the elastic moduli in both the pre- and post-transition region, which ranged from 0.78 to 0.96 MPa, were assumed to be the same. No significant differences were found between crosshead speeds within tissue orientation ($p=0.26$, $F=1.33$), or between tissue orientations ($p=0.18$, $F=1.94$). With the exception of the central core in the anterior-posterior orientation, the elastic moduli of this layer were higher than the two other tissue layers in the range of 2 to 8% strain. With the exception of the central core in a dorsal-ventral orientation at 5 mm/min, it had the lowest moduli values compared to the other tissues at strains greater than approximately 20%.

Ligamentous sheath and central core

The ligamentous sheath and central core generally displayed stress/stain behavior consistent with those of viscoelastic tissues. However, significant differences were present within the parameters that typify these patterns; i.e., length of the elongation in the pre-transition region, slope of the pre-transition region, initiation of the post-transition region, and slope of the post-transition region.

The extent of pre-transition elongation (x_0) of these two tissue layers was generally similar (2-6% strain), however, significant differences did exist within tissue and orientation, but interactions existed between tissue and orientation, and tissue, orientation, and speed (Table 5.2). The test specimens generally separated into two broad groups that were significantly different, although a considerable level of lack of

Table 5.2. Significant terms or interactions (+) from a generalized linear model to the coefficients obtained from a spline fit to the stress/strain relationships for the central core and ligamentous sheath, $p<0.005$.

Coefficient	Tissue	Orientation	Speed	Tissue: Orientation	Tissue: Speed	Orientation: Speed	Tissue: Orientation: Speed
End of pre-transition region x_0	+	+		+			+
Pre-transition modulus of elasticity, E_{pre} (b_1)		+	+		+	+	+
Beginning of post-transition region x_1	+	+		+		+	
Post-transition modulus of elasticity, E_{post} (b_3)	+	+	+	+		+	+

significance existed between several groups of means (Table 5.3). While no specific pattern was apparent, both of the central core's A-P orientations had the shortest elongation region while the ligamentous sheath's D-V orientation (5 mm/sec) had the most elongation before transition.

The values of the Young's moduli for the pre-transition region of both tissue layers were generally low, ranging from 0.00 to 0.38 MPa for both orientations and speeds. Although no significant differences were identified between tissues, they did exist for orientation and speed, although interactions between several of the factors confounded interpretation. However, most notable was the slope of the central core A-P orientation (5 mm/sec) with a value of 0.0, which was significantly lower than all the other groups based on the post-hoc test. Because this tissue orientation also had the shortest elongation (1.5% strain), this is not likely to be representative of its strength in the physiological range. In fact, over the range of 2-4% strain, this tissue layer had an average modulus of 1.53 MPa, a substantially higher pre-transition value than for all other tissue groups, even than the next closest pre-transition modulus, ligamentous sheath in the D-V orientation (5 mm/min) (0.38 MPa).

The beginning of the post-transition region (x_1) ranged from strains of 10% to 25% with significant differences between tissues and orientations, although interactions existed between these terms as well as between orientation and speed. Again, the central core A-P (5mm/sec) was significantly different from other tissues, having the highest strain values at the beginning of the post-transition region.

Table 5.3. Mean coefficients from a spline fit of the central core and ligamentous sheath by orientation and crosshead speed. Underlined coefficients that are connected indicate no significant difference based on a post-hoc Tukey's test, $p<0.05$.

CC – Central Core LS – Ligamentous Sheath AP – Anterior-Posterior DV – Dorsal –Ventral

Coefficient	Tissue / Orientation Crosshead speed							
End of pre-transition region x_0	CC / AP 5mm/sec	CC / AP 5mm/min	LS / DV 5mm/min	LS / AP 5mm/sec	CC / DV 5mm/sec	CC / DV 5mm/min	LS / AP 5mm/min	LS / DV 5mm/sec
	0.015	0.020	0.030	0.033	0.036	0.039	0.046	0.065
Pre-transition modulus of elasticity, E_{pre} (b_1)	CC / AP 5mm/sec	LS / AP 5mm/sec	LS / AP 5mm/min	LS / DV 5mm/sec	CC / DV 5mm/min	CC / DV 5mm/sec	CC / AP 5mm/min	LS / DV 5mm/min
	0.00	0.10	0.15	0.16	0.17	0.25	0.33	0.38
Beginning of post-transition region x_1	CC / DV 5mm/sec	LS / AP 5mm/min	LS / DV 5mm/min	LS / DV 5mm/sec	LS / AP 5mm/sec	CC / DV 5mm/min	CC / AP 5mm/min	CC / AP 5mm/sec
	0.10	0.12	0.12	0.13	0.16	0.16	0.18	0.28
Post-transition modulus of elasticity, E_{post} (b_3)	CC/ DV 5mm/min	CC / DV 5mm/sec	LS / AP 5mm/min	LS / AP 5mm/sec	CC / AP 5mm/sec	CC / AP 5mm/min	LS / DV 5mm/min	LS / DV 5mm/sec
	0.51	1.56	2.13	4.52	15.2	18.6	50.1	75.9

Otherwise, most of the other tissues performed similarly with significant differences lacking between all groups with strains between 10% and 16%.

In general, the post-transition moduli, which ranged from 0.51 to 75.7 MPa across all tissues, orientations, and speeds, were much higher than values associated with the pre-transition. In addition, there were significant differences between post-transition moduli at the tissue, orientation, and speed levels, although interactions also existed between all of these terms. However, unlike the pre-transition slopes, six of the eight post-transition slopes were significantly different from each other. Of greatest significance was the presence of a consistent pattern of increasing modulus based on predominate fiber orientation, from central core to ligamentous sheath. This pattern reflected significant differences not only between tissues with the same predominate fiber orientation (ligamentous sheath > central core) but also significant differences within tissues based on predominate fiber orientation (parallel > perpendicular).

The stress/strain curve obtained for the 50A durometer urethane was similar to the pattern of the relatively linear epidermis/dermal papillae layer, but with a higher elastic modulus (2.89 $\pm$ 0.1 SE MPa) up to 0.06 strain. However, this modulus was similar to that of the ligamentous sheath (A-P orientation) in the post-transition region.

Discussion

This study was the first to examine the material properties of the dorsal fin tissue of any small cetacean. Consequently, while these results cannot be compared with related species, some insights can be gained relative to other tissues.

Epidermis/dermal papillae

The behavior of the epidermis/dermal papillae was unlike collagen-bearing soft tissues, with generally linear behavior and relatively high stiffness at low strains. Its stress/strain curve is strikingly similar to rubber, although the stiffness of this tissue did not increase at higher strains, as do rubber-like materials (Mullin 1980, Vincent 1982). The low strain region has an elastic pattern similar to that of only the stratum corneum layer in humans and other terrestrial mammals (Wildnauer et al. 1971, Papir et al. 1975). However, despite the inclusion of the dermal papillae in the dorsal fin samples, its material properties were dissimilar to human dermis (Daly 1982). The presence of elastin in the dermal papillae may contribute to the ability of this layer to undergo relatively large deformations before yielding. A felt-work of fine filaments has been described in this layer in humans (Sanders et al. 1995) and may play a significant role in the relatively high stiffness of this layer in the expected physiological range, i.e. 2-5% strain (Parry and Craig 1984, Wainwright et al. 1982, Fung 1993). Intercellular bonds from the dermasomes and the muccopolysaccharides

of the ground substance likely contribute significantly to this layer's strength (Wildnauer et al. 1971, Mercer et al. 1968). The relatively high tissue strength suggests that the epidermis/dermal papillae layer plays a potentially important role in supporting telemetry tags.

Ligamentous sheath and central core

The results of this study also demonstrated that although the ligamentous sheath and central core behave like most viscoelastic tissues, the typical stress/strain pattern is less pronounced in the central core layer. The patterns observed in the central core, and the associated values of the spline coefficients are likely explainable based on collagen fiber orientation and density. When tissues are subjected to an applied load perpendicular to their fiber orientation, they typically exhibit greater elongation and delayed initiation of the post-transition, as well as lower post-transition moduli. The reasons for the consistently short elongation to the beginning of the transition phase (x_0) for the central core A-P at both speeds are unclear but may have been due to this tissue's fabric-like fiber arrangement (Chapter 4). Typically, the initial elongation that occurs is due to removal of crimp from an applied load when all the fibers are arranged parallel to this load. It may be possible that this tissue moves into the transition phase sooner because, like skin tissue, there may be a substantial number of bonds in the tissue matrix that are being pulled apart. This may offer more initial resistance, resulting in a greater pre-transition stiffness. However, at the faster

crosshead speed this may be due to the resistance of ground substance displacement (Potts and Breuer 1983). The breakage of the bonds in the matrix may also be responsible for the delayed onset of the post-transition stage. The post-transition moduli of the central core A-P were intermediate between a tissue with all fibers parallel to the applied load (ligamentous sheath D-V) and one in which they are perpendicular (ligamentous sheath A-P). Inasmuch as a substantial proportion of the fibers in this tissue run perpendicular (laterally), as well as at intermediate angles, such fiber arrangements will reduce a matrice's overall strength (Harris 1980) because there are fewer fibers to support the load in a particular direction. Also likely contributing to the weaker post-transition elastic moduli of the central core, compared to the ligamentous sheath, was its lower percentage of collagen (Chapter 4). The unique fiber arrangement of this layer may be important in supporting what are likely to typically be compressive loads from the tag attachments, particularly in the pre-transition region. However, because there appear to be no fibers running dorsal-ventral in this tissue layer (Chapter 4), it may provide little support if the tissue is subjected to loads in that direction, particularly if the strains are in the post-transition region.

It was not surprising that the ligamentous sheath in the dorsal-ventral orientation had the highest post-transition moduli. Although this layer is organized into the largest collagen structures in the fin, as well as having the highest collagen density (Chapter 4), its strength was substantially weaker than a sacrocaudulis tendon found in the tail stock of this species (1.52 GPa, Bennett et al. 1987). Compared to

humans and other animals, the collagen bearing tissues of the dorsal fin appear to have strength more similar to articular cartilage, which typically ranges from 5 to 50 MPa (Anderson et al. 1999). The resulting strength values confirm the importance of this layer as a support structure to resist perpendicular loads (Chapter 4). However, its ability to support loads that occur in the anterior-posterior plane, outside the pre-transition range, would be more limited.

Limitations

Although the coefficient values obtained in this study likely represent reasonable estimates of the stress/strain relationships of the associated tissue layers, at least some of the variability observed is likely due to small sample size. In addition, all fins used in this study were from beach-cast specimens. Consequently, although the tissues appeared to be in generally good condition, because the time since mortality was not known, a significant degree of tissue degradation may have occurred before recovery, which may not have been detectable from gross examination. In addition, the health status of these stranded individuals was unknown, but it might be expected that the problems that precipitated their stranding may have affected their physical condition. For example, if nutritionally stressed, fat might be expected to be used, which may be reflected as fewer adipose cells in the dorsal fin. Consequently, the use of fins from animals killed incidental to commercial fishing operations would be advantageous.

While additional work on harbor porpoises would be beneficial, comparative testing on the dorsal fins of other species would offer two benefits. Fins from a larger species would potentially allow testing of different orientations from the same fin. It also may be possible identify the potential sources of variability between species, particularly for those species where fin morphology differs as a secondary sex characteristic.

Other types of material property testing should be considered besides uniaxial testing. Given the anisotropic nature of this tissue, future testing would likely benefit from the use of a biaxial or triaxial tester. However, given the problems encountered with slippage in this study, particularly with the very oily central core (due to its high lipid content), more effective gripping techniques may need to be developed. Compression testing should also be considered because this is the type of loading the tissue is typically being subjected to from tag attachments. While tension and compression are generally considered to be inversely related, tissues may respond differently to compression in vitro, as well as in vivo (Buckwalter 1996).

Parameter estimation methods may also benefit from an alternative approach. Although the spline fitting routine generally provided good fits to the data, it suffered some sensitivity problems fitting the knot point x_0 and the pre-transition slope. This was a result of the sum of squares being dominated by the post-transition region fit. The high average value (6% strain) for the beginning of the transition region for the ligamentous sheath D-V orientation (5 mm/sec) appeared to be related to this lack of

sensitivity. A better approach might be the use of a smoothing function to estimate the pre- and post-transition moduli.

The material properties of the tissues tested in this study were generally a reflection of their predominate collagen fiber orientation, if collagen was present. While additional, more detailed, testing may reduce the observed variability, these results are likely within the true range of material properties for these tissues. The data generated in this study will be important to the development of a finite element model to examine the stress distribution caused by different tag designs and, hopefully, improve the understanding of those factors which influence attachment duration.

CHAPTER 6

FACTORS INFLUENCING TAG ATTACHMENT DURATION FOR SMALL CETACEANS: A FINITE ELEMENT ANALYSIS OF TELEMETRY TAGS ON A HARBOR PORPOISE DORSAL FIN

Introduction

The loss of telemetry tags from the dorsal fins of small cetaceans due to the degeneration of the dorsal fin tissue was first reported in the mid-1970s (Irvine et al. 1979). This problem has been observed in several subsequent studies (Tanaka et al. 1987, Martin and da Silva 1998, Orr et al. 1998). In some cases this tissue degradation and tag loss occurred within a few weeks of deployment (Irvine et al. 1982, Tanaka et al. 1987), yielding shorter than expected durations of transmitter signal contact. Some recent studies have made progress in attaining multi-month deployments (see Read and Westgate 1997, Martin and da Silva 1998, Larsen et al. in prep., Chapter 7). A general trend among some of these studies was the generally longer durations of contact when a single transmitter was attached to the side of the fin instead of the front of the fin. More recently, it has been shown that a pair of transmitters attached to the sides of the fin may yield even longer attachment durations than a single side-mounted tag (Chapter 7). However, in many of these studies there has continued to be considerable variability in attachment durations. In some cases there has been little or no resight data such that the underlying reasons for these results have remained unclear.

The pins that attach these telemetry tags to the dorsal fins of small cetaceans are essentially percutaneous devices exposed to dynamic loads an aquatic environment. There are at least four potential sources of tissue degeneration that might be expected to occur in association with these pins: 1) as a foreign body response due to the interaction of the pinning material and adjacent tissue (von Recum and Park 1981); 2) from infection due to a bacterial invasion of the wound (von Recum and Park 1981, Geraci and Smith 1990); 3) due to pressure necrosis, from chronic stress concentrations (Mak et. al. 1994); or 4) due to mechanical stresses disrupting the healing process (von Recum and Park 1981). The occurrence of the first two factors has been demonstrated in small cetaceans (Geraci and Smith 1990). The focus of this study will be the latter two, which are related to the static and dynamic loads, respectively, generated by the tags.

Pressure necrosis has been implicated as the source of tissue degradation in small cetacean tag attachments (Brill and Friedl 1993, Mate et al. 1995). This type of necrosis represents a structural breakdown of the tissue that results from load concentrations that occur for extended periods of time. It has most commonly been attributed to the occlusion of capillary blood flow (Kosiak 1961, Dinsdale 1974), or other changes that affect the structural properties of the tissues (Sanders et al. 1995). It is been demonstrated that there is an inverse logarithmic relationship between duration and pressure such that even low pressures can occlude blood flow over a long duration (Krouskop et al. 1983). However, because the pressures exerted on dorsal fin

tissues have never been quantified, it is unknown if this is the actual cause of this tissue breakdown.

It is also important to note that the loads these tag attachments create are changing (i.e., dynamic) as the animal accelerates, decelerates (Appendix A), and changes direction while swimming. In addition, every 2-3 minutes most species of small cetaceans surface several times to breathe. Consequently, during each of these short (1-2 second) surfacing events the tag's drag load drops to zero in air and then upon reentry to the much denser water, experiences an impact load. Interfacial tissue bridges that are forming during the wound healing process are thought to be weak (von Recum 1984) and thus would be highly susceptible to breakage from dynamic mechanical forces. These mechanical forces are also thought to cause focal bleeding, resulting in inflammation, which potentially allows for the onset of an infection (von Recum 1984). Consequently, an alternative, or additive source of load-related tissue necrosis could be due to these dynamic loads.

An initial attempt to relate tag load to duration of attachment examined the proportional drag increase for a given tag design on a model porpoise tested in a wind tunnel relative to the design's typical duration of attachment (Chapter 2). Although this approach was the first to quantify the total load that a tag generates and suggested that wind tunnel data appeared to be suitable for explaining some of the differences observed in attachment longevity, it could not explain all the observed differences. This result indicated that a more sophisticated model was required.

The performance of any material under load will be related to the magnitude and frequency of the loads it experiences as well as its strength, which is based on the composition and arrangement of its components. Dorsal fin tissue layers are essentially composite biomaterials (Chapter 4), with inherent strength characteristics that vary by tissue layer (see Chapter 5). Dorsal fins are less stiff than the pins and tag saddles that are typically attached to them. Thus, this mismatch in their material properties likely results in stress concentrations (Tramaglini et al. 1993) in the tissue surrounding the attachment site. Consequently, for a given tag's load regime, the stress distribution within the fin will be a function of the arrangement and strength of the tissue layers, as well as the attachment scheme's configuration, which is dependent on the position of the tag on the fin and the number, diameter, and location of pins and their associated material properties. By quantifying all these variables, this complexity can be simultaneously analyzed using a numerical model.

Finite element analysis (FEA) is a routinely used computer-based modeling procedure that allows the mechanical analysis of any structure. It can be used to approximate numeric solutions for the mechanical deformation and stresses on a structure exposed to external forces within the constraints of the laws of physics that underlie the force equilibrium equations. Using this technique to evaluate the stress distribution that various tag configurations create in the tissue of a dorsal fin requires the division of the fin's component parts into small, polygonal finite elements that together, fit the actual geometry. The tag components (transmitter, saddle, attachment

pins) are similarly defined. Together, these elements represent the mesh of the finite element model where the intersections of the vertices of the adjacent elements are defined as the nodes. The material properties (the stress/strain behavior under load) of each material component of the model are assigned to the appropriate element. These material properties are obtained from mechanical testing of these components. For manufactured materials, published values of their specifications are usually readily available. Other materials, such as dorsal fin tissue, need to be tested on a uniaxial or biaxial tester. Boundary conditions are specified to fix a portion of the model so that it remains in place rather than moving as a rigid body when the load cases of interest are applied. The nodal displacements are then solved for and estimates of the associated stresses are calculated and displayed graphically.

This report describes the development of a three-dimensional finite element model of a harbor porpoise dorsal fin with the three most commonly used telemetry tag placements subjected to loads that are expected to be encountered during typical swimming behavior. This is the first model of its kind and, thus, represents a preliminary attempt to quantify the stresses dorsal fin tissues experience for these different tag/attachment configurations for comparison to their attachment longevities.

Methods

Geometries

To define the fin's external geometry a fiberglass model of the dorsal fin was made from a mold taken from a carcass of a 1.54 m adult male harbor porpoise killed incidental to commercial fishing operations in Washington State. X, y, and z coordinates were measured relative to the base of the fin along a plane at its insertion point on the body. The external geometry of the fin was determined by tracing the outline of the base and sides of the fin on grid paper to provide the x and y coordinates, and the thickness of the fin was measured every 6 mm posterior to the leading edge on a series of lines spaced every 6 mm dorsal to the base, to determine the z dimension. Dorsal fins are an appendage primarily composed of connective tissue (Felts 1966, Elsner et al. 1974), of which collagen fibers predominate (Chapter 4), and its vascularization serves an important thermoregulatory role for internal reproductive organs (Rommel et al. 1992, 1993). The structural integrity of the fin is provided by the collagen, which composes a vertically oriented ligamentous sheath layer below the epidermis/dermal papillae (Chapter 4), surrounding a central core of fibers arranged as a matrix (Elsner et al. 1974, Chapter 4). Based on material property testing (Chapter 5), the strength of these three layers; the epidermis/dermal papillae, ligamentous sheath, and central core, were defined. The thickness of each of these

components was based on measurements taken from a porpoise fin for which a complete set of histological slides (anterior-posterior cross-section) existed (Chapter 4). Measurements of the internal layers at 2 cm dorsal to the base of the fin (insertion to the body) were: anterior end - overall thickness 1.8 cm, dermis 0.3 cm, and vertical sheath 0.1 cm; mid-fin - overall thickness 2.3 cm, dermis 0.3 cm, and vertical sheath 0.15 cm, posterior end - overall thickness 0.8 cm, dermis 0.25 cm, and vertical sheath 0.05 cm. Measurements were also made 6 cm dorsal to the base: all regions - overall thickness was 1.0 cm, dermis 0.25 cm, vertical sheath 0.07 cm. The thickness of each component layer was extrapolated between these two locations and coordinates were input relative to the external geometry of the fin.

Two of the three tag designs used in this analysis were based on dimensions of the front of the dorsal fin mount, and the single-side-mount configurations (Tags 2 and 3, respectively, Chapter 2) of Telonics ST-10 transmitters used by Read and Westgate (1997). The third design incorporated a pair of these side-mounted ST-10 transmitters as a proxy for the more geometrically complex streamlined urethane saddles of the paired side-mount tags (e.g., Tag 8, Chapter 3). Pin/saddle contact areas for the single side-mount and the streamlined paired side-mount tags were the same for the actual tags of each design. Pin diameters were 8 mm for the front-mount tag and 6.4 mm for both side-mounts.

All coordinates were entered into ABAQUS structural analysis software (Hibbitt, Karlsson, & Sorensen, Inc., Pawtucket, RI, Version 5.8). A finite element

mesh composed of 2368 eight-node composite brick elements (ABAQUS element type C3D8R) was used to complete all the component layers of the dorsal fin. The top 2.5 cm of the fin was excluded to minimize the number of elements in order to reduce file size and model processing time. Within the brick elements where the pins were located, wedge elements were used. The reduced element type was selected because the dorsal fin is a soft tissue. The front-mount tag was constructed of six-node isoparametric cylindrical elements (C3D6) and the saddle was constructed of eight-node brick elements (C3D8R) totaling 288 elements. For the single and paired side-mounts eight node brick elements (C3D8R) were used, with the number of elements totaling 554 and 1108, respectively. Each of the three pins was constructed of a total of 112 six node cylindrical elements. The complete finite element models (FEM) for each tag design are presented in Figure 6.1.

Boundary Conditions

All the nodes on the base of the dorsal fin model were set to zero displacement because no movement is expected where the base is connected to the body. The contacts used were: tag and fin; pin and fin; and fin and tag. No interface elements were used to model these surfaces due to a high degree of complexity. Instead, multi-point linear equations were used to constrain nodal displacement to zero.

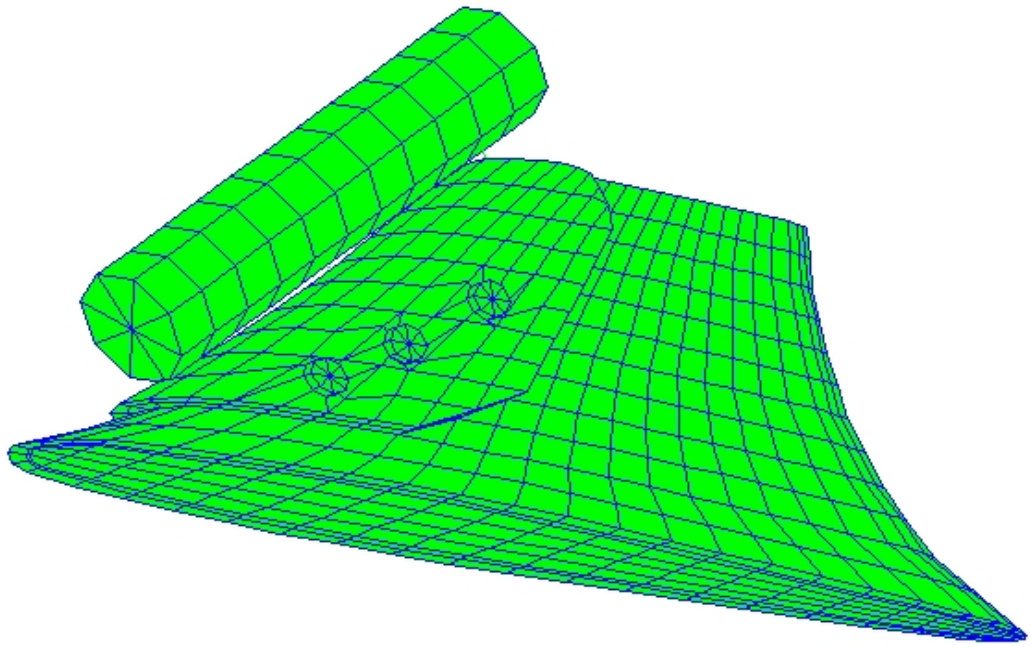

Figure 6.1a. Finite element model geometry of a harbor porpoise dorsal fin with a front mounted telemetry tag.

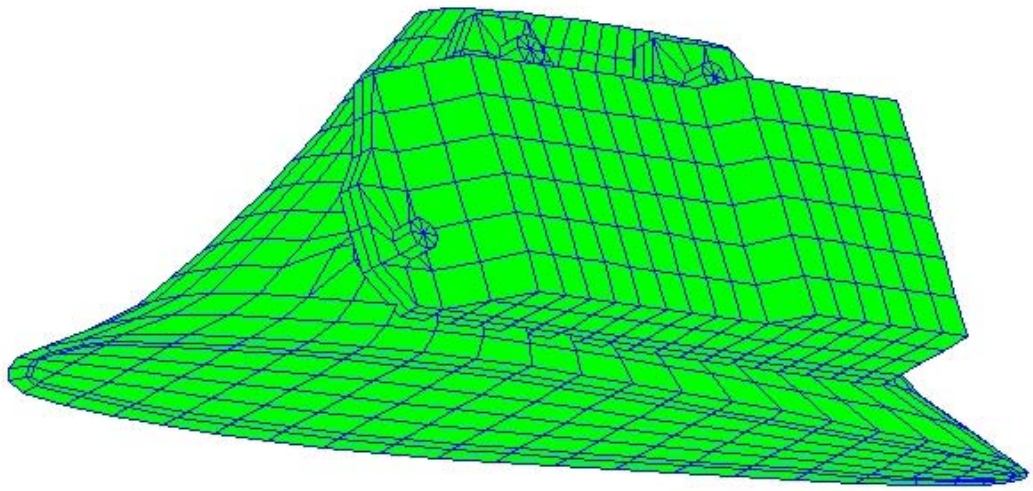

Figure 6.1b. Finite element model geometry of a harbor porpoise dorsal fin with single side mounted telemetry tag.

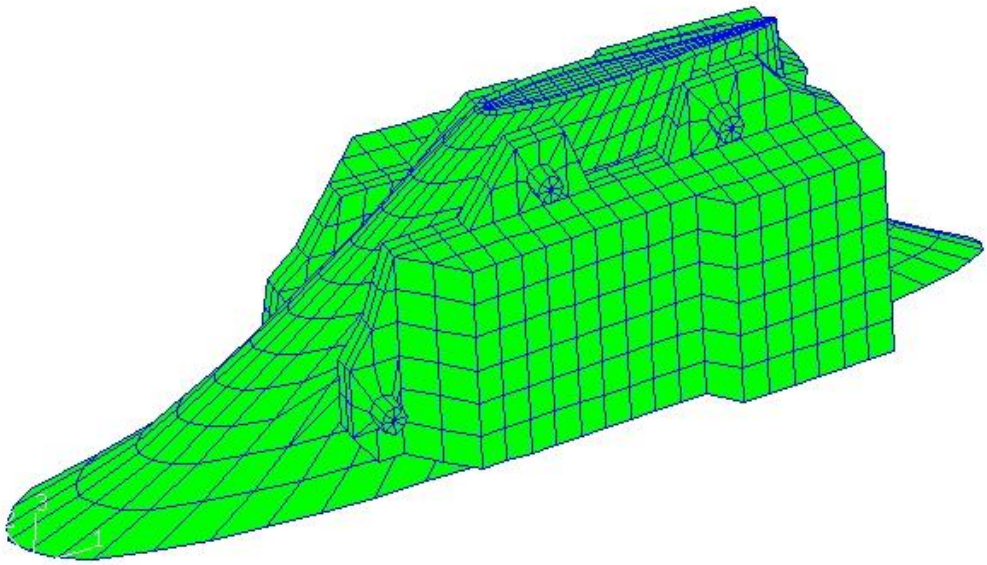

Figure 6.1c. Finite element model geometry of a harbor porpoise dorsal fin with paired side mounted telemetry tag.

Material Properties

Young's modulus (E) characterizes the stress/strain relationship (stiffness) of materials. It is determined by calculating the slope of the linear portions of the stress/strain relationships of the material as measured when subjected to tension or compression. Three regions have been described for the stress/strain curves of soft biological tissues; pre-transition, transition, and post-transition (Duck 1990). Relatively large elongations for small increases in applied loads occur with initial loading, the pre-transition region, whereas less elongation occurs for the same stress

increase in the post-transition area. Although the strain region that dorsal fin tissue operates in is unknown, the physiological strain range of most tissues that are primarily collagenous (e.g., tendons), is 2-5 percent, beyond which permanent damage typically occurs (Parry and Craig 1984, Wainwright et al. 1982, Fung 1993). The loads that tag attachments subject the tissue to during normal swimming and diving are expected to be in the pre-transition range whereas those associated with rubbing would most likely be in the post-transition range. As a result of this uncertainty, stress levels were determined initially for all the tags with both sets of materials properties for the static loads. Young's moduli for the component layers of the dorsal fin were measured experimentally under uniaxial tension (Chapter 5). Material properties for the tag components were obtained from published information by component manufacturers (Table 6.1). Shear moduli were estimated for each tissue component using the relationships presented in Appendix E.

The degree to which a deformable body contracts laterally as it elongates when put under tension is also a function of its material properties. The ratio of the elongation relative to original length, and the change in radius divided by its original radius (Poisson's ratio, ν) must be incorporated in the model. Biological tissues are generally considered to be incompressible and, thus, are typically assigned values between 0.45 and 0.49. Poisson's ratios were estimated for the each tissue component using the relationships in Appendix E and are presented in Table 6.1.

Table 6.1. Material properties of components of the dorsal fin/telemetry tag finite element models. Tissues include pre- and post-transition. Orientation subscripts are defined in Appendix E. Transmitter material properties were all set to E= 2756 MPa, ν=0.38, and density=1.96. E and ν for materials considered isotropic are listed only once.

Component		Dorsal fin						Front mount			Single side mount			Paired side mount	
Property	Units	Epidermis/ dermal papillae		Ligamentous sheath		Central core		Saddle	foam	pin	Saddle	foam	pin	Saddle	pin
		pre	post	pre	post	pre	post								
Young's modulus E_1	MPa	0.81	0.81	0.22	4.20	1.53	17.5	1619	1.80	2756	2377	1.80	2756	2.89	120000
Young's modulus E_2	MPa			0.22	4.20	0.33	1.50								
Young's modulus E_3	MPa			0.22	65.4	0.33	1.50								
Poisson's ratio ν_{12}		0.45	0.45	0.45	0.30	0.45	0.45	0.38	0.39	0.40	0.38	0.39	0.40	0.38	0.36
Poisson's ratio ν_{13}				0.45	0.03	0.45	0.45								
Poisson's ratio ν_{23}				0.45	0.03	0.30	0.30								
Shear modulus G_{12}	MPa			0.08	1.61	0.15	0.72								
Shear modulus G_{13}	MPa			0.08	2.04	0.15	0.72								
Shear modulus G_{23}	MPa			0.08	2.04	0.13	0.58								
Density ρ	g/cm^3	1.00		1.00		1.00		0.70	0.33	1.62	1.34	0.33	1.62	1.07	4.42

Load Cases

Five generalized force-related phases associated with surfacing/deep dive patterns have been identified based on analyses of time-depth recorder (TDR) data (which included a velocity meter) which was deployed on a free-ranging harbor porpoise (Appendix A). These general features include: 1) impact load at the air/water interface; 2) early dive acceleration; 3) mid-dive deceleration/acceleration; 4) late dive deceleration; 5) unload at the water/air interface. Within the mid-dive region the overall pattern has been deceleration with increasing depth to approximately maximum dive depth, followed by acceleration as the porpoise moves towards the surface. However, although there was variability within this general pattern, there were also short term, small scale, acceleration/deceleration events that lasted an average of 4 seconds, with an average rate of $0.16 m/s^2$. The distribution of the velocity readings for all the swimming behavior was bimodal with peak values at approximately 0.6 and 1.9 m/s, with the former associated with the intra-long dive surfacing bouts and the latter associated with dives greater than 30 seconds. Because the flow to the velocity turbine is likely disrupted by the suction cup that is located in front of it, the velocity meter requires calibration in order to correct the speed. An analysis of velocity meter readings compared to the rate of change of the depth pressure sensor indicated that the velocity meter was likely under-reporting the true velocity by at least 15% (S. Blackwell, pers. com.). Correction for this bias yields a

mean long dive swim velocity of 2.2 m/s. This speed in seawater corresponds to a dynamic pressure of approximately 0.38KPa for data collected on a life-size porpoise model in a wind tunnel (Chapter 2).

The load each tag design generated (Chapter 2, 3) was determined by subtracting the baseline load of the porpoise model from the load of the porpoise model and the tag (Table 6.2). The first load case examined was a static load at 0° yaw and an average swim speed of 2.2. m/s with no acceleration. This initial analysis was conducted with both the pre- and post-transition material properties for comparative purposes because it is uncertain in which region these tissues typically operate under normal behaviors.

Table 6.2. Load cases (N) used in the finite element models. To simulate loads during: impact at the air/water interface while submerging, a velocity of 1.1m/s was assumed; during swimming, an average speed of 2.2 m/s was used with 0° yaw and zero acceleration; and during turning, the same velocity (2.2 m/s) was used at -10° yaw.

Load case	Front-mount	Single side-mount	Paired side-mount
Impact at submergence	0.43	0.32	0.32
Average swim speed, 0° yaw	0.61	0.55	0.58
Average swim speed, -10° yaw	0.64	0.43	0.46

However, because many tendon-like, collagen-bearing tissues are known to sustain permanent damage if they exceed 5% strain (Parry and Craig 1984, Wainwright et al. 1982, Fung 1993), it was expected that these tissue layers only operate in the pre-transition region during typical swimming behavior. The analyses were limited to the post-transition material properties for the first load case due to the likelihood of potential biases from the output if these tissues have not experienced strains greater than 10-15% (Chapter 5). Consequently, the subsequent analyses for the other three loads cases were limited to pre-transition input values. The second load case estimated impact stresses at the air/water interface for an entry velocity of 1.1 m/s (Appendix A, Chapter 2, 3). The third load case used the same velocity and yaw position but incorporated an instantaneous change in acceleration to deceleration of 0.16 m/s^2 at a velocity of 2.2 m/s. The final load case estimated the stresses based on -10° yaw with a velocity of 2.2 m/s (Chapter 2, 3).

Of primary interest were the compressive stresses that develop at the pin/tissue interface. Consequently, for each tag design and load case, the maximum principal compressive stresses on the tissue layer at the pin/tissue interface were recorded. Subtracting the maximum principal compressive stress during acceleration from the maximum principal compressive stress during deceleration compared dynamic loads associated with acceleration/deceleration events. Similarly, the magnitudes of the maximum change in stresses were determined for each side of the tag between 0° and -10° yaw by subtraction.

Results

Static Loads

The maximum principal compressional stresses at the pin/tissue interface of the three tag designs at a simulated swim speed of 2.2 m/s with 0° yaw and zero acceleration had a smaller range across all tissue layers using pre-transition material properties (Table 6.3, Figure 6.2) than compared to the same models and loads cases using post-transitional coefficients. For the models using pre-transition coefficients the greatest stresses generally occurred in the epidermis, and the lowest in the ligamentous sheath (Figure 6.2a). The stress pattern was reversed using the post-

Table 6.3. Estimated maximum principal compressional stress levels (KPa) for static load cases associated with typical swimming. Values are based on inputs that assumed a velocity of 2.2 m/s (zero acceleration) and were recorded at the pin/tissue interface for the three tissue layers of a harbor porpoise dorsal fin for pre- and post-transition material properties.

	Front-mount		Single side-mount		Paired side-mount	
Tissue	Pre	Post	Pre	Post	Pre	Post
Epidermis/dermal papillae	5.37	2.28	4.13	0.84	1.03	0.14
Ligamentous sheath	1.37	10.8	0.90	4.39	0.34	2.10
Central core	2.75	2.49	2.61	2.83	1.10	1.06

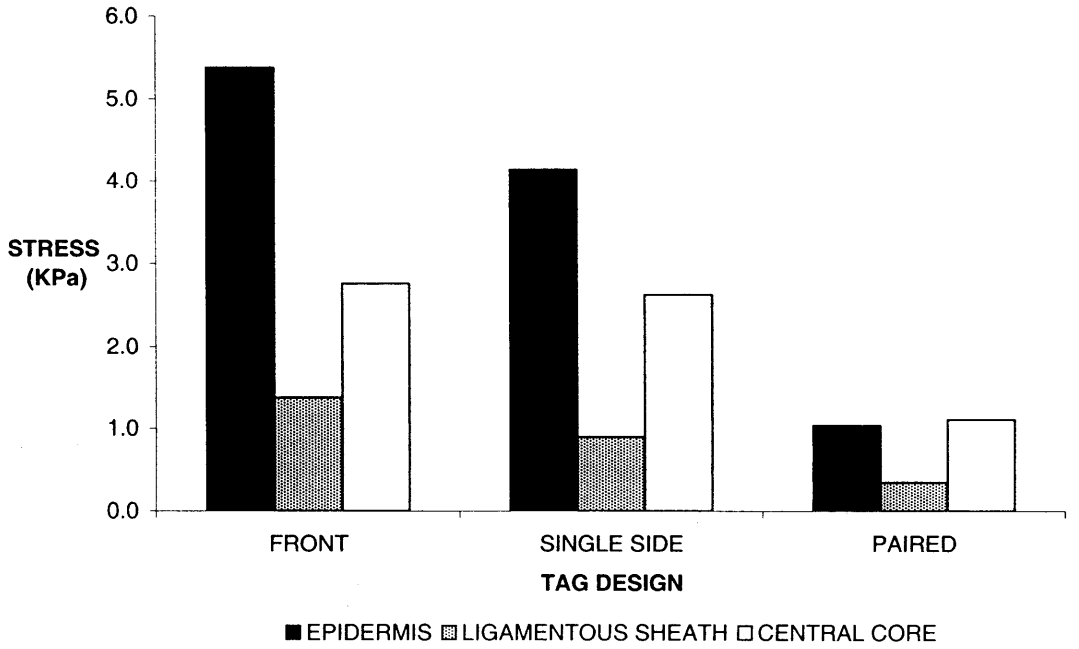

Figure 6.2a. Estimated maximum principal compressional stress levels (KPa) for a static load case associated with typical swimming using pre-transition material properties. Values were based on 2.2 m/s (zero acceleration) and recorded at the pin/tissue interface for the three tissue layers of a harbor porpoise dorsal fin.

transition coefficients with largest stress values in the ligamentous sheath and, lowest in the epidermis (Figure 6.2b). The trends observed in stresses between the pre- and post-transition material properties correspond with the stiffness patterns of the different tissue layers (Chapter 4), e.g., greater stresses were observed in the ligamentous sheath when the post-transition values were used because it has a significantly greater Young's modulus than other tissues. Although it is likely that these tissues typically operate in the pre-transition region during normal swimming, the possibility exists that these loads could cause displacements that would result in the tissue exhibiting the material properties of the post-transition region. The

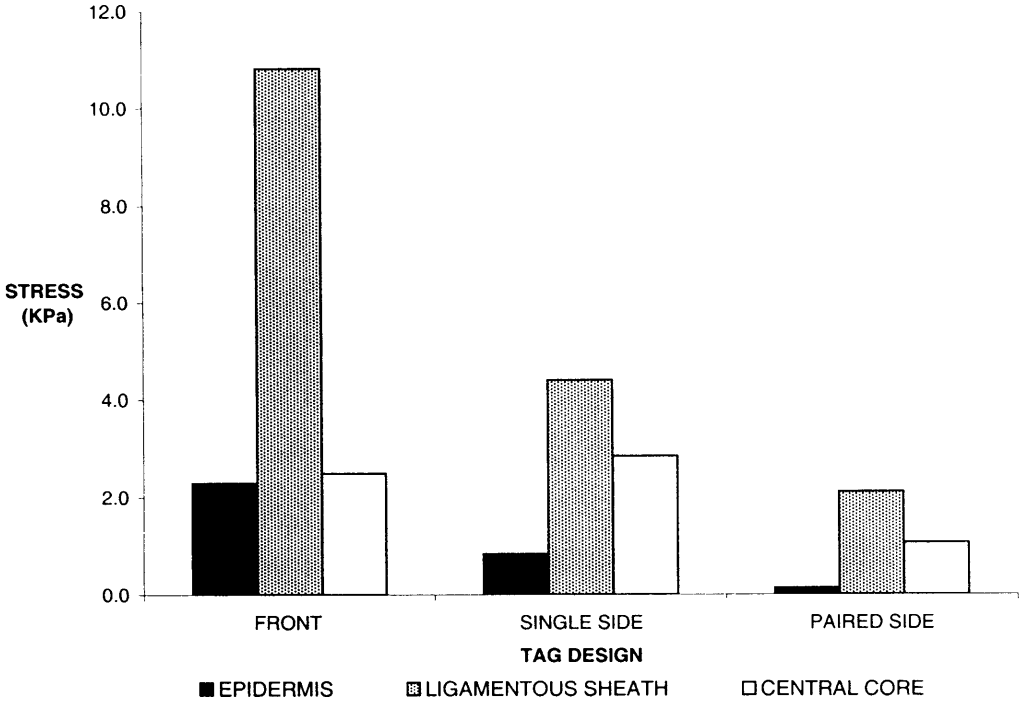

Figure 6.2b. Estimated maximum principal compressional stress levels (KPa) for a static load case associated with typical swimming using post-transition material properties. Values are associated with 2.2 m/s (zero acceleration) and recorded at the pin/tissue interface for the three tissue layers of a harbor porpoise dorsal fin.

consequences of these scenarios are that if the true displacements exceed 6-8%, the stresses obtained using pre-transition inputs will be underestimates. However, the reverse will be true using the post-transition properties, i.e., if the displacements are less than 10-15% the stresses obtained will likely be overestimates. This exercise illustrates that under high loads, with sufficient displacement, the ligamentous sheath will be the primary load-bearing tissue layer. Although differing in magnitude, the same general pattern of stress distribution was reflected between layers across tags for both sets of material properties. In both the pre- and post-transition material property

than the other two tags (Figure 6.2, Table 6.3). The paired side-mount consistently generated the lowest stresses and, in addition, the range of stress levels between tissue layers was also smallest for this tag. The front-mount and single side-mount produced a substantial amount of stress in the epidermis in the pre-transition region. The distribution of stress between the pin holes was not equal for all tags. Stress concentrations were located in the top hole of the front-mount tag, and similarly, the front hole on the single side-mount (Figure 6.3).

Dynamic Loads

Stresses generated by dynamic loads were estimated with only pre-transition material properties and included those pressures associated with impact at the air/water interface, acceleration/deceleration events, and turning to a yaw angle of –10° from 0°. The greatest impact stresses were consistently generated by the front and single side-mount, and the least by the paired side-mount (Table 6.4, Figure 6.4). Across tags, the epidermis generally sustained more of the highest stresses. In a comparison of the magnitude of stress differences resulting in a change from acceleration to deceleration at 2.2 m/s, the single side-mount and the paired side-mount had the highest overall changes (Table 6.5, Figure 6.5). Both these tags appeared to generate substantial stress levels in the epidermis and central core. In a comparison of the differences in stresses

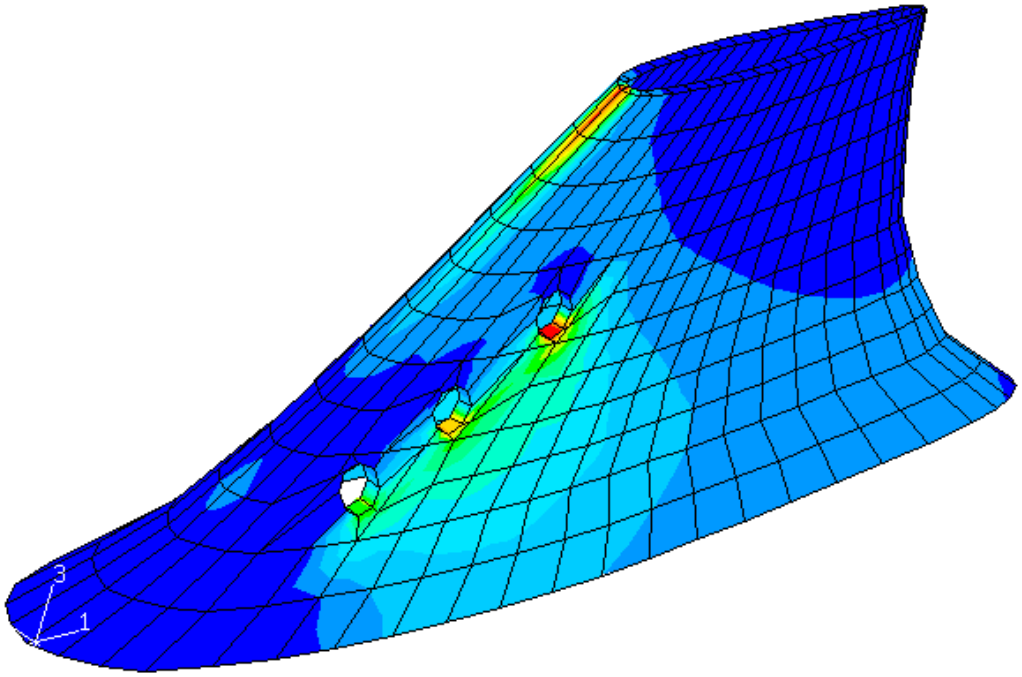

Figure 6.3a. Compressional stress contours in the epidermal/dermal papillae tissue layer of a harbor porpoise dorsal fin FEM for a front-mount tag. Based on inputs at a simulated swim speed of 2.2 m/s with 0° yaw and zero acceleration.

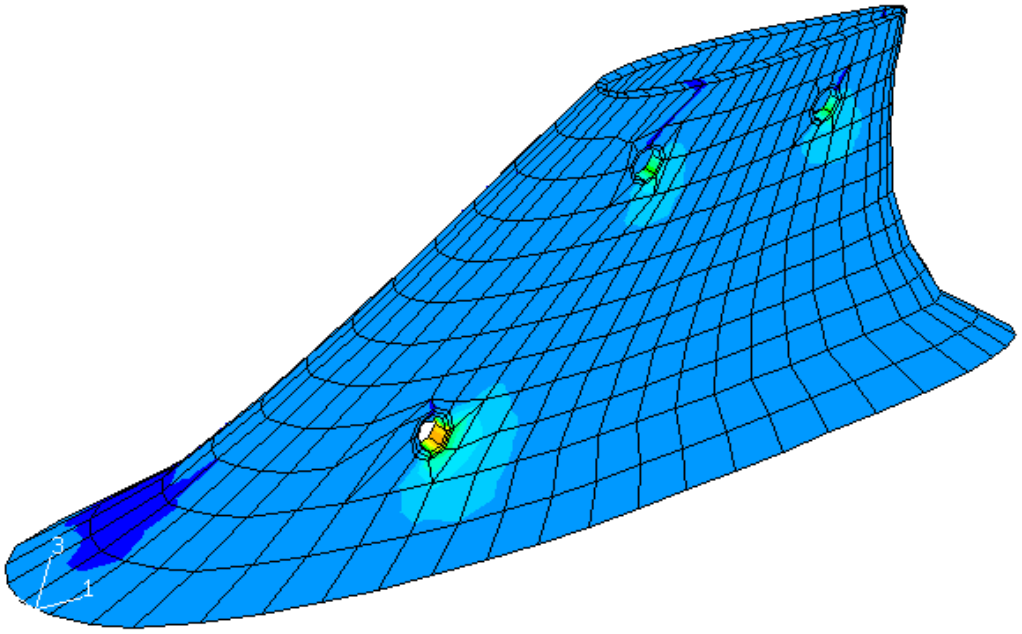

Figure 6.3b. Compressional stress contours in the epidermal/dermal papillae tissue layer of a harbor porpoise dorsal fin FEM for a single side-mount tag at a simulated swim speed of 2.2 m/s with 0° yaw and zero acceleration.

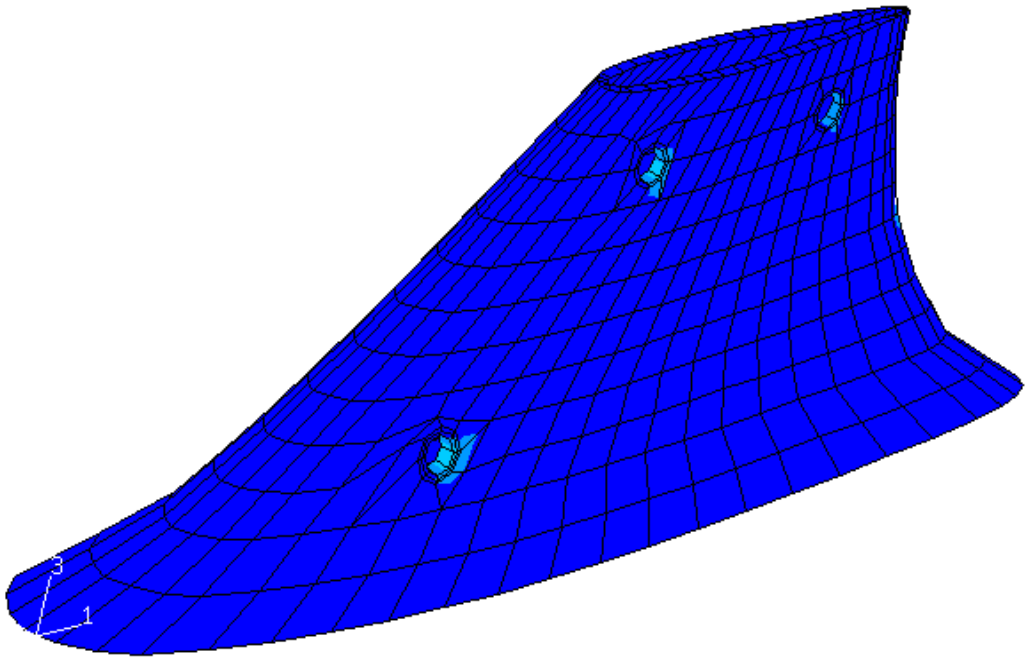

Figure 6.3c. Compressional stress contours in the epidermal/dermal papillae tissue layer of a harbor porpoise dorsal fin FEM for a paired side-mount tag at a simulated swim speed of 2.2 m/s with 0° yaw and zero acceleration.

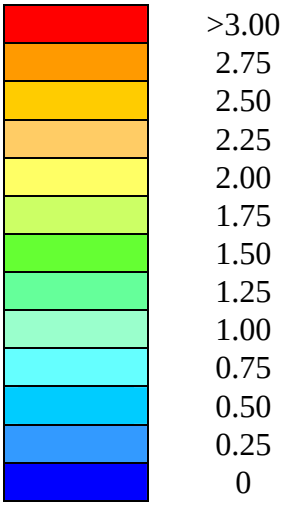

Figure 6.3d. Legend for maximum principal compressional stress contours (KPa).

Table 6.4. Estimated maximum principal compressional stress levels (KPa), for impact loads at the air/water interface. Inputs were based on an instantaneous velocity of 1.1 m/s using pre-transition moduli.

Tissue	Front-mount	Single side-mount	Paired side-mount
Epidermis/dermal papillae	1.61	0.65	0.15
Ligamentous sheath	0.91	0.18	0.05
Central core	0.81	0.39	0.01

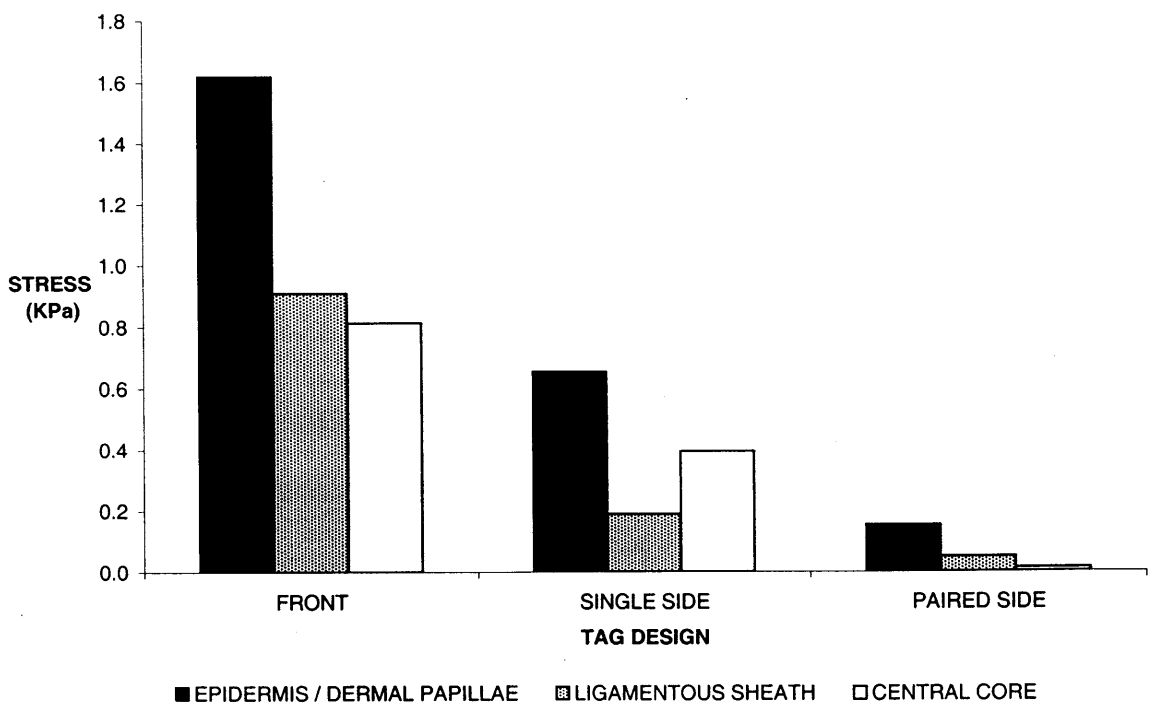

Figure 6.4. Estimated maximum principal compressional stress levels (KPa) for an impact load at the air/water interface. Values are based on an instantaneous velocity of 1.1 m/s using pre-transition moduli.

Table 6.5. Change in estimated maximum principal compressional stress levels (KPa) from acceleration to deceleration. An acceleration rate of $0.16 m/s^2$ and a deceleration rate of $-0.16 m/s^2$ were used based on an instantaneous velocity of 2.2 m/s, and using pre-transition moduli.

Tissue	Front-mount	Single side-mount	Paired side-mount
Epidermis/dermal papillae	0.13	0.94	0.44
Ligamentous sheath	0.09	0.24	0.15
Central core	0.09	0.76	0.49

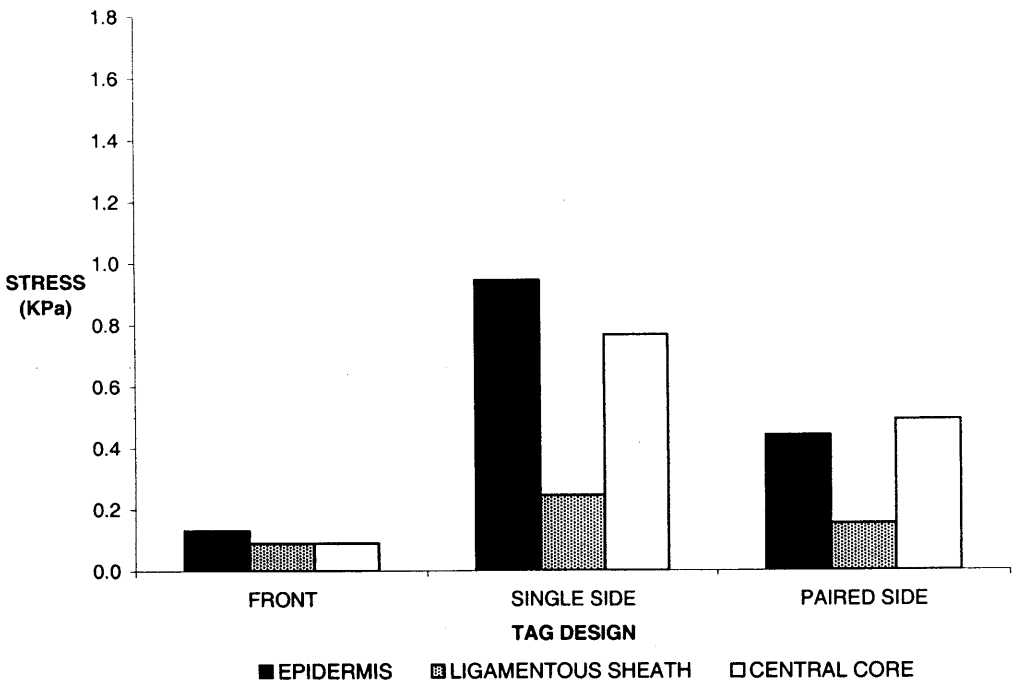

Figure 6.5. Change in estimated maximum principal compressional stress levels (KPa) from acceleration to deceleration. An acceleration rate of $0.16 m/s^2$ and a deceleration rate of $-0.16 m/s^2$ used at an instantaneous velocity of 2.2 m/s with pre-transition moduli.

side of the fin (Table 6.6, Figure 6.6). In general, the paired side-mount appeared to generate a slightly greater magnitude change in stress than the single side-mount, but for the single side-mount, both sides experienced decreases. The large changes displayed by the front-mount occurred primarily in the epidermis. The larger scale changes in the single side-mount tended to be in the epidermis or central core whereas the paired side-mount's changes occurred primarily in epidermis and ligamentous sheath.

Table 6.6. Change in estimated maximum principal compressional stress levels (KPa) between 0° and -10°. Models used inputs were associated with a velocity of 2.2 m/s, based on pre-transition moduli.

Tissue	Front-mount		Single side-mount		Paired side-mount	
	Right	Left	Right	Left	Right	Left
Epidermis/dermal papillae	3.65	-3.31	-1.44	-1.79	-0.48	2.20
Ligamentous sheath	1.03	-0.83	-0.41	-0.28	0.75	2.20
Central core	0.75	-0.90	-0.55	-1.03	-0.83	-0.76

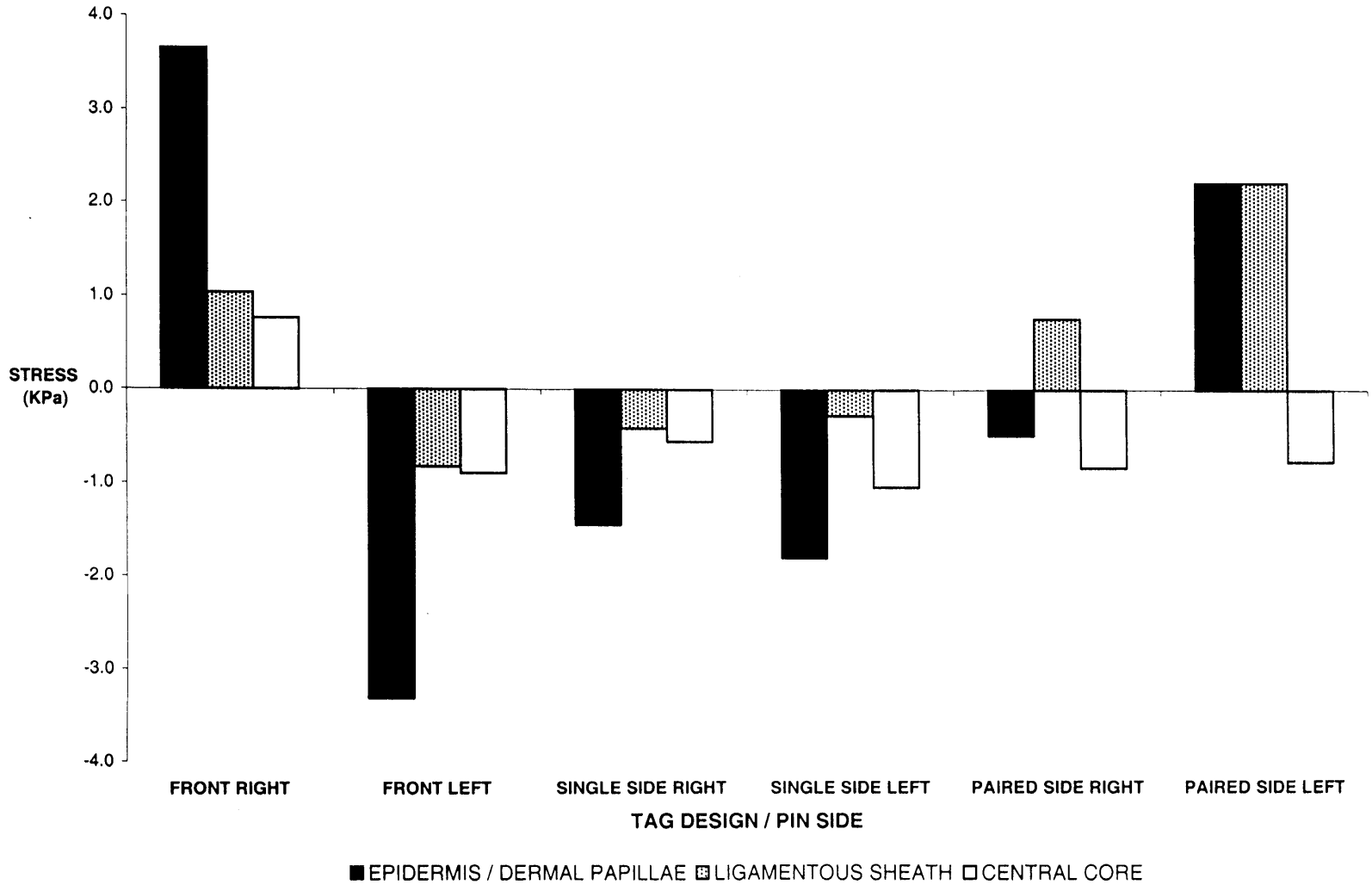

Figure 6.6. Changes in estimated maximum principal compressional stress levels (KPa) between 0° and -10°. Inputs were based on an instantaneous velocity of 2.2 m/s with on pre-transition moduli.

Discussion

The purpose of this study was to evaluate the stresses in dorsal fin tissue generated by static and dynamic loads from three different tag designs relative to their attachment durations. Although some variability exists within the results, there appears to be an inverse relationship with stresses developed for a given design and the duration of contact with a particular tag design observed from field studies. The front-mount design, which generally had shorter durations of contact (boto, 0-155 days, n=24, Martin and da Silva 1998; harbor porpoise, 2-21 days, n=5, Westgate and Read 1998), also generated the greatest stresses for the static load case and in two of the three dynamic load cases. The single side-mount tag, which has generally had longer durations of contact than the front-mount (boto, 0-290 days, n=10, Martin and da Silva 1998; harbor porpoise, 33-212 days, n=9, Westgate and Read 1998; 255 days, n=1, Larsen et al. in prep.) but shorter than the paired side-mount, had the highest magnitude stress differences for one of the dynamic load cases. The paired side-mount tag, which has demonstrated the longest attachment to date (Dall's porpoise, harbor porpoise, and bottlenose dolphins, 2-378 days, n=12, Chapter 7), either generated the lowest, or only moderate stresses.

Front-mount tag

The front-mount tag generated the highest static compressive stresses, the

largest magnitude impact loads at the air water/interface, and greatest changes in stress between 0° and -10° yaw, during turns. This design generated surprisingly high static stresses given that a much larger area, i.e., the leading edge of the fin, as well as larger diameter pins, supports its total load. The high impact loads that it generated are likely related to the fairly blunt surface area at the base of the tag. The high magnitude stresses that were generated for turns are likely the result of the tag developing a substantial moment relative to the center of the fin's axis of rotation. The low magnitude stress differences that developed during acceleration/deceleration are likely due to the truss-like support the saddle and pins formed around the leading edge of the fin. The relatively high stresses that occurred during typical swimming, impact at submergence, and turning, compared to the other tags, may be of particular significance because these were typically generated in the epidermis/dermal papillae and central core layers. Consequently, if these loads result in the tissues operating in the pre-transition region of their material properties, this likely means that these more highly vascularized tissues are bearing the greatest stresses.

Single side-mount tag

The relatively high stress concentrations the single side-mount developed are likely due to the moment associated with its asymmetrical design. It appeared to develop the greatest magnitude stress differences of all the tags for the acceleration/deceleration load case, which may be in part due to this moment.

However, the lack of any support structure between the pins on the side of the fin without the tag may allow for independent, dynamic, movement of the pins. The backing plate that Larsen et al. (in prep.) used on the opposite side of their side-mount may help explain the relatively long duration of contact they attained. Similar to the front-mount, the single side-mount appears to be generating substantial loads in the epidermal/dermal papillae layer. The low magnitude of the stress changes estimated during turning for the single side-mount might be due to a reduction in its moment, compared to the other two designs.

Paired side-mount tag

Although the paired side-mount tag did not generate the lowest stress changes in all cases, the lack of extremes in any of the load case scenarios may minimize its potential to damage tissue. The paired side-mount also generates moments, but its symmetrical design contributes to balancing these forces despite its greater momentum. The low impact stress this tag is estimated to generate is likely due in part to its streamlined shape. In addition, these lower stresses could be due to the material properties of the urethane used for the saddle on this design, because they are more similar to dorsal fin tissues than the thermoplastic or polycarbonate materials used for the saddles of the other two designs. This may reduce stress concentrations that the pin transmits to the tissue, performing a similar role to stress reduction regions

in percutaneous devices, as suggested by Grosse-Siestrup and Affeld (1984). Although the magnitude of the stress changes observed in the epidermis and ligamentous sheath for the paired side-mount are about the same magnitude as those developed by single side-mount in the epidermis, in the case of the former these large net changes are due to the relatively low static loads this tag develops in the 0° yaw position. The generally low stresses the single side-mount develops in the epidermis may be beneficial to maintaining the integrity of this layer, which is important because of the critical role it plays in preventing bacterial entry and infection (von Recum and Park 1981, Grosse-Siestrup and Affeld 1984, Geraci and Smith 1990). A combination of the saddle being contoured to fit the shape of the fin, the flexibility of the urethane saddle material, and the precision fit of the pin, saddle pinholes, and fin holes, may result in an epidermal seal similar to a percutaneous device with a stress reduction area. Some of these characteristics have been recommended to optimize the designs of percutaneous devices (see Grosse-Siestrup and Affeld 1984).

Limitations

There are numerous limitations associated with both the field studies to which comparisons have been drawn, and this modeling exercise, which are important to consider. The variability associated with differences in battery capacity and duty cycles used in the different tagging studies confounds the duration of transmitter

signal contact comparisons with the stresses generated by a given tag design. This is particularly true because most of these studies lacked resightings. In some studies the front-mount design was used initially and had either lower battery capacity or an increased duty cycle rate (Martin and da Silva 1998, Larsen et al. in prep.). Consequently, although there is still evidence that the previously outlined general trend of attachment duration relative to design is valid, some of the variability observed in these studies is due to differences in service life.

Part of any model's utility is its ability to simplify complex interactions. However, associated with this simplification process is the need to make assumptions and limit the scope of input variables. Consequently, there are several other sources of variability that may not have been possible to take into account and may affect tissue condition or tag attachment. The degree to which some of these simplifications, or restrictions on input variable ranges, potentially influenced analyses and their previously outlined significance are detailed below.

Material properties

The material properties used in this analysis were from normal tissues but several potential shortcomings associated with these tissues were noted (Chapter 5). In addition, several factors may act to modify the material properties of the fin tissues associated with tag attachment. The tag attachment is a combination of a wound

response to the surgical procedure of making the pin holes, as well as a foreign body response to a percutaneous device that is in contact with the tissue. Under the best of circumstances there will be an initial phase of acute inflation of about a week that precedes the deposition of any collagen (Woodward and Salthouse 1986). It then takes several weeks before encapsulation and the associated increase in strength from the greater amount and arrangement of collagen (in response to stress) to occur (Woodward and Salthouse 1986). Full strength is likely not attained for several months while cross-linking develops (Woodward and Salthouse 1986). Consequently, there is likely to be minimal strength at the tissue/pin interface initially before any increase in structural integrity occurs. Pressure on these tissues also has the potential to alter its structure. Although it has been well documented that controlled stress can increase the strength of a tissue (Sanders et al. 1995, Fischer 2000), it is important to note that dorsal fin tissues are unlikely to normally encounter the types of compressive loads that the pins typically generate. As a result, these tissues may respond differently. It is possible that the collagen fibers formed at these sites may be smaller than those normally occurring because fibers associated with load-bearing tissues such as cartilage are typically smaller than those in tendons (Kerr et al. 1999). In addition, there are differences in the component proteins of the ground substance in tissues under pressure (Reid and Flint 1974, Vogel 1995, Fisher 2000). Although the net effects are unclear, both of these factors may alter the tissue's material properties.

If necrosis does set in due to static or dynamic loads, or infection, the tissue

could be softer due to fluid accumulation and lack of collagen fiber development associated with chronic inflammation (Woodward and Salthouse 1986). Consequently, the tissue may be more deformable, such that its material properties would be weaker. This increased potential for deformation could potentially set up a viscous cycle of breakdown associated with dynamic loads. Rapid breakdown may increase the opportunity for bacterial access, resulting in infection. The irritation associated with an infection may also cause rubbing, with either factor leading to further tissue degradation.

A more fundamental problem of the material properties for a viscoelastic tissue may be associated with the appropriate region of the stress/strain relationship to use for model inputs. Although it is expected that the strains the tissues typically experience would likely be in the pre-transition region, it is possible that they could be in the post-transition region. However, there are several lines of evidence to suggest that these tissues typically operate in the pre-transition region. Most tendon-like tissues undergo irreparable damage at strains greater than 10% (Rigby et al. 1959). When porpoises surface to breathe there is no load, other than gravity, acting on the fin. No deformation of the dorsal fin is apparent in the anterior-posterior plane when the animal submerges, and although the fin does flex due to a bending moment during turns, the amount of elongation appears negligible. Elastin is known to allow large strains in other mammalian skin (Duck 1990), however, there appears to be no elastin in the ligamentous sheath of the dorsal fin (Chapter 5). Likely the best approach to

resolve the issue of which material property region is most appropriate in these types of analyses is to use more recent FEA software that allows the input of non-linear material properties.

Load cases

The load cases for tags used in this study are probably quite variable and potentially more complex than those analyzed here. Although this study likely identified many of the primary load cases, it is possible that it under- or over-estimated the magnitude of some, and missed others entirely. The impact loads that were estimated are at best a crude estimate of the true loads due to the complex shape (Xu et al. 1998) of the front of the tags. Because of the subjective nature of the estimate of each tag's drag coefficient (Chapter 2, 3), results of these analyses may be an artifact of the methodology used to estimate these loads. The loads associated with acceleration/deceleration are likely the most accurate of the dynamics loads examined. However, it is important to note that acceleration/deceleration changes occur over a wide variety of velocities compared to the single velocity used here. It is important to note that the frequency and magnitude of the heading changes these animals make, and their associated loads, are also unknown. These magnitudes have been estimated from wind tunnel data (Chapter 2, 3), and were based on an angle of attack of -10°, which may represent an overestimate.

All the models represent an idealized fit, assuming full contact of the pin and saddle, which may not have been the case in actual deployments on free-ranging animals. Whether the fit of the attachment in the actual tag deployments started out at a close tolerance, or what duration it may have remained in this condition, are unknown. However, if the tag does not have a close tolerance fit, momentum forces will magnify the expected dynamic loads. Several factors could cause this condition to occur. Compression of the foam padding between the saddle and the fin may result from pressure at depth, and this material is unlikely to fully recover as pressure is reduced. The front and single side-mount tags may be particularly susceptible to this problem. Improper pin hole alignment during tag application may cause initial pre-stresses in any or all of the tissue layers. Compressive stress concentrations may also occur due to over-tightening of the package, poor fit at the saddle/epidermal interface, or pressures during swimming. These problems may result in the redistribution of interstitial fluids in the tissues (Reddy 1986). Although the viscoelastic effects of creep and stress relaxation in tissues will generally reduce pressure concentrations (Gibson and Kenedi 1970), this may not be enough to reduce these stresses below those levels resulting in an adverse effect. The pressure that tags exert on the epidermis associated with the tightness of the fasteners at the time of attachment has never been quantified and likely varies between applications. The optimal pressure for securing attachments is unknown, as is the influence this may have had on tissue condition and attachment performance. There is likely a fine line between too much

pressure, and a tag that is loose enough for the effect of momentum during dynamic loading to cause stress peaks. Tags that do not conform to the shape of the fin would be predisposed to pressure concentrations. The single side-mount usually consists of a flat plate mounted on a curved dorsal fin. Consequently, there is a greater likelihood that it will have pressure concentrations than a front or paired side-mount, which are contoured to the fin. Because the front-mount is the only tag that wraps around the front of the fin, compression of the epidermal tissue during normal swimming may make it uniquely susceptible to this type of stress concentration. The potential for this problem is supported by the FEM for this tag that showed a stress concentration region near the top of the leading edge of the fin (Figure 6.3a). Although tissue will recover if the pressure is released, cyclic compression has shown to result in incomplete recovery of tissue deformation (Sakata et al. 1972).

A type of load that was not estimated but that likely occurs occasionally is associated with rubbing behavior (Bowers and Henderson 1972, Scott et al. 1990, Chapter 7). This behavior has the potential to generate extreme loads that exceed those examined in the current analysis. Front-mount tags are likely more vulnerable to this type of activity than are the other tags due to their more exposed position, potentially reducing their attachment durations not only due to tissue damage, but also due to attachment component failure (Read and Westgate 1997, Bloch et al. in prep.). Finally, because of the potential variability associated with these loads cases, this study was not able to fully account for each load's frequency of occurrence.

Consequently, a “stress budget” could not be estimated such that the contribution of each load case’s stress in the fin, and thus, its relative importance to tissue degradation, remains unclear at this time.

Pressure necrosis

One of the primary aspects of this study was to determine if the stresses that these models predicted for the different tags under a static load were sufficient to cause pressure necrosis. Pressure necrosis is typically thought to be the occlusion of blood flow, but other aspects of tissue function and structure may be impacted (Mak et al. 1994). The dorsal fin is an important thermoregulatory device such that blood flow might be able to be regulated, which may result in the mitigation of pressure necrosis. In addition, these animals dive to substantial depths such that the tissue and vascularization in their appendages may be more resistant to pressure than terrestrial animals. Despite the relatively high static pressure levels estimated for the front and single side-mount tags at an average swim speed, these were still less than those typically observed to cause occlusion of capillary blood flow (9-13 KPa) over extended periods in the skin of humans and other animals (Kosiak 1961, Dinsdale 1974, Sacks 1989). This pattern held true for either set of material properties, with the exception of the front-mounted tag’s stress on the epidermis in the post-transition region. While no pressure/duration relationship for ischemia has been determined for

dorsal fin tissues, in many respects their component layers resemble other mammalian tissues such that they might be expected to respond similarly to pressure. However, response to pressure may vary between tissues. For pressure sores in pigs, it was the deeper muscle tissue that broke down before the skin (Daniel et al. 1981). In addition, the large stress differences observed between most of the tissue layers for the front and single side-mount designs have the potential to create shear forces between these layers, which can reduce the pressure necessary to cause blood flow occlusion (Chow and Odell 1978, Bennett et al. 1979). Shear forces may also be a factor between tissue layers if the load is sufficient to result in a shift into the post-transition region because of the large differences between material properties in these two regimes.

Although pressure necrosis has generally been considered to be a result of occlusion of capillary blood flow, leading to hypoxia (Bader and Gant 1988) and the inhibition cellular waste product removal (Reddy 1986), it may result in additional effects on other aspects of tissue function. Mak et al. (1994) suggested that these effects may include changes in tissue hydrostatic pressure (Reddy 1986), reperfusion injury (Michel and Gillott 1990), and compromised interstitial transport processes (Reddy and Cochran 1981). An increase in tissue hydrostatic pressure may lead to increased cell contact and fibroblast inhibition (Reddy 1986), reducing collagen synthesis. Further, if the interstitial pressure is small and pressure is removed, the net effect may be the bursting of capillaries (Reddy 1986). Thus, although the stresses the tags generate appear to be below the threshold of blood flow occlusion, they may be

sufficient to affect other aspects of tissue health or strength.

Mechanical disruption of the healing process

The alternative factor under investigation was that tissue degradation, and subsequent pin out-migration, was due to the mechanical disruption of the healing process. This mechanical disruption has the potential to break the weak interfacial tissue bridges that are forming at the wound site (von Recum 1984) or cause focal vascular damage (von Recum 1984). Unfortunately, the magnitude, duration, and frequency of the force levels responsible for tissue breakdown have yet to be quantified in humans or other animal models (Urschel et al. 1988, Sanders et al. 1995, Fischer 2000). Consequently, the extent to which dynamic loads affect tissue condition remains unclear. However, there is evidence to suggest that dynamic loads may be associated with one component of the out-migration trajectories observed (Chapter 7). As noted previously, there appears to be a fine line between tissue adaptation and breakdown from loads on tissues (Sanders et al. 1995).

Conclusions

This study was the first attempt to evaluate load-related factors on tag attachment performance by quantitatively estimating the stresses the different designs

generate in dorsal fin tissues. The stress levels generated by the different tag designs generally reflect an inverse relationship with duration of attachment inferred by signal contact. However, there are numerous limitations associated with several of the assumptions and input values that will need to be improved to better understand this relationship. In particular, more accurate input data are needed on the material properties, and loads cases. While the results were not sufficient to unequivocally establish whether tissue degradation observed in field studies is due to pressure necrosis or the mechanical disruption of the healing process there is evidence that pressure necrosis may not be the primary factor associated with pin out-migration as previously suggested (Mate et al. 1995, Brill and Freidl 1993). The observed degradation may be more likely associated with dynamic loads. However, those aspects of tag design that are potentially related to static loads need to be given continued consideration, as are those that are likely associated with minimizing dynamic loads. Although this first generation FEM could benefit from the use of software that is specifically designed to allow analyses of dynamic load, this study has, at a minimum, succeeded in framing the question in the proper context and in identifying and highlighting many of the potential factors that may affect tag attachment. Future tag designs will hopefully benefit from careful consideration of these factors.

CHAPTER 7

ATTACHMENT PERFORMANCE OF A REDESIGNED SMALL CETACEAN TELEMETRY TAG SYSTEM

Introduction

Small cetaceans have been tagged with telemetry devices for over 30 years (see Norris et al. 1974, Leatherwood and Evans 1979, Dietz 1986, Scott et al. 1990 for reviews), but this technique has yet to gain its place as a standard research tool for these species (Reeves 1998). Premature signal loss, as a result of tag loss associated with breakdown of the dorsal fin tissue at the pin sites and subsequent pin out-migration (Irvine et al. 1982) is one problem that has likely discouraged researchers from fully embracing this technique. Until recently, dorsal fin mounted tags have typically remained attached (generally inferred from signal reception) for only a few days or weeks (Scott et al. 1990). While some recent efforts have yielded multi-month deployments (see Martin and da Silva 1998, Westgate and Read 1998, Larsen et al. in. prep.), some have experienced considerable variability in durations of signal contact compared to the expected durations. Like most previous tagging studies, the limited number of resights from more recent efforts has confounded a full assessment of the sources of variability associated with signal loss. Consequently, a lack of resights has contributed to the inability of most studies to identify the factors influencing signal loss. This limitation has likely resulted in the use of a wide variety of telemetry devices and attachment schemes, most of which have preformed poorly. The general

lack of reliability of these techniques, given the large investment required for captures and tags, has dissuaded many from using them such that only a relatively small number of animals have been tagged, further confounding a thorough analysis of this problem. In addition, reports of failures, while potentially of great benefit to other researchers, have typically not been published. The result has likely been the repetition of many of the same errors.

A lack of understanding of the failure modes of the tag systems has been demonstrated by the fact that little, if any, rationale is provided for the design of the instrument and attachment systems used in studies. Consequently, the reasons for "successes", as well as the failures, have remained unclear. The exception has been when resights of animals were made, because these data have been extremely important in determining the sources of failures. One of the problems identified early on was associated with degradation of the dorsal fin tissue (Irvine et al. 1979). Despite such observations, there has been a limited effort to identify the factors associated with this problem and no apparent attempts have been made to take these factors into account in tag redesigns.

One aspect of the problem that has been considered is tissue response to attachment materials. Summarizing the investigations of Bruce-Allen and Geraci (1985) and Geraci and Smith (1990) on small, dermal implants, Scott et al. (1990) noted the need for "a composite material that encourages growth in the implanted portion of the tag to immobilize the tag and prevent rejection, an epidermal seal to prevent wicking of pathogens, and an elasticity of the implanted portion which

matches that of the tissue but is strong enough to resist mechanical stress." A list of potential factors was developed by Brill and Friedl (1993), who noted three major concerns: attachment methods, tag reliability, and potential effects on the animals. For attachments, they noted that pressure necrosis, tag migration, and enlargement of holes with large or heavy transmitters were the important factors. Suggested research requirements included: material testing (mounts, biocompatible pins and antifouling treatments, etc.); flow dynamics testing (water flow around tag and tag mounts, migration of pins); "redesign of dorsal fin mount" (reflecting concerns about the role of fin vascularization in reproduction, see Rommel et al. 1992, 1993); and research into pin attachment and size and placement of the mount on the dorsal fin. For tag reliability, they suggested the use of both VHF and satellite transmitters with a potential for resights of coastal animals. In order to test the effects on the animals they suggested flow tank testing in order to develop an optimal design of the tag and its attachment. It was considered essential to test the tags on active animals, possibly with captive individuals, but ultimately on free-ranging animals, preferably on populations that have baseline movement data and that can be readily observed. In addition, they noted the need for tests on the physiological and energetic effects of tags, behavioral/social considerations, tissue damage and other health concerns (biocompatible materials research), and a failure analysis on existing tags. Most recently, Stone et al. (1998) noted only that size reduction in tags would solve retention problems.

In order to evaluate the factors influencing tag attachments relative to tissue degradation at pin sites, it was necessary to redefine the problem in terms of what the tag attachments actually are, i.e., percutaneous devices experiencing dynamic loads in an aquatic environment. For percutaneous devices, tissue degeneration might be expected to occur at these sites: 1) as a foreign body response due to the interaction of the pinning material and adjacent tissue (von Recum and Park 1981); 2) from infection due to a bacterial invasion of the wound (von Recum and Park 1981, Geraci and Smith 1990); 3) due to pressure necrosis, from chronic stress concentrations (Mak et. al. 1994); or 4) due to mechanical stresses disrupting the healing process (von Recum and Park 1981).

Previous studies to address tag retention factors only focused on the tissue response, i.e. foreign body response and infection (Geraci and Smith 1990). A systematic evaluation of the latter two factors, pressure necrosis and mechanical disruption of the healing process, was recently undertaken (Chapters 2,3,4,5,6). Because both of these factors are load-related, the focus of these recent efforts was to estimate the loads and evaluate their potential effect on the dorsal fin, and mitigate them through tag redesign. The initial step was to estimate the loads generated by the different tag designs under typical behaviors using a porpoise model in a wind tunnel (Chapter 2). This information and other basic engineering principles were used to redesign the tagging system (Chapter 3). Because the distribution of the loads these tags generate will be a function of the strength of the attachment materials as well as those of the fin tissues, a histological examination of the fin was undertaken to identify

those layers which would be expected to have unique material properties (Chapter 4). Based on the tissue types identified in that study, the strength of these layers was quantified with uniaxial testing (Chapter 5). Using the previously defined dorsal fin geometry (Chapter 4) and its material properties (Chapter 5) the stresses that three primary tag designs (Chapter 2, 3) potentially create in the fin tissue were estimated using a finite element analysis (Chapter 6). This report summarizes the final aspect of this project; to field test the redesigned tags (Chapter 3) on free-ranging animals to evaluate their attachment performance. Dall's porpoises (*Phocoenoides dalli*) and harbor porpoises (*Phocoena phocoena*) were tagged in the inland waters of Washington State, and bottlenose dolphins (*Tursiops truncatus*) were tagged on the central Atlantic coast of the U.S. (A. Hohn, unpubl. data). A tracking/resight effort was undertaken to evaluate the attachment performance of this system.

Methods and Materials

Capture and handling

Telemetry tags were deployed during opportunistic captures of three species of coastal small cetaceans between 1997 and 1999. In May of 1997, 1998, and 1999, the waters near the San Juan Islands were transited to locate Dall's porpoise, using a 7 m vessel with a 1 m bow platform extension. Using a breakaway hoop-net tethered to

the capture vessel, porpoise were captured while bow riding (see Ridgway 1966, Walker 1975, Asper 1975). The hoop was approximately 0.7 m in diameter and the net was constructed of 5 cm stretch-mesh knot-less nylon. As the porpoise surfaced next to the bow to breathe, the hoop was quickly placed in front of the animal such that it swam through the hoop, detaching the net (which surrounded the animal's body back to just behind the dorsal fin). The additional drag of the net slowed the animal substantially, but the design allowed the animal to still use its flukes to reach the surface to breathe. Approximately 25 m of line was attached from the net to the capture vessel to allow retrieval. Animals were maneuvered into a sling alongside the capture vessel and then the sling was transferred to a frame supported on each side by two small boats, similar to the porpoise chute system successfully used for dolphins in eastern tropical Pacific Ocean (Perrin et al. 1979). This system allows the animal to be partially supported in the sling by the water while the tag was attached.

In June 1998, areas where harbor porpoises have commonly been observed in the San Juan Islands were searched for concentrations of this species. When groups of porpoises were located, a specially designed gillnet was deployed from a 6.1 m vessel that had been outfitted to retrieve the net over the bow onto a hydraulic-powered reel. The net used measured 182 m in length and 9.1m deep, and was constructed of 30.5 cm (12") stretched mesh monofilament gillnet. The 1 cm corkline was equipped with white BL-S floats spaced every 1.1 m. The lead line used was the lightest commercially available, weighing 360 g/m (30lbs/100 fms). The net was set as a drift gillnet with one end attached to the reel, and a 4.2 m inflatable with an outboard

engine was used to check and, if necessary, disentangle the net to hang properly. Depending on the conditions of the tidal currents, the net orientation was kept linear by either occasionally backing the deployment boat or tying the 7.2 m tracking vessel off at the end opposite the deployment vessel. The net was only deployed in Beaufort sea states 0-2. The corkline was closely monitored for areas that were submerged, or had bunched corks, which might indicate an animal entanglement. The 4.2 m inflatable was used to investigate potential entanglements. This boat was equipped with a 10 cm thick open cell pad on the deck to serve as the processing platform for captured animals. This method of processing was similar to a method previously used during the capture of a harbor porpoise on the outer Washington coast (Osmek et al. in prep.). It provides non-rigid support for the porpoise and retains water on their flippers and flukes (that has been poured over them to keep their skin moist), which aids in thermoregulation.

In October 1998, a bottlenose dolphin was captured near Norfolk, Virginia using the hoop net procedure described previously for Dall's porpoise. Dolphins were also captured in November 1999 near Beaufort, North Carolina using a seine net technique previously used in Florida (Asper 1975, Irvine et al. 1982, Wells 1991). Dolphins were brought aboard a specially designed 7m boat with a low work deck where the animal was placed on foam padding and kept wet.

Instrument attachment was conducted as quickly as possible in order to minimize stress. Stress was monitored by timing the animal's respirations and observing general behavior.

Telemetry tags and attachments

The redesigned telemetry tags deployed on the porpoises and dolphins generally consisted of pair of tags mounted on the sides of the fin (Chapter 3). This pair of tags included either a satellite transmitter and a VHF transmitter or two VHF transmitters. Although the tags were of the same general design (Chapter 3), their component and attachment configurations varied slightly (Table 7.1, Chapter 3). Both sides of Tag 4 were equipped with a VHF transmitter (ATS, Isanti, MN). Tags 8, 15, and 16 consisted of a satellite transmitter (Telonics ST-10, Mesa, AZ) in the left side and a VHF transmitter on the right side. Three Dall's porpoises were equipped with Tag 4 in 1997, one with Tag 8 in 1998 and one in 1999, and two with Tag 16 in 1999. A harbor porpoise was also instrumented with Tag 8 in 1999. In 1998 and 1999, four bottlenose dolphins were equipped with Tag 15.

A pair of tags were attached with three or four 6.3 mm diameter acetal (Delrin), polyetherimide (Ultem 1000), or titanium (CP GR2) pins (Table 7.1), threaded on both ends to accept a 6 mm nut. The exception was one of the dolphins, which was tagged with only the right half of the tag. In this case, the pins on the left side of fin were backed with 39 mm diameter, 6.3mm thick, foam spacers against the

Table 7.1. Summary of tag designs and attachment systems deployed on porpoises and dolphins. Minimum duration of attachment based on telemetry signals or resights.

Animal number	Age class, sex	Tag design	Number of pins	Type of pins (6.3mm dia.)	Nut type (all 6 mm tread)	Expected service life - PTT (days)	Expected service life – VHF (days)	Minimum duration of attachment (days)
Dall's porpoise								
97-01	SAM	# 4	3	Delrin	High carbon jam		180 [a]	2
97-02	SAF	# 4	3	Delrin	High carbon jam		180 [a]	6
97-03	SAF	# 4	3	Delrin	Zinc plated nylock		180 [a]	4
98-02	SAM	# 8		Ultem 1000	Zinc plated nylock	90-120	150 [b]	5
99-01	SAM	# 16	4	Titanium	Zinc plated nylock	300	330 [b]	184
99-02	AF	# 16	3	Titanium	Zinc plated nylock	300	330 [b]	378
99-03	SAM	# 8	4	Delrin/ titanium**	Zinc plated nylock	90-120	150 [b]	21
Harbor porpoise								
98-02	AF	# 8	3	Titanium	Zinc plated nylock	90-120	150 [b]	215
Bottlenose dolphins								
FB 401	SAF	# 15	4	Delrin	Zinc plated nylock	90-120	180	194
FB 403	SAF	# 15 [c]	4	Delrin	Zinc plated nylock	90-120	30	159
FB 407	AF	# 15	4	Delrin	Zinc plated nylock	90-120	180	21
FB 408	SAM	# 15	4	Delrin	Zinc plated nylock	90-120	180	280

[a] based on warranty, assuming 25% time at surface [b] based on warranty [c] right side only

** tag attached with three Delrin pins and one titanium pin.

skin and stainless steel washer between it and the nut (A. Hohn, unpubl. data). The process for attaching the tags included application of a local anesthetic at the approximate site of the pins holes (bottlenose dolphins only). The tags were positioned on the fin and 18 gauge hypodermic needles were inserted through the pin holes and the fin tissue. This procedure generally allowed for the detection of major blood trunks prior to boring the pin holes. The primary purpose of these needles was to serve as alignment guides after the tags had been removed. Attachment pin holes were made with a tool similar to a laboratory cork borer, which had been cold sterilized. The pins were inserted in the holes and the tags positioned on the pins. The tags were secured with zinc plated-high carbon nuts next to a stainless steel flat washer, which acted as a corrodible link to allow the package to be released from the animal after the batteries were exhausted. Just prior to release, most porpoises also had suction-cup attached time depth recorder tags placed on their back. When possible, tagged porpoises were followed for several hours to monitor their condition.

Monitoring

Tag attachment duration and attachment condition were monitored by satellite location data received from Service Argos, reception of VHF signals, and directed or opportunistic resightings. Attachment duration was determined from satellite data, reception of VHF signals, or resightings. In the absence of satellite data, attempts were made to monitor VHF signals from boats, aircraft, or positions on land.

Opportunistic resights were obtained from local efforts incidental to photo-identification studies (bottlenose dolphins). Tag attachment condition for porpoises was monitored by direct efforts to periodically relocate the animals by their VHF signal from a boat, or opportunistic resight efforts. Relocations of porpoises were attempted approximately every other day by monitoring from boat, aircraft, or land during the first two weeks following release. Subsequent attempts were made to relocate them 1-2 times every two weeks. During the winter each good weather opportunity was utilized to attempt relocation. Attempts to relocate bottlenose dolphins were made at least monthly by monitoring the VHF tag's signals from boats or aircraft. Resights were also obtained during opportunistic encounters from a coast-wide network of researchers conducting photo-identification studies.

Results

The twelve small cetaceans, seven Dall's porpoise, one harbor porpoise, and four bottlenose dolphins, instrumented with this redesigned tagging system were documented to have durations of attachment that ranged from 2 to 378 days (Table 7.1). One tag remained attached for over a year, and five of the other deployments were verified to have exceeded five months. Of the other six, there is circumstantial evidence that suggests at least two remained attached for several months. Only one tag was documented to have suffered a failure of a component of the attachment

system. However, attachment failure was strongly suspected for a second tag. The fate of the other two tags is uncertain.

Of the six tags that were known to have remained attached for at least five months, two were observed to have had no attachment related problems. The longest duration was for a Dall's porpoise (Pd 99-02), which was resighted and radio-tracked periodically for 378 days. This duration represents the longest period a small cetacean has been monitored with a functioning telemetry device. Of additional significance was that no migration of the tag from its original attachment position on 12 May 1999 (Figure 7.1a) was apparent when the porpoise was last observed on 5 May 2000, 359 days after deployment (Figure 7.1b,c). The reason for signal loss was likely due to the VHF transmitter reaching the end of its service life. Similarly, when Dall's porpoise Pd99-01 was last resighted 184 days after tag attachment, its tag had not undergone any migration. Failure of the VHF transmitter antenna was suspected as the reason for subsequent signal loss.

In the cases of the five other long-term attachments, resights were made for three. Although the tags had remained attached, dorsal fin tissue degradation had developed as evidenced by pin migration. However, there were differences in the pin migration trajectories. Two of these tags were observed on the bottlenose dolphins (Mazzarella in prep., K. Rittmaster, pers. comm.), and based on the tag position, the pin migration trajectories were posterior-dorsal. When dolphin FB408 was resighted 280 days after deployment (Mazzarella in prep.), the tag was still attached but the posterior pins were no longer in the fin. Based on the position of the scar from the

Figure 7.1a. Tag position on the right side of Dall's porpoise 99-02 at time of capture, 12 May 1999. Note tag is approximately 10-15 mm back from leading edge.

Figure 7.1b. Right side of Dall's porpoise 99-02 on 30 April 2000. Note that tag position is in approximately the same location as on the day of attachment.

Figure 7.1c. Left side of Dall's porpoise 99-02 on 21 April 2000. Note that tag position is in approximately the same location as on the day of attachment.

front bottom pin, it appeared the tag had moved approximately 4.5 cm almost parallel to the leading edge of the fin. From the slow rate of migration it appeared the tissue in the migration track had healed. The other dolphin, FB403 was last observed 159 days after deployment with its single tag still attached (K Rittmaster, pers. comm.). However, even by 123 days post-deployment, photographs showed that this tag had migrated approximately 2.5 cm, with the bottom posterior pin out of the fin, and the fin bent over to the right side (K. Rittmaster, pers. comm.). By 13 July when it was next resighted it was missing the tag (Mazzarella in prep.). The fin had two approximately 5 cm migration tracks leading posterior-dorsally from the original position of the front pins. The length of the scars suggests that the tag remained attached for several more weeks. The pattern of the tracks were similar to those for FB408, both having migration trajectories almost parallel to the leading edge of the fin. The migration rate of the pins on FB403 appeared to be fast enough that that the tissue was not healed completely by the time the track was visible. In case of the harbor porpoise (98-02), the tag had migrated approximately 3.0 cm posterior-ventrally when it was observed 203 days after deployment. The last previous observation had been 143 days after attachment and no change in tag position had been apparent. The relatively slow rate of movement and the appearance of light-colored tissue in the pin tracks suggested that the tissue was healing following migration.

Two of the other deployments, one on a Dall's porpoise and one on a bottlenose dolphin are suspected to have lasted several months. Approximately 5

months after all the Dall's porpoises were tagged in 1997 and the signals subsequently lost, an anonymous report was received from a fishermen near Victoria, British Columbia of a Dall's porpoise with a "light-colored" tag on its dorsal fin. Although the signals from all these porpoises were lost in less than a week, this signal loss was thought to have been the result of a faulty saltwater switch design, rather than an attachment failure, because similar problems were later detected on some of the other tags that had not been deployed. In the second case, the tags from a bottlenose dolphin (FB407) that had been tagged in November 1999 in North Carolina were recovered on a beach in Virginia in December 2000 (A. Hohn, unpubl. data.). Two factors suggest that the tag had remained attached long-term. One was that the ventral, posterior pin still connected the two tags, indicating that it had migrated out of the fin, a process that been observed on other animals to take several months. The second was that four barnacles (base diameter 5-7 mm) had settled in the unused alternate posterior pin sites. These recesses are the only sites marine growth has been observed to get a foothold on these tags while on the animals and their relatively large size suggests that it would take several months to grow to that size even if they settled immediately after deployment.

Only one attachment failure was documented, although in another instance, a similar outcome was strongly suspected. For Dall's porpoise 99-03, the satellite transmitter was observed missing 13 days after deployment, but the VHF tag was still attached. From close proximity resightings, it appeared that the attachment nuts were still present such that the urethane fairing would have most likely failed. The lack of

VHF signals in the general area 23 days after tagging suggests that the VHF transmitters detached too. In the other instance, both signals were lost from Dall's porpoise 98-02 within 10 days of deployment. The last satellite transmitter signal was six days after attachment and no signals from the VHF transmitter were received in an aerial check four days later. The porpoise was last observed three days before satellite transmitter signal loss and the VHF signal was received one day before satellite transmitter signal loss.

Discussion

The purpose of this study was to evaluate the attachment performance of a redesigned small cetacean tag system. It was observed that this telemetry system remained attached for longer than any other system without necessarily causing tissue damage to the dorsal fin. The previous record for duration of attachment of a functioning transmitter was 290 days on a boto (*Inia geoffrensis*), however no resight information was reported to assess the fin condition at that time (Martin and da Silva 1998). The resight observations showing that the tag remained in place on a Dall's porpoise for 378 days demonstrated that the four previously noted factors which are known or suspected to cause tissue breakdown had at least been minimized, or potentially overcome.

One of these factors is a foreign body response due to the interaction of the pinning material and adjacent tissue. Titanium is used extensively in humans due to

its good biocompatibility qualities (Keller and Lautneschaler 1986). Although an acute foreign body response (followed by extrusion) was observed for titanium in the skin of small cetaceans, it was suggested that the rejection of this material had little to do with its physical properties (Geraci and Smith 1990). Similarly, although stainless steel had the most severe reaction in the same implant study, this same material yielded one of the longest attachment durations recorded for cetaceans when used as the attachment pins for a killer whale tag (4.5+ months, Erickson 1978). No information is available on chronic foreign body response for titanium. Delrin (acetal) pins like those used in the bottlenose dolphins and some of the porpoises have never been tested in a controlled implant study but would be expected to have minimal effects like other similar polyolefin polymers (Leininger and Bigg 1986). Although a foreign body response does not appear likely to play a dominant role in tissue degradation, careful consideration should be given to the biocompatibility of the materials used for the attachment pins.

A second, and potentially more significant factor that may cause tissue breakdown is infection. The potential seriousness of this problem is emphasized by the observation that only the complete removal of the percutaneous device allowed for healing to proceed in lab studies (von Recum and Park 1981). All pins and coring tools used in this study were, at a minimum, cold sterilized to minimize this potential infection vector. Although this factor has not been reported in tagged free-ranging small cetaceans (Irvine et al. 1982, Martin and da Silva 1998), it has been documented in association with the rejection of a number of materials implanted in captive

bottlenose dolphins and beluga whales, *Delphinapterus leucas* (Geraci and Smith 1990). They attributed the infections to bacteria being carried in with the implant or deposited from the water that bathed the opening. As a potential mitigation they suggested that a collar should be designed to provide a tight seal at the surface of the skin. The contoured fit to the dorsal fin of the redesigned tag in this study, combined with the urethane's flexibility and its close tolerance fit with the pins, may have acted as an epidermal seal, preventing infection.

A third factor that may result in tissue breakdown is pressure necrosis. This type of tissue degradation has been suggested as the source of tissue degeneration in small cetacean tagging studies (Brill and Friedl 1993, Mate et al. 1995). The design of these tags attempted to minimize this factor by streamlining the tags to reduce drag loads and using a paired design on the sides of the fin to reduce forces associated with moments. A finite element analysis suggests that this tag design would be the least likely to generate pressures sufficient to cause pressure necrosis due to blood flow occlusion (Chapter 6). Nonetheless, blood flow occlusion may occur at levels below those estimated in the finite element model (Chow and Odell 1978, Bennett et al. 1979) and there are several other adverse impacts that could be related to the effects of pressure (Reddy et al. 1981, Reddy 1986, Michel and Gillott 1990). Some of these factors may also affect tissue material properties (Reid and Flint 1974, Vogel 1995, Kerr et al. 1999). The potential for the influence of these aspects suggests continued implementation of tag design factors that may reduce pressure necrosis.

The fourth factor that could cause tissue breakdown is the mechanical disruption of the weak bonds that are forming during the tissue healing process (von Recum and Park 1981). The load levels that can cause this breakdown are unknown (Urschel et al. 1988, Sanders et al. 1995, Fischer 2000). In addition to bond breakage, small-scale vascular damage may also result from these mechanical disruptions (von Recum 1984), and similarly, the load levels that can cause these are unknown. This mechanical disruption is likely associated with dynamic loading. The redesign of this tag was an attempt to mitigate the potential effects of dynamic loads by potting the transmitters in a urethane whose material properties were close to those of the fin tissue (Chapter 5), and using a close tolerance fit between the pin, pin hole in the tag, and pin hole in the fin (Chapter 3). A finite element analysis that examined dynamic load cases suggested that, compared to other designs, this design minimizes the effect of impact on the tissues at the air/water interface (Chapter 6). Impact loading that occurs due to submergence at the air/water interface has a vertical force component that may account for the dorsal portion of the pin migration trajectories observed in spinner and bottlenose dolphins (Norris and Dohl 1980, Irvine et al. 1982, Mazzerella in prep., K. Rittmaster, pers. comm.). Despite the relative infrequency of this type of loading compared to other dynamic loads, tissue in this plane may be more vulnerable to degradation. This vulnerability is likely due in part to the weakness of the central core tissue layer of the dorsal fin in this orientation, and the inability of the ligamentous sheath to support compressive loads (Chapter 5). This result suggests that dynamic loads may be the primary factor associated with pin migration. However,

like static loads, the dynamic loads free-ranging animals experience are likely of numerous types. In addition to impact loads, two other types of dynamic loads were apparent from data obtained from the velocity meter on time-depth recorders attached to porpoises and from observations of free-ranging animals. These included acceleration/deceleration during swimming (Appendix A) and yawing during turns. Because the magnitude of the forces necessary to break these weak bonds (Urschel et al. 1988, Sanders et al. 1995, Fischer 2000), or cause small-scale vascular damage (von Recum 1984) is unknown, the effects of these dynamic loads are unclear. Consequently, design efforts should focus on reducing the angle of the front of the tag at the base of the fin to minimize the force of the impact load vectors. In addition, continued emphasis should be placed on maximizing the stability of tag attachments in order to minimize the effect of momentum associated with dynamic loads. It is also possible that reducing tag size, as noted by Stone et al. (1998), could potentially decrease the effect of dynamic loading two ways. One aspect has to do with a dynamic load known as the acceleration reaction (Daniel 1984). Not only are greater forces associated with increasing velocity and acceleration of tag mass, but it is also necessary to accelerate the mass of the displaced fluid, i.e., the acceleration reaction (Vogel 1994, Denny 1988). This ‘added mass’ will depend on the object’s shape, as well as its volume (Vogel 1994). As a result, tag volume is also a factor in the loads it generates. It has been noted that added mass plays a role in limiting the size of organisms in a wave swept environment (Denny et al. 1985). Thus, there may be an upper limit to tag volume relative to the strength of the dorsal fin tissue, attachment

pin number, and size. The greater volume of the bottlenose dolphin's tags compared to the Dall's porpoise tags may have played a role in the pin migration observed with the dolphin tags. A second potential aspect is related to the size of the "footprint" of the attachment pins. By reducing the tag size, and the distance between pins, the relative amount of strain might be reduced.

Another type of impact load that may have affected tag attachment duration is related to rubbing behavior. If an animal rubs on the bottom substrate, the associated impact load has the potential to be extremely high, possibly causing tissue damage (Torzilli et al. 1999), or tag component damage or failure. The observed loss of the PTT on Dall's porpoise 99-03 was most likely due to rubbing. The loss of both transmitter signals from Dall's porpoise 98-02 five days after tagging also strongly suggests an attachment failure due to rubbing. The reason these porpoises lost their tags and harbor porpoise 98-02 (which had evidence of rubbing) did not, was that all three of the pins in the latter's attachment were titanium versus all but one being plastic for the two former animals (Table 7.1). Despite an attempt to mitigate rubbing loss by reducing the acute angles on the front of the tag as part of its streamlining, this design is still vulnerable to attachment failure. Although it is unclear why only some of these animals rubbed their tags, it is possible that they may have been experiencing some discomfort. While there is likely some sensation associated with the healing process (Woodward and Salthouse 1986), this may be accentuated if pressure concentrations or looseness exists due to poor fit, or if an infection has developed.

This underscores the need to prevent infection and use shape(s) that fit the contours of the fin.

Like some previous studies, a substantial amount of variability was associated with attachment duration in this study. Some of this was explainable based on transmitter or attachment component failure. However, while some aspects of the variability in the long-term attachment durations were consistent with expectations, others were not. The observation of the shorter attachment of the single side-mount compared to the paired side-mount on the bottlenose dolphin is consistent with the higher stresses estimated in the finite element analysis for this single side-mount (Chapter 6). The greater stresses it generates are likely due to its greater moment, a factor associated with its asymmetrical design. However, it is not clear why the tags remained in the same position on the Dall's porpoise 99-02 for over a year, while the tags on the bottlenose dolphin FB408 had begun migrating at nine months. In two regards, this outcome was the opposite of what might have been expected. Dall's porpoises are noted for their fast swimming behavior (Law and Blake 1994), such that they likely have higher average velocities compared to bottlenose dolphins. In addition, this fast swimming behavior commonly occurs at, or near, the surface (roostertailing), such that wave drag and impact loads would be substantially greater. Therefore, the tags would be expected to generate greater static and dynamic loads in Dall's porpoise dorsal fin tissues. Consequently, if these factors were underlying tissue degeneration, tag migration or loss would have been expected to occur sooner, or at a faster rate on Dall's porpoises. In addition, the tag on the Dall's porpoise that

remained in position for over a year was attached with only three pins, all titanium, compared to the four Delrin pins on the bottlenose dolphins. The fewer, stiffer, pins in the Dall's porpoise would been expected to cause greater stress concentrations in the tissues, such that pin migration would have been expected to be observed in that species first. Three possible explanations for this apparent inconsistently might be related to differences in pin material, tissue structure, or loading related to the position on the fin. As noted previously, the tissue response of Delrin (acetal) has never been tested in small cetaceans. Although there is a possibility that a foreign body response may have occurred, this material has been used extensively in these species, such that this factor is considered unlikely. It is also possible that the material properties of Dall's porpoise and bottlenose dolphin dorsal fins, may be significantly different, although neither have been tested. However, the larger size of the bottlenose dolphin fins would suggest that these fins require greater support, such that the tissue layers of the dolphin would be expected to have greater strength. The most plausible reason for the observed inconsistency is that the tags were mounted much higher on the fins of the bottlenose dolphins (A.Hohn unpubl. data) such that the fins were more susceptible to a bending moment. This additional flexing potentially could result in more movement at the pin/tissue interface such that these greater dynamic loads may be more likely to cause tissue breakdown.

An additional aspect of the observed variability that appears to be inconsistent is the apparent delayed onset of pin migration. The tissue surrounding the pins might be expected to be in its weakest state just after tag attachment. This is because it takes

a few weeks before collagen synthesis and deposition begins as part of the wound response (Woodward and Salthouse 1986). In addition, it takes several months before a tissue's full strength is attained (Woodward and Salthouse 1986). Consequently, it might be expected that the tissues are most vulnerable to breakdown during the first few weeks following deployment and thus, pin migration might be expected to be most readily manifested during that period. However, if necrosis sets in, the tissue's strength may actually decrease such that there is a potential for a cycle of tissue degradation to begin. Although the pressure from tag load would not change during this time, tag fit could gradually loosen, with a cycle of accelerating tissue breakdown, due to gradually increasing dynamic loads, associated with greater momentum. Additional tag deployment studies with frequent monitoring will be needed to address this issue.

This study has demonstrated that the redesigned tag has the capability to remain attached to a small cetacean for over a year without apparent damage to the dorsal fin. Keeping a telemetry tag on a small cetacean for this duration is an important milestone because animal movements and habitat use are typically assumed to follow annual cycles. In addition, maintaining an attachment for a year without tissue damage is important because any long-term impacts to the animal have likely been minimized, such that its health and behavior have not been compromised. Although tissue damage was observed on some animals, in the case of some (bottlenose dolphins) these attachment durations represented a substantial improvement over other designs and previous studies. Additional studies are needed

to better understand the variability that was observed. An approach that combines a component that builds on previously developed models (Chapter 6) and field deployments that incorporate a dedicated resight/tracking effort are most likely to make advances to this important research tool. In particular, resight data will be extremely valuable in guiding future tag design refinements.

CHAPTER 8

CONCLUSIONS AND RECOMMENDATIONS

Conclusions

This was the first study that has attempted to comprehensively identify and quantify the factors related to the duration of telemetry tag attachments in small cetaceans. Its most notable achievement was the development of a new tag design concept that attempted to take these factors into account. When this tag design was deployed, it appeared to provide consistently longer tag attachment durations than other designs, and in some cases, did so with little or no tissue damage.

While this study has succeeded in identifying some of the important factors affecting these tag attachments it has also demonstrated that the factors that affect tag attachment are both numerous and complex. In the process of carrying out this study, deficiencies in the currently available data became apparent. In addition, areas were identified that exceeded the scope of this study. Throughout these analyses it was necessary to make numerous assumptions. Some of these assumptions were based on a substantial amount of accurate data, while others were based on data that were only approximations. In other cases data were limited or completely lacking, resulting in the use of educated guesses. Taken together, the uncertainties represent areas that require additional research. While the assumptions used in these analyses may be faulted, the overall framework of the approach appears valid. It is hoped that this work will encourage other researchers to make a paradigm shift and take a more

appropriate perspective toward the challenge of tagging small cetaceans. For those that are stimulated to undertake future investigations, the following aspects and approaches are recommended to better illuminate many of the factors influencing small cetacean tag attachment durations.

Recommendations

Chapter 2

- Collect additional velocity TDR data from free-ranging animals to determine variability between animals and different species. The use of TDRs equipped with accelerometers, to measure the frequency and magnitude of direction changes, would be most valuable.

- Quantify impact loads for different tag designs via lab-based drop tests.

- Conduct further full-scale model testing in the 190-290 Pa dynamic pressure range, particularly using flow visualization in order to investigate the generally observed drag decrease as well as the large degree of variability in the results associated with this region.

- Undertake glide deceleration studies on captive animals by temporarily attaching the tags. This will provide an important validation to the data obtained in the wind tunnel.

- Use a smaller wind tunnel with a more sensitive drag balance to measure tag drag with greater accuracy, particularly at lower dynamic pressures, which may be more representative of these animal's typical swim speeds. The use of a smaller tunnel with a model of the fin-only and tags will be useful to investigate the effect of tags on the fin's ability to generate lift as well as the degree to which the tag itself generates lift. The use of urethane dorsal fins should be considered in order to try to approximate chord-wise flexing during turns.

- The relatively high drag levels observed suggest that there could be a considerable energetic cost associated with carrying a tag by porpoises. This could best be evaluated by metabolic studies on captive animals to directly measure this cost.

Chapter 3

- Most of the reccomendations outlined for Chapter 2 also apply to Chapter 3. However, several addition aspects deserve study.

- Conduct additional mockup testing which incorporate current and next generation satellite transmitter hardware.

- Determine the potential for antenna streamlining while maintaining, or enhancing performance and structural integrity, particularly the stress reduction region at the base of the antenna.

Chapter 4

- Use dorsal fins for subsequent histological analyses from freshly dead animals. These should preferably be from a source such as animals taken incidental to commercial fisheries, with initial preservation by fixation rather than freezing to provide the best results.

- Conduct additional histological studies using stains specific to nerves to determine their distribution.

- More comprehensive analyses should be conducted within fins to determine if regional differences exist in collagen density and arrangement. Similar analyses would be beneficial for examining the variability within species, particularly between sex and age classes. These analyses should include

histology, percent collagen composition, vascular distribution, as well as a quantitative approach to determining predominant collagen fiber angles.

- Due to the variety of species being instrumented with telemetry devices, some, if not all of the previously noted analyses would be beneficial for a comparison between species, particularly Dall's porpoise and bottlenose dolphins.

Chapter 5

- Additional tissue material property testing should be conducted, preferably using dorsal fins that are fresh and from healthy specimens, such as animals taken incidental to commercial fishing operations.

- More tissue sites should be tested within fins. This may require the use of smaller tissue samples.

- Experiment with new gripping techniques to reduce slippage. This is particularly important for the central core due to the high lipid content of this tissue layer.

- Conduct biaxial or triaxial tissue testing. Material properties estimates could likely be improved by these methods because the collagen fiber orientation of

these tissues, particularly the central core, is anisotropic. In addition, because the dorsal fin tissues are typically being subjected to compressive loads by the attachment pins, compression testing may provide a valuable perspective.

- Explore other parameter estimation procedures. Although the spline-fitting routine used in this study performed well, the sum of squares tended to be dominated by the post-transition values. A smoothing function may be a more robust approach to determining these values.

- Conduct a comparative study of material properties from the fins of other commonly tagged small cetaceans, particularly Dall's porpoise and bottlenose dolphins. Differences in fin sizes and velocities of different species of small cetaceans suggest that there may be differences between the strength of the tissue layers of their fins.

Chapter 6

- Examine a wider range of loads cases. In particular, examinations of attachment performance under extreme loads associated with rubbing would be desirable.

- Develop a true dynamic model that simultaneously incorporates pre- and post-transition material properties using more advanced FEA software.

- Models should also include forces due to the acceleration reaction.

- Develop models for other tags that have been relatively large sample sizes and good resight histories.

Chapter 7

- Evaluate transmitter performance, identify failure modes of components and redesign tags accordingly.

- Conduct additional tagging studies with dedicated resight efforts on populations in areas that are relatively accessible, such that resight information is maximized.

- Tag designs used in future studies should be based on previously proven designs and use transmitter components with a reliable track record of performance. Any design or material changes should be specifically justified. Small, seemingly benign changes can have catastrophic consequences.

- Redesign tags to minimize static loads. Basic hydrodynamic principles should be used to minimize drag, i.e., a fineness ratio of less than 10:1 and tapering the leading and trailing edges. However, extending the tag anterior and posterior to the leading and trailing edges of the fin should be avoided due to the substantial moments that may be generated during turns.

- Redesign tags to minimize effects of dynamic loads. Decrease the transition angle between the ventral face of the tag and the dorsal fin. Locate pins to act more like a truss relative to this load vector. Tags should be positioned closer to the base of the fin to minimize the moment associated higher positions. Explore the availability of pin materials that have material properties closer to those of the dorsal fins but maintain a high shear strength. Similarly, lower durometer urethanes should be considered for tag saddles.

- Conduct captive studies of tissue response similar to those of Geraci and Smith (1990), but use load bearing percutaneous devices.

- Develop corrodible links that better match the transmitter service life. A key aspect will be the need to incorporate a locking mechanism that does not require excessive pressure from tightening the attachment. Alternatively, the potential for use of biodegradable materials for pins should be investigated.

- Attempt to improve biocompatibility, and possibly reduce loading, by revisiting the use of fine-mesh porous materials as sleeves for attachment pins.

LIST OF REFERENCES

Alexander, R. McN. 1975. Biomechanics. Chapman and Hall, London. 62 pp.

Anderson, D.D., D.J. Adams, and J.E. Hale. 2000. Mechanical effects of forces acting on the bone, cartilage, ligaments, and tendons. Pp. 283-306, in B.M. Nigg, B.R. MacIntosh, and J. Mester (eds.), Biomechanics and the biology of movement. Human Kinetics, Champaign, IL.

Anderson, J.M., and P.A. Kerrebrock. 1997. The Vorticity Control Unmanned Undersea Vehicle – An autonomous vehicle employing fish propulsion and maneuvering. Pp.189-195, in Tenth International Symposium on Unmanned Untethered Submersible Technology: Proceedings of the Special Section on Bio-engineering Research Related to Autonomous Underwater Vehicles. September 7-10, Autonomous Undersea Systems Institute, Durham, NH.

Asper, E.D. 1975. Techniques of live capture of smaller Cetacea. J. Fish. Res. Bd. Can. 32:1191-1196.

Bader, D.L, and C.A. Gant. 1988. Changes in transcutaneous oxygen tension as a result of prolonged pressures at the sacrum. Clin. Phys. Physiol. Meas. 9:33-40.

Bannasch, R. 1995. Hydrodynamics of penguins - an experimental approach. Pp. 141-176, in P. Dann, I. Norman, and P. Reilly (eds.), The Penguin. Surrey Beatty and Sons, Berlin.

Bannasch, R. 1996. Zur strömungsdynamischen Formoptimierung von Telemetriegeräten für Schweinswale (*Phocoena phocoena*). Meer and Museum 12:11-16.

Bannasch, R., R.P. Wilson, and B. Culik. 1994. Hydrodynamic aspects of design and attachment of a back-mounted device in penguins. J. Exp. Biol. 194:83-96.

Bennett, L.D., Kavner, B.K. Lee, and F.A. Trainor. 1979. Shear vs pressure as causative factors in skin blood flow occlusion. Arch. Phys. Med. Rehabil. 60:309-14.

Bennett, M.B., R. F. Ker, and R. McN., Alexander. 1987. Elastic properties of structures in the tails of cetaceans (*Phocoena* and *Lagenorhynchus*) and their effect on the energy cost of swimming. J. Zoo., Lond. 211:177-192.

Blackwell, S.B., C.A. Haverl, B.J. LeBoeuf, and D.P. Costa. 1999. A method for calibrating swim-speed recorders. Mar. Mamm. Sci. 15(3): 894-905.

Blake, R.W. 1983. Fish Locomotion. Cambridge University Press, Cambridge, U.K.

Bloch, D., M.P. Heide-Jørgensen, E. Stefansson, R. Dietz , L. Andersen, B. Mikkelsen and, L. H. Ofstad. In prep. Short-term movements of pilot whales around the Faeroe Islands.

Bowers, C.A., and R.S. Henderson. 1972. Project Deep OPS: Deep object recovery with pilot and killer whales. NUC TP 306. Undersea Surveillance and Oceans Sciences Dept., Naval Undersea Center, San Diego, Calif. 86 pp.

Brill, R.L., and W.A. Friedl. 1993. Reintroduction to the wild as an option for managing Navy marine mammals. Naval Command, Control and Ocean Surveillance Center, RDT&E Div. Tech. Rept. 1549.

Bruce-Allen, L.J., and J.R. Geraci. 1985. Wound healing in the bottlenose dolphin (*Tursiops truncatus*). Can. J. Fish. Aquat. Sci. 42:216-228.

Buckwalter, J.A. 1996. Effects of early motion on healing of musculoskeletal tissues. Hand Clinics 12(1):13-24

Carson, F.L. 1997. Histotechnology. ASCP Press, Chicago. 304 pp.

Chow, W.W., and E.I. Odell. 1978. Deformations and stresses in soft body tissues of a sitting person. J. Biomech. Eng. 100:79-87.

Croll, D.A., S.D. Osmek, and J.L. Bengtson. 1991. An effect of instrument attachment on foraging trip duration in chinstrap penguins. Condor 93: 777-779.

Culik, B.M., R. Bannasch, and R. Wilson. 1994. External devices on penguins: how important is shape? Mar. Biol.(Berl.) 118:1851-1855.

Daly, C.H. 1982. Biomechanical properties of dermis. J. Invest. Dermatol. 79:17s-20s.

Daniel, R.K., D.L. Priest, and D.D. Wheatley. 1981. Etiologic factors in pressure sores: an experimental model. Arch. Phys. Med. Rehabil. 62:492-98.

Daniel, T.L. 1984. Unsteady effects of aquatic locomotion. Amer. Zool. 24:121-34.

Davis, R.W., G.A.J. Worthy, B. Würsig, and S.K. Lynn. 1996. Diving behavior and at-sea movements of an Atlantic spotted dolphin in the Gulf of Mexico. Mar. Mamm. Sci. 12(4):569-581.

Denny, M.W. 1988. Biology and the mechanics of the wave-swept environment. Princeton University Press, Princeton, NJ. 329 pp.

Denny, M.W., T.L. Daniel, and M.A.R. Koehl. 1985. Mechanical limits to size in wave-swept organisms. Eco. Mono. 55(1):69-102.

Dietz, R. 1986. A feasibility study on satellite and VHF tracking of marine mammals. Unpubl. rept. to the Commn. for Sci. Res. in Greenland and Greenland Fish. and Enviro. Res. Inst. 94 pp.

Dinsdale, S.M. 1974. Decubitus ulcers: role of pressure and friction in causation. Arch. Phys. Med. Rehabil. 55(4):147-52.

Duck, F.A. 1990. Physical properties of tissue. Academic Press, San Diego, CA.

Elsner, R., J. Pirie, D.D. Kenney, and S. Schemmer. 1974. Functional circulatory anatomy of cetacean appendages. Pp.143-159, in R. J. Harrison, (ed.), Functional anatomy of marine mammals. Vol. 2. Academic Press, London.

Erickson, A.W. 1978. Population studies of killer whales (*Orcinus orca*) in the Pacific Northwest: A radio-marking and tracking study of killer whales. Natl. Tech. Inform. Serv. Rep. No. PB-285615. 34 pp.

Evans, W.E. 1974. Radio-telemetric studies of two species of small cetaceans. Pp. 385-394, in W.E. Schevill (ed.), The whale problem: A status report. Harvard Univ. Press, Cambridge, MA.

Felts, W.J.L. 1966. Some functional and structural characteristics of cetacean flippers and flukes. Pg. 255-276, in K.S. Norris (ed.), Whales, dolphins and porpoises. University of California Press, Berkeley.

Fischer, K.J. 2000. Biological response to forces acting in the locomotor system. Pp. 307-329, in B.M. Nigg, B.R. MacIntosh, and J. Mester (eds.), Biomechanics and the biology of movement. Human Kinetics, Champaign, IL.

Fish, F.E., and J.J. Rohr. 1999. Review of dolphin hydrodynamics and swimming performance. Technical Report 1801, SPAWAR Systems Center, San Diego. 136 pp.

Fraser, F.C. 1952. Handbook of R.H. Burne's cetacean dissections. British Museum (Natural History), London. 70 pp.

Fung, Y.C. 1993. Biomechanics: mechanical properties of living tissues. Springer-Verlag, New York. 568 pp.

Geraci, J.R., and G.J.D. Smith. 1990. Cutaneous response to implants, tags, and marks in Beluga whales, *Dephinapterus leucas*, and bottlenose dolphins, *Tursiops truncatus*. Pp. 81-95, in T.G. Smith, D.J. St. Aubin, and J.R. Geraci, (eds.), Advances in research on the beluga whale, *Dephinapterus leucas*. Can. Bull. Fish. Aq. Sci. 224.

Geraci, J.R., D.J. St. Aubin, and B.D. Hicks. 1986. The epidermis of odontocetes: a view from within. Pp. 3-21, in M.M. Bryden and R. Harrison (eds.), Research on dolphins. Clareden Press, Oxford.

Gibson, T., and R.M. Kenedi. 1970. The structural components of the dermis and their mechanical characteristics. Pp. 19-38, in W. Mountagna (ed.), The Dermis. Appleton – Century- Croft, NY.

Gollwitzer, R.M. and R. Petersen. 1996. Drop tests and planing boat dynamics modeling for investigating repeated water-entry shock mitigation. Proceedings, small craft marine engineering, Resistance and Propulsion Symposium, Ann Arbor, MI. 10 pp.

Green, R.F. 1972. Observations on the anatomy of some cetaceans and pinnipeds. Pg. 247-297, in S.H. Ridgway (ed.), Mammals of the sea, biology and medicine. C.C. Thomas Publisher, Springfield, IL.

Grosse-Siestrup, C., and K. Affeld. 1984. Design criteria for percutaneous devices. J. Biomed. Mat. Res. 18:357-382.

Hansen, A.G. 1987. Dynamic similarity. Pp. 157-158, in S.P. Parker, (ed.), Fluid dynamics source book. McGraw-Hill Book Company. New York.

Hanson, M.B., and R.W. Baird. 1998. Dall's porpoise reactions to tagging attempts using a remotely deployed suction-cup tag. Mar. Tech. Soc. J. 32(2):18-23.

Harris, B. 1980. The mechanical behavior of composite materials. Symp. Soc. Exp. Biol. 34:37-74.

Hoerner, S.F. 1965. Fluid dynamic drag. Published by the author. Bricktown, New Jersey, v.p.

Hooker, S.K., and R.W. Baird. 1999. Deep-diving behaviour of the northern bottlenose whale, *Hyperoodon ampullatus* (Cetacea: Ziiphidae). Proceedings of the Royal Society of London B. 266:671-676.

Irvine, A.B., M.D. Scott, R.S. Wells, J.H. Kaufmann, and W.E. Evans. 1979. A study of the activities and movements of the Atlantic bottlenosed dolphin, *Tursiops truncatus*, including an evaluation of tagging techniques. U.S. Dep. Commer., Natl. Tech. Inform. Serv., Rep. No. PB298042. Available from NTIS, 5285 Port Royal Road, Springfield, VA 22167.

Irvine, A.B., R.S. Wells, and M.D. Scott. 1982. An evaluation of techniques for tagging small odontocete cetaceans. Fish. Bull. U.S. 80:135-143.

Keller, J.C., and E.P. Lautenschlager. 1986. Metals and alloys. Pp. 3-23, in A.F. von Recum (ed.), Handbook of biomaterials evaluation, scientific, technical, and clinical testing of implant materials. Macmillan. NY.

Kerr, R.F. 1999. The design of soft collagenous load-bearing tissues. J. Exp. Biol. 202:3315-3324.

Kosiak, M. 1961. Etiology of decubitus ulcers. Arch. Phys. Med. Rehabil. 42:19-29.

Krouskop, T.A., P.C. Noble, and S.L. Garber. 1983. The effectiveness of preventive management in reducing the occurrence of pressure sores. J. Rehabil. Res. Dev. 20(1):74-83.

Larsen, F., J. Teilmann, and G. Desportes. in prep. Satellite tracking of harbour porpoises (*Phocoena phocoena*) in Danish waters.

Law, T.C., and R.W. Blake. 1994. Swimming behaviors and speeds of wild Dall's porpoises (*Phoeonoides dalli*). Mar. Mamm. Sci. 10: 208-213.

Leatherwood, S., and W.E. Evans. 1979. Some recent uses and potentials of radio-telemetry in field studies of cetaceans. Pp. 1-31, in H. E. Winn and B. L. Olla (eds.), Behavior of marine animals, Vol. 3. Plenum Press.

Leininger, R.I., and D.M. Bigg. 1986. Polymers. Pp. 24-37, in A.F. von Recum (ed.), Handbook of biomaterials evaluation, scientific, technical, and clinical testing of implant materials. Macmillan. NY.

Mak, A.F.T, L. Huang, and Q. Wang. 1994. A biphasic poroelastic analysis of the flow dependant subcutaneous tissue pressure and compaction due to epidermal loadings: Issues in pressure sore. J. Biomech. Eng. 116:421-429.

Martin, A.R., and V.M.F. da Silva. 1998. Tracking aquatic vertebrates in dense tropical rainforest using VHF telemetry. Mar. Tech. Soc. J. 32(1):82-88.

Martin, H., W.E. Evans, and C.A. Bowers. 1971. Methods of radio tracking marine mammals in the open sea. Pp. 44-49, IEEE 1971 Conf. Eng. Ocean Environ.

Mate, B.R., K.A. Rossbach, S.A. Nieukirk, R.S. Wells, A. B. Irvine, M.D. Scott, and A.J. Read. 1995. Satellite-monitored movements and dive behavior of a bottlenose dolphin *(Tursiops truncatus*) in Tampa Bay, Florida. Mar. Mamm. Sci. 11(4):452-463.

Mazzarella, K. In prep. Movement patterns of Beaufort freezebranded bottlenose dolphins in Roanoke Sound, North Carolina.

Mercer, E.H., R. John, and H. Maibach. 1968. Surface coat containing polysaccharides on human epidermal cells. J. Invest. Dermatol. 51:204–214.

Michel, C.C., and H. Gillott. 1990. Microvascular mechanisms in stasis and ischaemia. Pp. 153-163, in D.L. Bader (ed.), Pressure sores: Clinical practice and scientific approach. MacMillian Press, London.

Mullin, L. 1980. Theories of rubber-like elasticity and the behaviour of filled rubber. Symp. Soc. Exp. Biol. 34:274-288.

Nachtigall, W. 1981. Hydromechanics and biology. Biophys. Struct. Mech. 8:1-22.

Nigg, B.M. 2000. Forces acting on the human body. Pp. 253-282, in B.M. Nigg, B.R. MacIntosh, and J. Mester (eds.), Biomechanics and the biology of movement. Human Kinetics, Champaign,IL.

Norris, K.S., and K.W. Pryor. 1970. A tagging method for small cetaceans. J. Mamm. 51(3):609-610.

Norris, K.S., and T.L. Dohl. 1980. Behavior of the Hawaiian spinner dolphin, *Stenella longirostris*. Fish. Bull. U.S. 77(4):821-849.

Norris, K.S., W.E. Evans, and G.C. Ray. 1974. New tagging and tracking methods for the study of marine mammal biology and migration. Pp. 395-408, in W.E. Schevill (ed.), The whale problem: A status report. Harvard Univ. Press, Cambridge, Mass.

Norris, K.S., B. Würsig, R. S. Wells, M. Würsig, S. M. Brownlee, C. Johnson, J. Solow. 1985. The behavior of the Hawaiian spinner dolphin, *Stennella longirostris*. NOAA, NMFS Admin. Rept. LJ-85-06C.

Obrecht III, H.H., C.J. Pennycuick, and M.R. Fuller. 1988. Wind tunnel experiments to assess the effect of back-mounted radio transmitters on bird body drag. J. Exp. Biol. 135:265-273.

Orr, J., D.J. St. Aubin, P.R. Richard, and M.P. Heide-Jørgeson. 1998. Recapture of belugas, *Delphinapterus leucas*, tagged in the Canadian arctic. Mar. Mamm. Sci. 14(4):829-834.

Osmek, S.D., M.B. Hanson, and R.L. DeLong. In prep. First directed live-capture and movements of a harbor porpoise from the northeast Pacific Ocean.

Özkaya, N., and M. Nordin. 1999. Fundamentals of biomechanics: equilibrium, motion, deformation. Van Nostrand Reinhold, New York. 393 pp.

Pabst, D.A., S.A. Rommel, and W.A. McClellan. 1999. The functional morphology of marine mammals. Pg. 15-72, in J.E. Reynolds III and S.A. Rommel (eds.), Biology of Marine Mammals. Smithsonian Institution Press, Washington.

Papir, Y.S., K-H. Hsu, and R.H. Wildnauer. 1975. The mechanical properties of the stratum corneum. I. The effect of water and ambient temperature on the tensile properties of newborn rat stratum corneum. Biochim. Biophys. Acta 399:170-180.

Parry, D.A.D., and A.S. Craig. 1984. Growth and development of collagen fibers in connective tissues. Pp. 34-64, in A. Ruggeri and P.M. Motta (eds.) Ultrastructure of the connective tissue matrix. Martinus Nijhoff, Boston.

Perrin, W.F., W.E. Evans, and D.B. Holts. 1979. Movements of pelagic dolphins, (*Stenella* spp.) in the eastern tropical Pacific as indicated by results from tagging with a summary of tagging operations, 1969-1976. NOAA Tech. Rept. NMFS SSRF-737.

Potts, R.O., and M.M. Breuer. 1983. The low-strain viscoelastic properties of skin. Bioeng. Skin 4:105-114.

Purves, P.E. 1969. The structure of the flukes in relation to laminar flow in cetaceans. Z. Saeugertierkd 34(1):1-8.

Purves, P.E., W.H. Dudok van Heel, and A. Jonk. 1975. Locomotion in dolphins. Part I: Hydrodynamic experiments on a model of the bottle-nosed dolphin, *Tursiops truncatus*, (Mont.). Aq. Mamm. 3:5-31.

Rae, Jr., W.H., and A. Pope. 1984. Low-speed wind tunnel testing. John Wiley and Sons, New York.

Read, A.J. 1999. Harbor porpoise, *Phocoena phocoena*, (Linnaeus, 1758). Pg. 323-355, in S.H. Ridgway and R. Harrison (eds.), Handbook of marine mammals,Vol. 6. The second book of dolphins and porpoises. Academic Press, Harcourt, Brace and Co., San Diego, CA.

Read, A.J., and D.E. Gaskin. 1985. Radio tracking the movements and activities of harbor porpoises, *Phocoena phocoena* (L.), in the Bay of Fundy, Canada. Fish. Bull. 83(4):543-552.

Read, A.J., and A.J. Westgate. 1997. Monitoring the movements of harbour porpoises (*Phocoena phocoena*) with satellite telemetry. Mar. Biol. 130:315-322.

Reddy, N.P. 1986. Mechanical stress and viability of the skin and subcutaneous tissue. Pp. 215-241, in A. R. Hargens (ed.), Tissue nutrition and viability. Springer-Verlag, NY.

Reddy, N.P., and G.V.B. Cochran. 1981. Interstitial fluid flow as a factor in decubitus ulcer formation. J. Biomech. 14(12):879-881.

Reid, T. and M.H. Flint. 1974. Changes in glycosaminoglycan content of healing rabbit tendon. J. Embrol. Exp. Morphol. 31:489-95.

Reeves, R.A. 1998. History of marine mammal tagging. Pp. 28-36, in G.S. Stone, H.C. Tausig, and J.R. Schubel (eds.), Marine animal telemetry tags. New England Aq. Aquatic Forum Series Rept. 98-3.

Ridgway, S.H. 1966. Dall's porpoise, *Phocoenoides dalli* (True): observations in captivity and at sea. Norsk Hvalfangst-Tidende 55:97-110.

Rigby, B.S., N. Hirai, J.D. Spikes, and H. Eyring. 1959. Mechanical properties of the rat tail tendon. J. Gen. Phyiol. 43:265-83.

Rommel, S.A., D.A. Pabst, W.A. McLellan, J.G. Mead, and C.H. Potter. 1992. Anatomical evidence for a counter current heat exchanger associated with dolphin testes. The Anatomical Record 232:150-156.

Rommel, S.A., D.A. Pabst, and W.A. McLellan. 1993. Functional morphology of the vascular plexus associated with the cetacean uterus. The Anatomical Record 237:538-546.

Ross, M.H., and E.J. Reith. 1985. Histology: a text and atlas. Harper and Row, New York, NY. 766 pp.

Sacks, A.H. 1989. Theoretical prediction of a time-at-pressure curve for avoiding pressure sores. J. Rehab Res. Dev. 26:27-34

Sakata, K., G. Parfitt, and K.L. Pinder. 1972. Compressive behaviour of a physiological tissue. Biorheology 9(3):173-84. .

Sanders, J.S., B.S. Goldstein, and D.F. Leotta. 1995. Skin response to mechanical stress: adaptation rather than breakdown – A review of the literature. J. Rehab. Res. Dev. 32(3):214-226.

Sandor, B.I. 1972. Fundamentals of cyclic stress and strain. Univ. of Wisconsin Press. 167 pg.

Scott, M.D., R.S. Wells, A.B. Irvine, and B.R. Mate. 1990. Tagging and marking studies on small cetaceans. Pp. 489-514, in S. Leatherwood and R.R. Reeves (eds.), The Bottlenose Dolphin. Academic Press, San Diego.

Scott, M.D., A.J. Read, R.S. Wells, D.A. Pabst, W.A. McClellan, A.J. Westgate, F.I. Townsend, H.L. Rhinehart, and M.B. Hanson. In prep. Dorsal fin morphology and radio-tag attachment on small cetaceans.

Simpson, J.E., and M.B. Gardner. 1972. Comparative microscopic anatomy of selected marine mammals. Pg. 298-418, in S.H. Ridgway (ed.), Mammals of the sea, biology and medicine. C.C. Thomas Publisher, Springfield, IL.

Sokolov, V.E. 1982. Mammal skin. University of California Press, Berkeley. 695 pp.

Stewart, B.S., P.H. Thorson, and P.K. Yochem. 1995. Development of a satellite – linked radio-transmitter package for small cetaceans. Abstract only, Eleventh Biennial Conf. on the Bio. of Mar. Mamm., 14-18 Dec. 1995. Orlando, FL. Pg. 110.

Stone, G.S., H.C. Tausig, and J.R. Schubel (eds). 1998. Marine animal telemetry tags. New England Aq. Aquatic Forum Series Rept. 98-3.

Streeter, V.L, E.B. Wylie, and K.W. Bedford. 1998. Fluid Dynamics. WCB McGraw Hill, Boston, Massachusetts.

Tanaka, S., K. Takao, and N. Kato. 1987. Tagging techniques for bottlenose dolphins, *Tursiops truncatus*. Nippon Suisan Gakkaishi 53(8): 1317-1325.

Thompson, S.W., and R.D. Hunt. 1966. Selected histochemical and histopathological methods. C.C. Thomas, Springfield IL. 1639 pp.

Torzilli, P.A., R. Grigiene, J. Borelli, Jr., and D.L. Helfet. 1999. Effect of impact load on articular cartilage: Cell metabolism and viability, and matrix water content. J. Biomech. Eng. 121:433-441.

Tramaglini, D., D.L. Powers, and J. Black. 1993. The influence of flange compliance and mechanical loading on the tissue response to percutaneous devices. J. Appl. Biomat. 4:183-194.

Urschel J.D., P.G. Scott, and H.T. Williams. 1988. The effect of mechanical stress on soft and hard tissue repair; a review. Br. J. Plast. Surg. 41(2):182-6

Venables, W.N., and B.D. Ripley. 1994. Modern applied statistics with S-Plus. Springer-Verlag, New York. 462 pp.

Vincent, J.F.V. 1982. Structural biomaterials. Halsted Press, John Wiley and Sons, New York. 206 pp.

Vogel, K.G. 1995. Fibrocartilage in tendon: a response to compressive load. Pp. 205-215, in S.L. Gordon, S. J. Blair, L.J. Fine (eds.), Repetitive motion disorders of the upper extremity. Am. Acad. Orthorpaedic Surgeons. Rosemount IL.

Vogel, S. 1994. Life in moving fluids: the physical biology of flow. Willard Grant, Boston.

von Mises, R. 1945. Theory of flight. Dover Publications, New York.

von Recum, A.F. 1984. Applications and failure modes of percutaneous devices: a review. J. Biomed. Mater. Res. 18:323-336.

von Recum, A.F., and J.B. Park. 1981. Permanent percutaneous devices. Crit. Rev. Bioeng. 5(1):37-77.

Wainwright, S.A., W.D. Bigg, J.D. Currey, and J.M. Gosline. 1982. Mechanical design in organisms. Princeton University Press, Princeton, NJ. 423 pp.

Walker, B.G., and P.L. Boveng. 1995. Effects of time-depth recorders on maternal foraging and attendance behavior of Antarctic fur seals (*Arctocephalus gazella*). Can. J. Zool. 73:1538-1544.

Walker, W.A. 1975. Review of the live-capture fishery for smaller cetaceans taken in southern California waters for public display. J. Fish. Res. Bd. Can. 32:1197-1211.

Webb, P.W. 1975. Hydrodynamics and energetics of fish propulsion. Bull. Fish. Res. Bd. Can. 190:1-158.

Wells, R.S. 1991. The role of long-term study in understanding the social structure of a bottlenose dolphin community. Pp. 199-225, in K.S. Pryor and K.S. Norris (eds.), Dolphin societies, discoveries and puzzles. Univ. of California Press. Berkeley, CA.

Westgate, A.J., and A.J. Read. 1998. Applications of new technology to the conservation of porpoises. Mar. Tech. Soc. J. 32(1):70-81.

Wildnauer, R.H., J.W. Bothwell, and A.B. Douglas. 1971. Stratum corneum biomechanical properties. I. Influence of relative humidity on normal and extracted human stratum corneum. J. Invest. Dermatol. 56(1):72-78.

Williams, T.M. 1987. Approaches for the study of exercise physiology and hydrodynamics in marine mammals. Pp. 127-145, in A.C. Huntley, D.P. Costa, G.A.J. Worthy and M.A. Castellini (eds.), Approaches to marine mammal energetics, Spec. Pubs. Soc. Mar. Mamm. No 1. Allen Press, Kansas.

Williams, T.M., R.W. Davis, L.A. Fuiman, J. Francis, B.J. Le Boeuf, M. Horning, J. Calambokidis, and D.A. Croll. 2000. Sink or Swim: Strategies of cost-efficient diving by marine mammals. Science 288:133-136.

Woodward, S.C., and T.N. Salthouse. 1986. The tissue response to implants and its evaluation by light microscopy. Pp. 364-378, in A.F. von Recum (ed.), Handbook of biomaterials evaluation, scientific, technical, and clinical testing of implant materials. Macmillan, NY.

Würsig, B. 1982. Radio tracking dusky porpoises in the south Atlantic. Pp. 145-160, in Mammals in the seas, Vol 4. FAO Fish Ser. No. 5.

Xu, L., A.W. Roesch, and R. Peterson. 1999. Asymmetric hydrodynamic impact and dynamic response of vessels. J. Offshore Mech. and Arct. Eng. 121:83-89.

Yasui, W.Y. 1980. Morphometrics, hydrodynamics, and energetics of locomotion for a small cetacean, *Phocoena phocoena* (L.). Unpubl. Master's thesis, Univ. of Guelph. 86 p.

APPENDIX A

ESTIMATES OF FREE-RANGING HARBOR PORPOISE VELOCITIES

Velocity data were collected from a free-ranging harbor porpoise using a suction-cup attached time-depth recorder (TDR) equipped with a velocity turbine (Mk6, Wildlife Computers, Redmond, WA). The TDR and a VHF transmitter were housed in a syntactic foam body that allowed the tag to be located when released (Hanson and Baird 1998). A 164 cm female harbor porpoise was captured by gillnet entanglement for dorsal fin transmitter attachment on 16 June 1998 near Pt. Doughty, Orcas Island, Washington State. When the porpoise was released this tag was placed on her back. The tag remained attached for 38.7 hr as the porpoise moved within Presidents Channel and the southern Strait of Georgia. Depth and velocity readings were recorded every second and temperature was recorded every 5 seconds.

Velocity was estimated based on the assumption that 600 rpm= 1 m/s (Blackwell et al. 1999). However, disruptions of the flow into the turbine can affect the accuracy of the velocity readings (Blackwell et al. 1999). Because flow into the turbine inlet may be disrupted by the close anterior proximity of the hub of the suction cup that attaches the tag to the porpoise, an underestimate of the porpoise's true velocity may result. In addition, differing flow regimes (laminar versus turbulent), which are dependent on the animal's velocity (Fish and Rohr 1999) and position of the tag on the body, may also alter the flow through the turbine (Blackwell et al. 1999). A technique to calibrate TDR velocity was developed by Blackwell et al. (1999). Data

calibrated from this deployment indicate that the TDR may have been underestimating velocity by approximately 15% during this deployment. However, the uncorrected velocity values were used in the wind tunnel analysis as a conservative estimate of velocity.

An examination of the velocity data over the entire data record suggested that during approximately the first hour post-release the porpoise swam faster than the subsequent 37.7 hours, presumably as a response to the capture/restraint. A histogram of the resulting 134,666 velocity readings is shown in Figure A.1. The distribution of these values was bimodal with peak values at approximately 0.6 and 1.9 m/s. The median velocity was 1.25m/s, with 90% of the speeds being between 0.4 and 2.3 m/s. The maximum velocity was 6.5 m/s. The peaks appear to be associated with surfacing behavior and diving behavior, respectively, as illustrated by the example from 1600-1700 hr shown in Figure A.2. Approximately 11% of the velocity readings were zero and coincided with logging behavior of the porpoise at the surface. Although this type of behavior has been documented for some tagged harbor porpoises (Read and Gaskin 1985), it underestimates the velocities for the near surface dives between deep dives for animals that actively swim most or all of the time. Because the resolution of the depth sensor was $\pm$2m, and the large variation between surface water and deep-water temperatures caused the depth sensor to lag the true depth readings, it was not possible to know exactly when the porpoise surfaced, or the velocities associated with each surface/dive event.

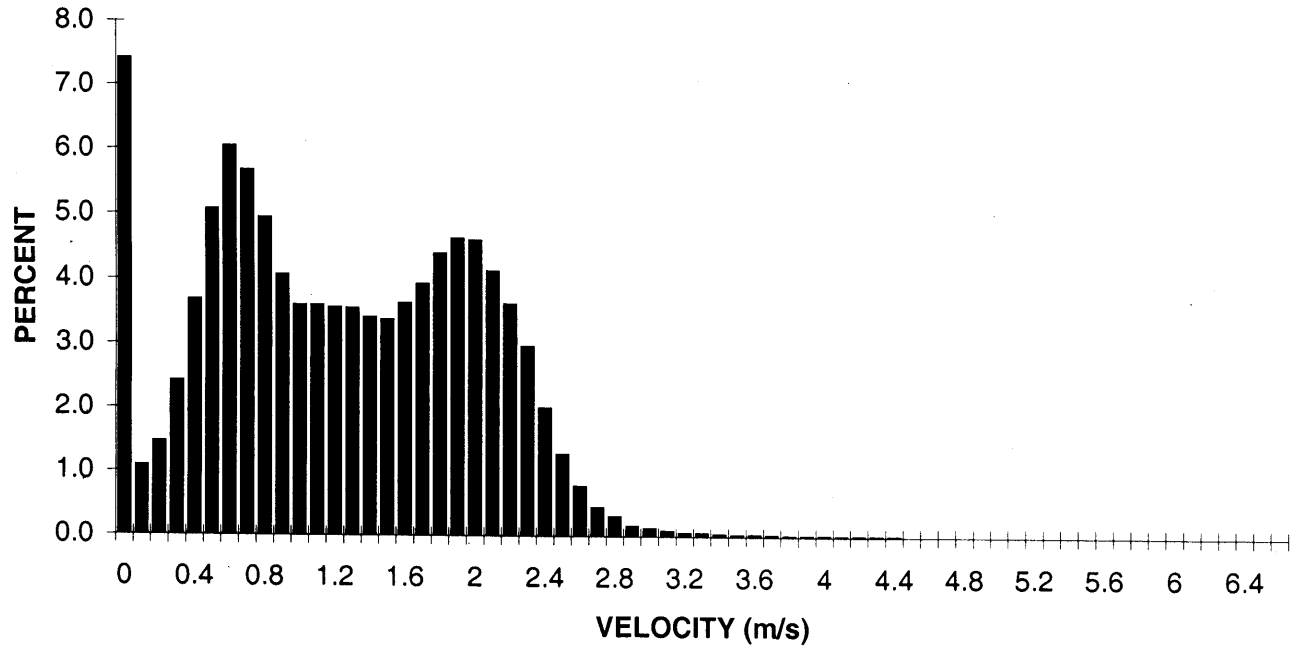

Figure A.1. Frequency distribution of velocity readings obtained from a time–depth recorder during 37.7 hours of a deployment on a free-ranging harbor porpoise.

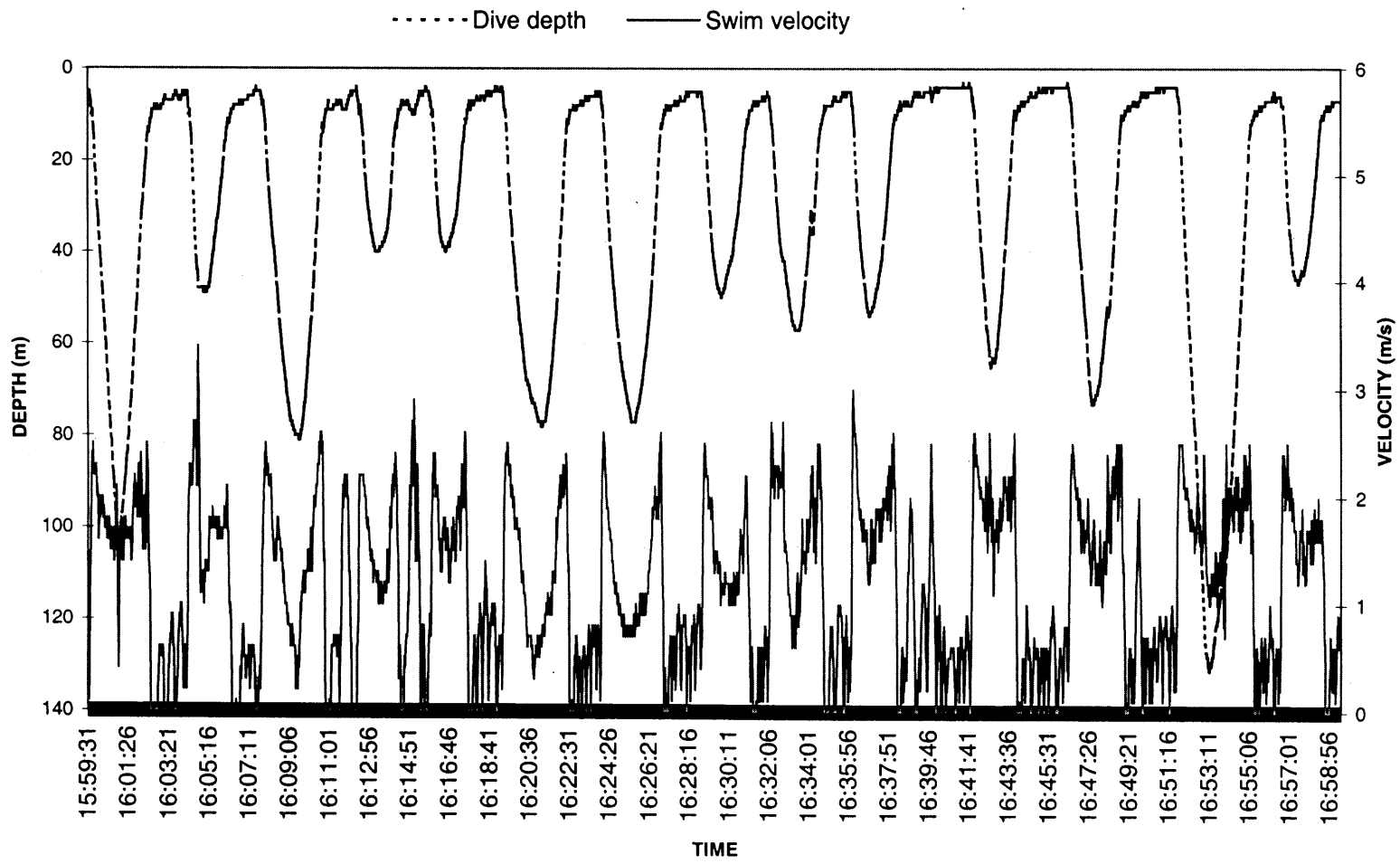

Figure A.2. Depth and velocity readings from a time-depth recorder plotted against time from 1600-1700 on 17 June 1998 during a 38.7 hour deployment on a free-ranging harbor porpoise.

In order to estimate the velocity of the porpoise as it surfaced and began its next dive a video analysis was conducted from three phases of 24 surfacing events, 10 from the tagged harbor porpoise and 14 from another slightly smaller porpoise during normal surfacing behavior. The original video tape was copied on a Sony EVO 9500A Hi8 videocassette recorder which time stamped the tape with hours : minutes : seconds: frame number (30/second). The time and frame count were recorded for all surfacings that were approximately perpendicular to the field of view when: 1) the tip of the snout emerged, 2) the anterior insertion point of the dorsal fin emerged, 3) the tip of the dorsal fin emerged, 4) snout submerged, 5) anterior insertion point of the fin submerged, 6) tip of fin submerged, 7) mid-peduncle submerged. Time differences were calculated for three phases of the surfacing event: 1) the snout emerged and the dorsal fin insertion point emerged, 2) snout submerged and anterior insertion point of dorsal fin submerged, and 3) snout submerged and mid–peduncle submerged. Velocity (m/s) was calculated for the tagged porpoise by dividing the elapsed time into 0.71m (distance from the snout to the anterior insertion point of the dorsal fin) for the first two calculations and into 1.05 m for the latter. For the smaller porpoise, 0.65 m and 0.96 m were used for these same calculations based on its size relative to the tagged porpoise.

The overall average velocity of all surfacing events was 1.1 $\pm$ 0.03 (SE) m/s. The average velocity for the snout out to base of fin was greater (1.2 m/s) than the latter two estimates, (0.95 and 1.0 m/s, respectively), suggesting that a porpoise decelerates as its surfaces.

Acceleration/deceleration patterns and rates were estimated for a haphazard sample of 88 of the approximately 931 deep dives logged during this deployment. The data record for the beginning of each long dive was marked at the first velocity greater than 1.1 m/s associated with an increase in depth that exceeded 10m. Consequently, all dives began with an acceleration event. The end of this acceleration event (beginning of deceleration event) was determined to be the time at which the velocity change occurred when it was followed by a consistently decreasing trend (> 2 seconds). Deceleration events were defined in a similar fashion, but where the velocity trend was increasing. The acceleration/deceleration rate was calculated as the change in velocity between the beginning and end of the event divided by the change in time between the beginning and end of the event. The average acceleration rate was defined as the average of the absolute value of all acceleration and deceleration rates. There were 2531 acceleration/deceleration events in the 88 dives examined with the overall average acceleration rate of $0.16 \pm 0.001 m/s^2$.

APPENDIX B

MALLORY'S ANILINE BLUE COLLAGEN STAIN

Acid Fuchsin Solution

Acid Fuchsin	0.5 g
Distilled water	100 ml

Aniline Blue – Orange G solution

Aniline Blue	0.5 g
Orange G	20 g
Phosphotungstic acid	1.0g
Distilled water	100 ml

Technique

1. Deparffinize sections and hydrate
2. Stain in Acid Fuchsin solution 2 minutes
3. Transfer directly to aniline blue solution 10 minutes
4. Dehydrate, clear and coverslip

Results

Nuclei – red

Collagenous fibrils – blue

Ground substance, cartilage, mucin, amyloid – varying shades of blue

Erythrocytes, myclin – yellow

Elastic fibrils – pale pink, pale yellow or unstained

APPENDIX C

VERHOEFF ELASTIC STAIN

Reagents

Lugol iodine

Iodine	10g	-	5 g	-	2.5 g
Potassium Iodide	20 g	-	10g	-	5 g
Distilled water	1000 ml	-	500 ml	-	250 ml

Put iodine and potassium iodide in a flask with 200ml of distilled water. Stir with mechanical stirrer until iodine dissolves and add rest of distilled water.

Ferric Chloride 10%

Ferric Chloride	25 g
Distilled water	250 ml

Alcoholic Hematoxylin 5%

Hematoxylin	5 g
95% Ethyl alcohol	100 ml

Verhoeff Elastic stain

Prepare fresh each time and mix in order

1. Alcoholic Hematoxylin 5%
2. Ferric Chloride 10%
3. Lugol iodine

Light green SF counterstain

Stock solution

Light green SF yellowish	1 g
Distilled water	500 ml
Glacial acetic acid	1 ml

Mix well and filter

Working solution

Stock solution light green SF	10 ml
Distilled water	50 ml

Sodium Thiosulfate 5%

Sodium Thiosulfate	50 g	-	5 g
Distilled water	1000 ml	-	100ml

Procedure

1. Deparffinize sections and hydrate to distilled water
2. Stain in Verhoeff stain - 1 hour
3. Wash into changes of distilled water
4. Differentiate microscopically in 2% ferric chloride until elastin fibers are distinct and background is colorless to light gray. If sections are differentiated too far, restain.
5. Rinse sections in distilled water
6. Place sections in Sodium Thiosulfate 1 minute

7.	Wash in running tap water	5 minutes
8.	Counterstain in light green SF if necessary	1-2 minutes
9.	Dehydrate, clear and coverslip.	

Results

Elastic fibers – blue-black to black

Nuclei – blue to black

APPENDIX D

COLLAGEN PERCENT AREA ANALYSIS PROTOCOL

All camera settings used were the defaults. The upper and lower diaphragms of the microscope were set to wide open and magnification set to 20x (20x was selected because it was high enough power to be able to discern the lipid cell walls and low enough that each image would sample an area of about 10% of the slide). This allowed an image of the ligamentous sheath and central core to be sampled from each quadrant of each specimen slide. An area of ligamentous sheath or central core for each slide was centered and focused manually. The microscope was then switched to the photographic mode and the photo preview of Digital Microscope Camera (DMC) software was initialized. The focus box was turned on in the DMC preview window and the image was focused on the scope manually to attain the highest value of the DMC focus index before capture and enhance was selected. The brightness level for all images was adjusted to 45% (most images had default brightness values in the range of 42-47% when captured) before saving. The image was opened in Optimus. In Percent Area, the color thresholds were set to: red, 0, 200, blue, 0, 255, and green, 0, 255. Percent area of Mallory's stained collagen was most sensitive to the red setting. An upper value of 200 was selected as the optimal setting after comparisons of several slides at 175 and 225. The value of 200 was found to consistently detect the relatively subtle stained collagen in the walls of the artery and veins but not detect the lightly stained lipid cell walls. For the ligamentous sheath, a

region of interest was manually traced which excluded the subpapillary layer and central core tissue, and a measurement was taken. For the central core tissue the percent area for the entire image was measured.

APPENDIX E

DETERMINATION OF ENGINEERING CONSTANTS

The Young's moduli were based on the values obtained for uniaxial testing (Chapter 5) and a Poisson's ratio of 0.45, which was selected as an approximate for an incompressible material. Due to the composite structure of the ligamentous sheath and central core, Young's modulus of elasticity (E), Poisson's ratio (ν) and shear modulus (G) were modified for each principle axis relative to the fiber orientation for input into the finite element model. They are designated as E_1, E_2, E_3, ν_{12}, ν_{13}, ν_{23}, G_{12}, G_{13} G_{23}, in which 1, 2, 3 represent orthogonal directions along with materials characteristic directions. If fiber direction is parallel to the predominant fiber direction of the central core, it is assigned a value of 1. If the fiber direction is parallel to the predominant fiber direction of the ligamentous sheath it is assigned a value of 3. It is assigned a value of 2 if the fiber angle is perpendicular to either of these two layers.

E_1 = Emax if maximum elastic modulus material direction coincides with direction 1.

E_1 = Emin if minimum elastic modulus material direction coincides with direction 1.

E_2 = Emax if maximum elastic modulus material direction coincides with direction 2.

E_2 = Emin if minimum elastic modulus material direction coincides with direction 2.

E_3 = Emax if maximum elastic modulus material direction coincides with direction 3.

$E_3 = Emin$ if minimum elastic modulus material direction coincides with direction 3.

$\nu_{12} = 0.45$ if $E_1 > E_2$, i.e., loading is || to the stronger material direction

$\nu_{12} = 0.30$ if $E_1 = E_2$, i.e., loading is in the isotropic material plane.

$\nu_{12} = 0.45 / E_1 \times E_2$ if $E_1 < E_2$, i.e., loading is $\perp$ to the weaker material direction.

$\nu_{13} = 0.45$ if $E_1 > E_3$, i.e., loading is || to the stronger material direction.

$\nu_{13} = 0.30$ if $E_1 = E_3$, i.e., loading is in isotropic material plane.

$\nu_{13} = 0.45 / E_1 \times E_3$ if $E_1 < E_3$, i.e., loading is $\perp$ to the weaker material direction.

$\nu_{23} = 0.45$ if $E_2 > E_3$, i.e., loading is || to the stronger material direction.

$\nu_{23} = 0.30$ if $E_2 = E_3$, i.e., loading is in the isotropic material plane.

$\nu_{23} = 0.45 / E_2 \times E_3$ if $E_2 < E_3$, i.e., loading is $\perp$ to the weaker material direction.

$G_{12} = E_1 / 2 \ (1 + \nu_{12})$ if $E_1 < E_2$, i.e., using smaller elastic modulus and Poisson ratio.

$G_{12} = E_2 / 2 /(1 + \nu_{21})$ if $E_1 > E_2$, i.e., using smaller elastic modulus and Poisson ratio.

$G_{13} = E_1 / 2 \ (1 + \nu_{13})$ if $E_1 < E_3$, i.e., using smaller elastic modulus and Poisson ratio.

$G_{13} = E_3 / 2 (1 + \nu_{31})$ if $E_1 > E_3$, i.e., using smaller elastic modulus and Poisson ratio.

$G_{23} = E_2 / 2 (1 + \nu_{23})$ if $E_2 < E_3$, i.e., using smaller elastic modulus and Poisson ratio.

$G_{23} = E_3 / 2 (1 + \nu_{32})$ if $E_2 > E_3$, i.e., using smaller elastic modulus and Poisson ratio.

The shear moduli of orthotropic materials need to be independent constants and should be measured from tests. Lacking such test data, an empirical equation has to be used. This equation was borrowed from the equation for isotropic materials and uses smaller E and ν values. The Poisson ratios ν_{21}, ν_{31} and ν_{32} used are obtained from theoretical equations:

$\nu_{21} = \nu_{12} / E_1 \times E_2$

$\nu_{31} = \nu_{13} / E_1 \times E_3$

$\nu_{32} = \nu_{23} / E_2 \times E_3$

A subroutine was run in Abaqus to convert the physical direction associated with 1, 2, and 3 to x, y, and z coordinates.

VITA

Brad Hanson was born in Seattle, Washington. He earned a Bachelor of Arts degree in Zoology at the University of Washington and Master of Science in Fisheries from the University of Washington. In 2001 he earned a Doctor of Philosophy at the University of Washington in Aquatic and Fishery Sciences.